

ALGERIAN DEMOCRATIC AND POPULAR REPUBLIC
MINISTRY OF HIGH EDUCATION AND SCIENTIFIC RESEARCH



UNIVERSITY OF SAAD DAHLAD BLIDA 1
INSTITUTE OF AERONAUTICAL AND SPACE STUDIES AIRCRAFT
CONSTRUCTION DEPARTMENT

Master's dissertation

Option: SPACE PROPULSION

Theme:

**Modeling and analysis of hydrogen enriched Methane
Combustion in Confined Chambers using ANSYS Fluent**

Written by:

Winnie Mwangemi Mwalewa

Supervised by:

Dr. Allouche

Dr. R. Renane

Defence date:7/7/2025

Member of the Jury

President, Dr Neche Ahmed

Ex1 Dr. Bekka Nadir

Ex2 Dr. Oueldbessi Hamid

Academic year:2024/2025

Acknowledgement

I would like to express my sincere gratitude to all those who have supported and guided me throughout the course of this work.

First and foremost, I am deeply thankful to Dr. R. Renane whose expertise, patience, and insightful feedback have been invaluable. Their encouragement and guidance have helped me stay focused and motivated.

I also extend my appreciation to Institute of Aeronautical and Space Studies Aircraft Construction Department for providing the necessary resources and a supportive environment in which to complete this project.

My heartfelt thanks go to my family and friends for their constant encouragement and understanding, especially during challenging times. Their support has been a source of strength throughout this journey.

Lastly, I acknowledge everyone who contributed to this work, whether through direct assistance, moral support, or by inspiring me in ways they may not even realize.

Thank you all.

Abstract

This study investigates the combustion characteristics of methane-air mixtures using ANSYS Fluent, focusing on three main aspects: global reaction modeling, the effects of hydrogen addition, and a detailed chemical reaction mechanism. The global reaction analysis explores the fundamental combustion behavior of methane in air, establishing a baseline for comparison with more complex scenarios. The second part of the study examines the impact of adding hydrogen to the methane-air mixture, with particular attention to the changes in combustion efficiency, flame characteristics, and pollutant emissions. Finally, a detailed mechanism involving a comprehensive set of chemical reactions is implemented to capture the complex interactions within the combustion process, providing deeper insight into species formation, temperature distribution, and reaction pathways.

The results from these three approaches are compared to highlight the effects of hydrogen on combustion dynamics and the accuracy of global versus detailed reaction models in predicting real-world behavior. This comparative analysis reveals that hydrogen addition enhances combustion efficiency, reduces emissions, and alters the flame structure, while the detailed mechanism offers a more accurate prediction of temperature profiles and species concentrations compared to the global reaction model. Overall, this study underscores the importance of selecting the appropriate modeling approach based on the desired level of accuracy and computational resources.

Key words: methane combustion, non-premixed combustion, Ansys-Fluent, Navier-Stokes, RANS, $k-\omega$ SST, confined combustion chamber, hydrogen addition, global reaction, equivalence ratio, lean combustion regime, NO_x emissions

Résumé

Cette étude explore les caractéristiques de la combustion des mélanges méthane–air à l’aide d’ANSYS Fluent, en se concentrant sur trois aspects principaux : la modélisation par réaction globale, l’effet de l’ajout d’hydrogène, et l’utilisation d’un mécanisme chimique détaillé. La première partie analyse la combustion fondamentale du méthane dans l’air à l’aide d’une réaction globale, servant de référence pour des scénarios plus complexes. Ensuite, l’ajout d’hydrogène au mélange méthane–air est étudié, en mettant l’accent sur l’efficacité de la combustion, la structure de la flamme et les émissions polluantes. Enfin, un mécanisme détaillé comprenant un ensemble complet de réactions chimiques est mis en œuvre pour capturer les interactions complexes du processus de combustion, permettant une meilleure compréhension de la formation des espèces, de la distribution de température et des chemins réactionnels.

Les résultats issus de ces trois approches sont comparés afin de mettre en évidence les effets de l'hydrogène sur la dynamique de la combustion, ainsi que la précision des modèles globaux par rapport aux mécanismes détaillés. Cette analyse comparative montre que l'ajout d'hydrogène améliore l'efficacité de la combustion, réduit les émissions, et modifie la structure de la flamme. Le mécanisme détaillé offre quant à lui une prédiction plus précise des profils de température et des concentrations d'espèces. Dans l'ensemble, cette étude souligne l'importance de choisir une approche de modélisation adaptée au niveau de précision souhaité et aux ressources de calcul disponibles.

Mots-clés: combustion du méthane, combustion non prémélangée, Ansys-Fluent, équations de Navier-Stokes, RANS, $k-\omega$ SST, chambre de combustion confinée, addition d'hydrogène, réaction globale, rapport d'équivalence, régime de combustion pauvre, émissions de NOx

المخلص

مع التركيز على ثلاثة محاور، ANSYS Fluent، تتناول هذه الدراسة خصائص احتراق خلطات الميثان مع الهواء باستخدام برنامج رئيسية: نمذجة الاحتراق باستخدام تفاعل كلي مبسط، تأثير إضافة الهيدروجين، وتطبيق آلية كيميائية تفصيلية. يهدف الجزء الأول إلى تحليل سلوك الاحتراق الأساسي للميثان في الهواء باستخدام نموذج تفاعل مبسط، مما يشكل قاعدة مقارنة للحالات الأكثر تعقيداً. في الجزء الثاني، يتم دراسة تأثير إضافة الهيدروجين إلى خليط الميثان والهواء، مع التركيز على تغييرات كفاءة الاحتراق، خصائص اللهب وانبعثات الملوثات. أما الجزء الأخير فيعتمد على آلية كيميائية مفصلة تشمل مجموعة من التفاعلات الكيميائية بهدف فهم التفاعلات المعقدة أثناء الاحتراق، والتنبؤ بتوزيع درجات الحرارة وتكوين الأنواع الكيميائية المختلفة.

تمت مقارنة نتائج النماذج الثلاثة لإظهار تأثير الهيدروجين على ديناميكية الاحتراق، وكذلك تقييم دقة النماذج المبسطة مقارنةً بالنماذج الكيميائية التفصيلية. أظهرت النتائج أن إضافة الهيدروجين تعزز من كفاءة الاحتراق، وتقلل الانبعثات، وتغير من شكل اللهب، في حين توفر الآلية التفصيلية تنبؤاً أكثر دقة بدرجات الحرارة وتركيز الأنواع الكيميائية. وتؤكد هذه الدراسة على أهمية اختيار نموذج الاحتراق المناسب بناءً على مستوى الدقة المطلوب والموارد الحسابية المتاحة.

الكلمات المفتاحية:

نموذج (RANS) احتراق الميثان، الاحتراق غير المسبق الخلط، أنسيس-فلونت، معادلات نافير-ستوكس، نمذجة رانس غرفة احتراق محصورة، إضافة الهيدروجين، تفاعل كيميائي عالمي، نسبة التكافؤ، نظام الاحتراق $k-\omega$ SST، الاضطراب (NOx) الفقير، انبعثات أكاسيد النيتروجين

Table of contents

Acknowledgement	i
Abstract	ii
Résumé	ii
Table of contents.....	iv
List of figures.....	viii
Nomenclature.....	xi
Introduction	1
Chapter 01 Literature review and Generalities of combustion	4
1.1 Introduction.....	4
1.2 Literature review	4
1.2.1 Experimental work	4
1.2.2 Previous works	7
1.3 Fundamentals of Combustion.....	9
1.3.1 Definition of combustion.....	9
1.3.2 Importance and applications of combustion	9
1.4 Types of Combustion	10
1.4.1 Premixed flames.....	10
1.4.2 Non-Premixed Flames (Diffusion Flames).....	10
1.4.3 Complete combustion.....	12
1.4.4 Incomplete combustion	12
1.5 Thermodynamics of combustion(ΔH_C°)	13
1.5.1 Enthalpy of combustion	13
1.5.2 Heat of reaction and adiabatic temperature	14
1.5.3 Stoichiometry and equivalence ratio	15
1.5.4 First and second laws of thermodynamics in combustion.....	16
1.6 Chemical Kinetics of Combustion.....	17
1.6.1 Reaction mechanisms and elementary reactions.....	17
1.6.2 Arrhenius equation and activation energy	19
1.6.3 Autoignition and ignition delay	21
1.7 Combustion Equilibrium	21
1.7.1 Equilibrium composition of combustion products.....	21
1.7.2 Gibbs free energy minimization	23

1.7.3	Water-Gas Shift and Dissociation Reactions:.....	23
1.7.4	Effects of pressure and temperature on equilibrium	24
1.8	Flame Characteristics	26
1.8.1	Flame speed and flame structure	27
1.8.2	Laminar and Turbulent flames	28
1.8.3	Quenching Distance and Flammability Limits	29
1.8.4	Detonation and Deflagration	29
1.9	Pollutants Formation in Combustion.....	29
1.10	Combustion of Different Fuels.....	30
1.11	Methane and hydrogen combustion.....	31
1.11.1	Combustion Chemistry of Methane and Hydrogen	31
1.12	Conclusion	32
Chapter 02	Mathematical Modeling	34
2.1	Introduction.....	34
2.2	The Fundamental Equations of Fluid Dynamics	35
2.2.1	Equation of Continuity	35
2.2.2	Momentum Equation (Navier-Stokes Equations).....	35
2.2.3	Energy Equation.....	36
2.2.4	Species transport equation.....	37
2.2.5	The eddy dissipation model (EDM)	38
2.2.6	The Eddy Dissipation Concept (EDC)	39
2.3	Turbulence Modeling.....	40
2.3.1	Transport equation for turbulent kinetic energy (k):.....	41
2.3.2	Transport equation for specific dissipation rate (ω):.....	41
2.3.3	Turbulent eddy viscosity (μ_t):	42
2.4	Reaction Rate	43
2.4.1	Global One-Step Reaction Mechanism	43
2.6.2	Reduced Detailed Mechanism (DRM)	44
2.5	Numerical Discretization	45
2.6	Conclusion	46
Chapter 03	Numerical resolution.....	47
3.1	Introduction.....	47
3.2	Numerical Resolution Methods.....	47
3.3	Discretization Method	47
3.4	Pressure based solver	48

3.4.1	Coupled Algorithm (Fully Coupled Pressure-Based Solver).....	49
3.5	Turbulence Modeling.....	49
3.6	Combustion Modeling.....	50
3.7	Solver Settings and Convergence.....	50
3.8	Mesh and Grid Independence.....	51
3.9	Conclusion	51
Chapter 04	Simulation Setup	52
4.1	Introduction.....	52
4.2	Combustor Modeling	52
4.3	Mesh Generation.....	53
4.4	Boundary conditions	56
4.4.1	Section naming.....	56
4.4.2	Boundary conditions identification	58
4.5	mesh sensitivity study	59
4.5.1	Quantitative Mesh Convergence Analysis.....	60
4.5.2	Grid Convergence Index (GCI)	61
4.6	Fluent Setup	62
4.7	Conclusion	64
Chapter 05	Results and Discussion.....	65
5.1	Introduction.....	65
5.2	Methane-air combustion results for a global reaction.....	65
5.2.1	Results for Stoichiometric conditions.....	65
5.2.2	Lean combustion regimes in my simulation	69
5.2.3	NOx effects at different equivalence ratios	70
5.3	Effects of Hydrogen Addition on Combustion	71
5.3.1	Hydrogen addition at equivalence ratio of 1	71
5.3.2	NOx effects on addition of hydrogen	76
5.4	Comparison and validation of results	77
5.4.1	Validation of Adiabatic Flame Temperature at Stoichiometric Conditions	77
5.4.2	Validation of Flame Temperature Rise with Hydrogen Addition	79
5.4.3	Validation of Velocity Field.....	80
5.4.4	Pressure Field Validation	81
5.4.5	Density Field Validation	81
5.4.6	Overall Combustion Behavior with Hydrogen Addition	81
5.5	Conclusion	82

Conclusion.....	94
Key Findings.....	94
References	96
Appendix A	100
A.1 Methane-air Simulation Setup using a Global reaction	100
A. 2 Hydrogen addition to Methane-air Simulation Setup	104
Appendix B.....	106
B.1 Cold Flow Simulation Setup for DRM22 Mechanism.....	106
Objective of the Cold Flow Simulation	106
Chemical Mechanism and Import Process	106
Initialization and Patch	108
Convergence Criteria	109
Remarks	111

List of figures

Figure 1 Schematic diagram of an experimental flat-flame burner setup with optical access. [37].....	5
Figure 2 Z-type Schlieren optical arrangement for visualizing flame fronts and flow-field gradients [39]	6
Figure 3 Snapshots of premixed flame at different flow conditions [16]	10
Figure 4 Snapshots of Non-Premixed Flame at different flow conditions [16]	11
Figure 5 Arrhenius plot [20]	20
Figure 6 2D geometry used by C. E. L. Pinho, J. M. P. Q. Delgado, R. Pilao, J. Conde and C. Pinho in their study titled “Numerical Study of Propane-Air Mixture Combustion in a Burner Element” [52]	52
Figure 7 2D asymmetric geometry of a burner element	53
Figure 8 full view of the mesh	54
Figure 9 zoomed view of the mesh	54
Figure 10 skewness histogram	55
Figure 11 orthogonal quality histogram	55
Figure 12 skewness and orthogonal quality mesh spectrum [53]	55
Figure 13 Combustion chamber fuel inlet.....	56
Figure 14 Combustion chamber air inlet.....	56
Figure 15 Combustion chamber outlet.....	57
Figure 16 Combustion chamber axis.....	57
Figure 17 Combustion chamber wall	58
Figure 18 Mesh independence study, at equivalence ratio of 1, plot for the four meshes	60
Figure 19 A Temperature contour for methane-air combustion for a global reaction at the equivalence ratio Φ of 1	66
Figure 20 Temperature plot at the axis for methane-air combustion for global reaction at the equivalence ratio Φ of 1	66
Figure 21 Velocity contour for a methane-air combustion for a global reaction at the equivalence ratio Φ of 1.....	67
Figure 22 velocity plot at the axis for methane-air combustion for a global reaction at the equivalence ratio Φ of 1	67
Figure 23 Pressure contour for methane-air combustion for global reaction at the equivalence ratio Φ of 1	68

Figure 24 pressure plot at the axis for methane-air combustion for a global reaction at the equivalence Φ ratio of 1	68
Figure 25 Density contour for methane-air combustion for a global reaction at the equivalence Φ ratio of 1	69
Figure 26 Temperature contour of methane-air combustion at the equivalence ratio of 0.8.....	69
Figure 27 Temperature contour of methane air combustion T equivalence ratio of 0.7	69
Figure 28 NOx mass fraction contour at the equivalence ratio of 0.7	70
Figure 29 NOx mass fraction contour at the equivalence ratio of 0.8	70
Figure 30 NOx mass fraction contour at the equivalence ratio of 1.1	70
Figure 31 NOx mass fraction contour at the equivalence ratio of 1.2	71
Figure 32 Temperature contours from 0% to 35% addition of hydrogen at equivalence ratio of 1	72
Figure 33 Temperature plots from 0% to 35% addition of hydrogen at equivalence ratio of 1	73
Figure 34 Velocity contours from 0% to 35% addition of hydrogen at 3atm	75
Figure 35 Velocity plots from 0 to 35 addition of hydrogen at 3atm	75
Figure 36 NOx mass fraction at 5% hydrogen addition in methane-air combustion	76
Figure 37 NOx mass fraction at 15% hydrogen addition in methane-air combustion	76
Figure 38 NOx mass fraction at 25% hydrogen addition in methane-air combustion	76
Figure 39 NOx mass fraction at 35% hydrogen addition in methane-air combustion	77
Figure 40 Mean temperature contour of the Sandia D methane–air flame from RANS-FGM simulation representing a benchmark for turbulent jet flames under stoichiometric conditions, side by side with the results of this simulation.	78
Figure 41 Temperature field of the Sandia D Simulated with Flamelet Model	78
Figure 42 A side by side comparison between the reference data and the results of the simulation.....	79
Figure 43 A side by side comparison between the velocity contour results and references at hydrogen additions of 0%, 5%, 15%, 25% and 35%.....	80
Figure 44 General Steady configuration step	100
Figure 45 Energy equation step	100
Figure 46 Model choice step (Species transport)	100
Figure 47 Selection of the viscous model step	101
Figure 48 Setting the Mass flow rate Step for air inlet.....	101
Figure 49 Setting the initial temperatures	102
Figure 50 Setting the Species mass fractions at the air inlet.....	102
Figure 51 Setting the Mass flow rate at the fuel inlet.....	103
Figure 52 Setting the initial temperatures	103

Figure 53 Setting Species mass fractions	103
Figure 54 Addition of hydrogen to the available materials list	104
Figure 55 Addition of Hydrogen to the species list.....	104
Figure 56 Addition of the Hydrogen reaction equation.....	105
Figure 57 mechanism importing process.....	106
Figure 58Mechanism importing process	107
Figure 59 Mechanism importing process	107
Figure 60 Scaled Residuals	109
Figure 61 Mass balance check for air inlet.....	110
Figure 62Mass balance check for fuel inlet.....	110
Figure 63 Mass balance check for outlet.....	111
Figure 64 Temperature contour during cold flow	111
Table 1-1 Differences between Premixed and Non-premixed flames	11
Table 1-2 Enthalpy of combustion for common fuels [17]	14
Table 4-1 Labels and dimensions of the Combustion chamber	53
Table 4-2 Meshing details.....	54
Table 4-3 Maximum temperatures at equivalence ratio of 1 for 4 meshes with different refinements	59
Table 5-1 Maximum temperatures and different hydrogen percentage addition	73
Table 5-2 Maximum temperatures and different hydrogen percentage addition	79
Table 5-3 Summary of Validation Results	82
Table 0-1 Solver and model settings.....	108
Table 0-2 Boundary Conditions.....	108
Table 0-3Material Properties	108
Table 0-5 Solution controls.....	109

Nomenclature

Chapter 1: Generalities of Combustion

Symbol	Description
CO	Carbon monoxide
CO ₂	Carbon dioxide
CH ₄	Methane
H ₂	Hydrogen
O ₂	Oxygen
N ₂	Nitrogen
UFL	Upper Flammability Limit
LFL	Lower Flammability Limit
AIT	Autoignition Temperature
T	Temperature
P	Pressure
ΔH^c	Enthalpy of combustion
Φ (Phi)	Equivalence ratio
kJ/mol	Kilojoules per mole
NO _x	Nitrogen oxides

Symbol	Description
UHC	Unburned hydrocarbons
G	Gibbs free energy
ΔG	Change in Gibbs free energy
S	Entropy
K	Equilibrium constant
WGSR	Water-Gas Shift Reaction

Chapter 2: Mathematical Modeling

Symbol	Description
ρ	Density (kg/m ³)
u, v	Velocity components
μ	Dynamic viscosity
μ_t	Turbulent (eddy) viscosity
p	Pressure
k	Turbulent kinetic energy
ω	Specific dissipation rate
ε	Turbulent dissipation rate
C _p	Specific heat at constant pressure
T	Temperature
h	Enthalpy
t	Time
Y _i	Mass fraction of species <i>i</i>
R	Universal gas constant

Symbol	Description
τ_{ij}	Stress tensor components
∇	Gradient operator
$\nabla \cdot$	Divergence operator
D_i	Diffusion coefficient for species i
S_i	Source term for species i
χ	Fine structure mass fraction (EDC model)
τ	Residence time (EDC model)

Chapter 3: Numerical Resolution

Symbol	Description
$\Delta x, \Delta y$	Grid spacing in x and y directions
CFL	Courant–Friedrichs–Lewy number
GCI	Grid Convergence Index
FVM	Finite Volume Method
PISO	Pressure-Implicit with Splitting of Operators
SIMPLE	Semi-Implicit Method for Pressure-Linked Equations
URF	Under-relaxation factor

Chapter 4: Simulation Setup

Symbol	Description
MFR	Mass Flow Rate

Symbol	Description
mm	Millimeter
K	Kelvin
s	Seconds
Q	Heat source/supply
T ₀	Initial temperature
Y _{CH₄}	Mass fraction of methane
Y _{H₂}	Mass fraction of hydrogen
Y _{O₂}	Mass fraction of oxygen
Y _{N₂}	Mass fraction of nitrogen

Chapter 5: Results and Discussion

Symbol	Description
T _{max}	Maximum flame temperature
V	Velocity magnitude
p	Static pressure
ρ	Gas density
Φ	Equivalence ratio
NO _x	Nitrogen oxide emissions
CO	Carbon monoxide
CO ₂	Carbon dioxide
U	Axial velocity component
T(x)	Temperature along axis

Symbol	Description
ΔT	Temperature difference

Introduction

Introduction

As the global energy sector shifts toward sustainable and low-carbon solutions, the role of cleaner and more efficient combustion systems has become increasingly important. Methane, the primary component of natural gas, has long been favored as a fuel due to its high availability, established infrastructure, and relatively low carbon content compared to heavier hydrocarbons. Despite these advantages, methane combustion still results in significant emissions of carbon dioxide (CO₂), carbon monoxide (CO), and unburned hydrocarbons (UHCs), particularly under sub-optimal conditions. Consequently, there is a growing interest in exploring strategies to enhance methane combustion performance while mitigating its environmental impact.

One such strategy involves the addition of hydrogen to methane-air mixtures. Hydrogen offers several favorable combustion characteristics: it has a high laminar flame speed, low ignition energy, and a wide flammability range. These properties make it particularly effective in stabilizing lean flames, allowing combustion to occur at lower equivalence ratios, which in turn helps reduce CO and UHC emissions while improving thermal efficiency. However, hydrogen enrichment can also lead to higher flame temperatures, which may result in increased formation of nitrogen oxides (NO_x), especially under stoichiometric or rich conditions. Understanding the balance between improved combustion performance and potential pollutant formation is essential to safely integrating hydrogen into existing and future combustion technologies.

Computational Fluid Dynamics (CFD) has emerged as a powerful tool for investigating the complex interactions that occur during combustion. CFD enables detailed simulation of flow behavior, heat transfer, and chemical reactions under controlled and repeatable conditions, eliminating the need for costly experimental setups. It is especially well-suited for analyzing methane-hydrogen combustion, where the interaction between turbulence and chemistry is highly nonlinear and sensitive to changes in boundary conditions, fuel composition, and geometry. Moreover, CFD allows researchers to explore a wide range of operating conditions efficiently through parametric studies, making it an invaluable tool for modern combustion research.

In this study, CFD simulations were carried out using ANSYS Fluent 2024 to examine the combustion behavior of pure methane-air and hydrogen-enriched methane-air mixtures in a confined burner geometry. A key feature of the study is the comparison between two different chemical kinetic modeling approaches: a simplified global one-step reaction mechanism and a reduced detailed mechanism

(DRM22) comprising 21 species and 84 reactions. The global mechanism is computationally efficient and useful for capturing general trends in flame temperature and stability, whereas the detailed mechanism allows for more accurate prediction of intermediate species, reaction pathways, and pollutant formation. This comparative approach enables a balanced assessment of the trade-offs between chemical accuracy and computational cost.

Although previous studies have investigated hydrogen addition in both experimental and numerical settings, there remains a notable gap in systematically comparing global and detailed chemical mechanisms across a wide range of combustion parameters. Most existing simulations either focus on detailed kinetics under laminar flow conditions or apply overly simplified models in turbulent scenarios. Additionally, the combined effects of equivalence ratio, preheat temperature, and hydrogen content have rarely been explored in a single CFD framework that is applicable to real-world combustion systems. This research addresses that gap by investigating how hydrogen enrichment influences flammability limits, particularly under lean conditions; how preheat temperature affects flame stabilization; and how different chemical kinetic models perform in predicting realistic combustion behavior.

The simulations were conducted in a two-dimensional axisymmetric burner geometry, with the computational domain discretized using a structured mesh that was validated through a mesh independence study. The setup included separate inlets for fuel and air, allowing for both pure methane and hydrogen-enriched mixtures to be evaluated. Two types of chemical mechanisms were employed. The global mechanism consisted of a one-step reaction for methane. The DRM22 detailed mechanism, imported using CHEMKIN files, was applied specifically to pure methane-air combustion to serve as a high-fidelity reference for validating the global approach.

The simulations were performed using both the Eddy Dissipation Model (EDM) and the Eddy Dissipation Concept (EDC), depending on the mechanism used. EDM was applied in conjunction with the global model due to its ability to model turbulent, non-premixed flames where reaction rates are limited by turbulent mixing. EDC, on the other hand, incorporates finite-rate chemistry effects and was therefore more appropriate for use with the detailed mechanism, particularly in identifying flammability limits and ignition-extinction behavior. Turbulence was modeled using the $k-\omega$ SST model, which provides accurate near-wall resolution and robustness in the freestream region, making it well-suited for reacting flows.

To evaluate flame behavior, the study explored a range of equivalence ratios and hydrogen blending percentages. The outputs of interest included temperature fields, velocity profiles, flame shape and

anchoring behavior, and species distributions. Results from the global and detailed models were compared to assess predictive capability, with emphasis on temperature profiles, flame structure, and species formation.

This research makes several important contributions. It presents a validated CFD methodology for assessing hydrogen-enriched methane combustion, provides a direct comparison between simplified and detailed kinetic models, and enhances the understanding of how hydrogen affect flame dynamics in confined geometries. These findings have practical implications for the design and optimization of industrial burners, gas turbines, and other combustion systems that aim to incorporate hydrogen as a clean fuel additive, supporting broader efforts toward decarbonization and improved energy efficiency.

Chapter 1:

Generalities of Combustion

Summary

1.1	Introduction.....	4
1.2	Literature review	4
1.3	Fundamentals of Combustion.....	9
1.4	Types of Combustion	10
1.5	Thermodynamics of combustion(ΔH_C°)	13
1.6	Chemical Kinetics of Combustion.....	17
1.7	Combustion Equilibrium	21
1.8	Flame Characteristics	26
1.9	Pollutants Formation in Combustion.....	29
1.10	Combustion of Different Fuels.....	30
1.11	Methane and hydrogen combustion.....	31
1.12	Conclusion	32

Chapter 01 Literature review and Generalities of combustion

1.1 Introduction

Combustion is a fundamental chemical process that involves the rapid reaction of a substance with oxygen, accompanied by the release of energy in the form of heat and light. It is a key process in many natural and industrial applications, including energy production, transportation, and various manufacturing processes. At its core combustion is an exothermic chemical redox reaction between a fuel and an oxidant, typically oxygen from the air.

This chapter presents a literature review on previous works done on methane-air combustion and addition of hydrogen and the approach I took in the numerical analysis of this phenomena. Apart from that a general review on combustion to help us better understand these phenomena.

1.2 Literature review

1.2.1 Experimental work

Although this study is entirely numerical, the modeling work is designed to reflect conditions that can be realistically replicated in an experimental setting. To provide a framework for future validation and to ensure that the numerical assumptions align with practical combustion systems, this section outlines the experimental procedures that would accompany the simulation work described in this thesis. These procedures are based on standard practice in methane and hydrogen combustion research, and their design parallels the input conditions, flame configurations, and data extracted from CFD.

In a laboratory context, the combustion experiments would be conducted in a horizontal or vertically oriented axisymmetric burner, enclosed in a quartz-walled chamber to allow for optical diagnostics. This burner would accommodate both pure methane and hydrogen-enriched methane-air mixtures. A simplified schematic of such a setup, commonly used in flame stability and structure investigations, is shown in **Figure 1-4**, which illustrates the burner, quartz chamber, and **Schlieren optical arrangement** [37].

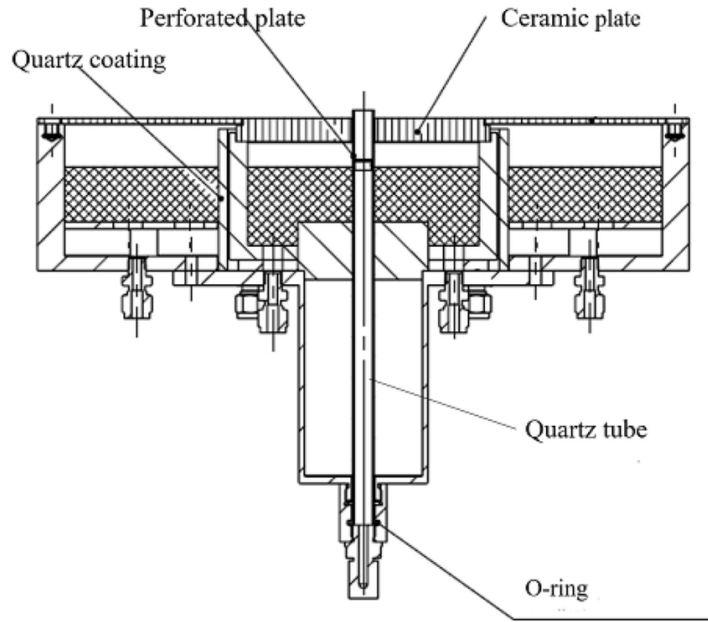


Figure 1 Schematic diagram of an experimental flat-flame burner setup with optical access. [37]

The fuel delivery system would consist of high-purity methane and hydrogen cylinders connected to mass flow controllers (MFCs) to ensure precise regulation of flow rates. Similarly, dry, filtered air would be supplied as the oxidizer. The MFCs allow for the careful adjustment of equivalence ratios over a broad range, from lean to rich conditions, typically between 0.6 and 1.2. In addition to controlling the fuel–air ratio, the hydrogen content in the fuel mixture would be varied incrementally, often by volume percentage (e.g., 0%, 10%, 20%, 30% H₂), to study its influence on flame stability and structure, just as was done in the simulation stage [2].

To replicate the effects of preheated reactants observed in simulation, the fuel–air mixtures would be passed through inline electric heaters or recuperative heat exchangers. The preheat temperature could be precisely controlled, ranging from ambient (300 K) up to 600 K. Preheating is essential for experiments focused on determining flammability limits and ignition behavior, particularly for lean mixtures where flame stability becomes increasingly sensitive to inlet temperature [38].

Combustion would be initiated using a spark ignitor positioned at the burner exit. Upon ignition, the flame would be allowed to stabilize at the nozzle to emulate the flame anchoring observed in CFD. In experiments involving premixed conditions, this stabilization is crucial for measuring flammability limits and ensuring a consistent flame zone for diagnostics. For stability studies, a lean blow-off or rich extinction condition would be induced by gradually adjusting the fuel or air flow until the flame detaches or extinguishes, replicating the CFD-based method of flammability limit detection.

Literature review and Generalities of combustion

Data collection in such an experimental setup would involve a combination of optical and probe-based diagnostics. **Schlieren imaging** is among the most effective techniques for visualizing flame fronts and flow-field gradients. A **Z-type Schlieren optical setup**, similar to that shown in **Figure 1-5**, would be used to capture high-speed images of flame dynamics, including flame length, curvature, and instabilities [39]. These images would be directly comparable to temperature contours and flame zones obtained in Fluent.

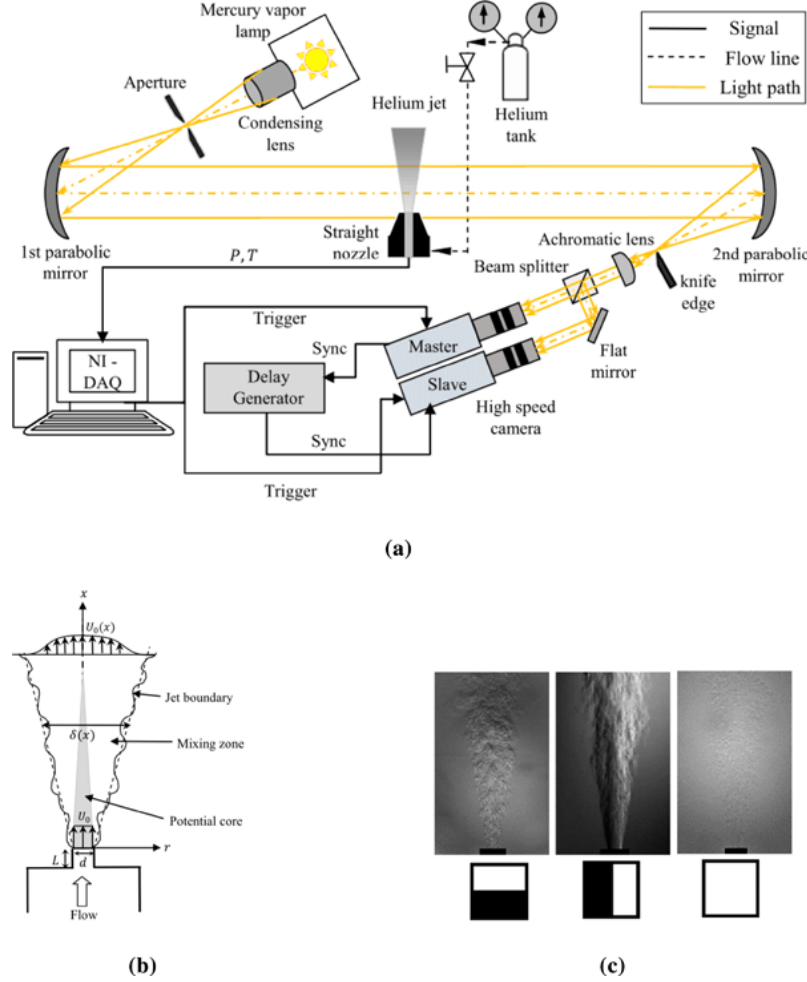


Figure 2 Z-type Schlieren optical arrangement for visualizing flame fronts and flow-field gradients [39]

In parallel, **OH*** chemiluminescence could be used to map the active reaction zone and estimate peak heat-release regions. When superimposed with Schlieren images, this provides a rich visual understanding of flame structure and local combustion intensity [40].

Temperature measurement within the flame would be performed using fine-wire thermocouples (typically 0.05 mm in diameter) inserted through ports in the combustion chamber wall. These

thermocouples would allow for measurement of both pre-flame and post-flame temperatures. Additionally, **thin-filament pyrometry** could be employed to record flame temperature non-invasively, particularly when dealing with hydrogen-rich flames where steep gradients exist and probe intrusion might disturb the flame structure [41].

Gas analyzers positioned downstream of the flame would quantify the concentration of major species such as CO, CO₂, and unburned hydrocarbons. In hydrogen-enriched conditions, H₂ detectors and NO_x analyzers would also be required to understand the environmental and safety implications of using hydrogen in practical combustion systems [42].

To determine the flammability limit of the mixtures, a slow reduction or increase in the equivalence ratio would be carried out until the flame could no longer sustain itself. The limiting equivalence ratio values at which blow-off (lean) or extinction (rich) occurred would be noted and compared against the thresholds predicted by the CFD simulations. This procedure would be repeated for various preheat temperatures to observe how temperature shifts the limits.

Finally, all collected data—such as flame shape, ignition behavior, temperature profiles, and flammability limits—would be compared with the numerical predictions. The visual flame front captured by Schlieren and chemiluminescence imaging could be matched against the Fluent-generated flame contours. Similarly, temperature data from thermocouples could validate simulated maximum flame temperatures at various operating points. This integrated approach ensures that simulation results are grounded in experimentally measurable quantities, thereby reinforcing the credibility and applicability of the numerical findings.

1.2.2 Previous works

In the pursuit of optimizing methane-air combustion, I reviewed several key studies that investigated the effects of hydrogen enrichment. These works vary in their approach—ranging from experimental to computational methods—but all contribute valuable insight into how hydrogen influences flame behavior, combustion efficiency, and pollutant emissions. Below is a critical summary of these studies, which collectively inform the direction and methodology of my research.

1. Guo et al. (2007) conducted a benchmark study on the laminar flame speed and flammability limits of methane-hydrogen-air mixtures [1]. Using both experimental measurements and numerical analysis, they found that increasing the hydrogen content in the mixture significantly boosts the laminar flame speed due to hydrogen's high diffusivity and chemical reactivity. Furthermore, the flammability limits expanded on

Literature review and Generalities of combustion

both the lean and rich sides. This ability to sustain combustion under ultra-lean conditions supports the feasibility of stable and efficient operation in conditions where pure methane would fail. Their findings directly inform my decision to explore lean combustion regimes in my CFD simulations.

2. Ji and Wang (2009) examined the combustion and emission characteristics of hydrogen-enriched methane in a spark-ignition engine [3]. Their experiments revealed improved thermal efficiency in lean mixtures, primarily due to hydrogen's fast flame speed, which promotes more complete combustion. Notably, the addition of hydrogen reduced CO and unburned hydrocarbon (UHC) emissions but increased NO_x formation. Their suggestion of using exhaust gas recirculation (EGR) or equivalence ratio adjustments to mitigate NO_x is highly relevant to my work, where flame temperature and pollutant profiles are analyzed across different equivalence ratios.

3. Medwell et al. (2008) used advanced laser diagnostics to investigate the effects of hydrogen addition on turbulent non-premixed methane jet flames [5]. Their use of planar laser-induced fluorescence (PLIF) provided visual confirmation that hydrogen leads to shorter, more intense flames, with earlier ignition points and higher flame curvature. These changes were attributed to hydrogen's lower ignition energy and faster reaction rates. While this supports my use of hydrogen for flame stabilization, their warning about increased NO_x in near-field regions also underscores the trade-offs I aim to quantify in my simulations.

4. Ren et al. (2007) carried out a comprehensive computational and experimental analysis of laminar premixed methane-air flames with hydrogen [8]. They focused on the concentrations of radicals like H, O, and OH, discovering that hydrogen enhances radical formation and reduces flame thickness. This compact and more intense flame structure is useful for designing high-performance combustors. Their detailed chemical mechanism serves as a validation reference for the skeletal reaction mechanism I employ in my Fluent simulations.

5. Porpatham et al. (2011) analyzed the effects of hydrogen on the performance of a compressed natural gas (CNG) engine [2]. They demonstrated that hydrogen addition leads to quicker combustion, improved brake thermal efficiency, and reduced CO and HC emissions. However, similar to previous studies, NO_x emissions increased. Importantly, they showed that hydrogen allows operation under ultra-lean conditions, which would be otherwise unsustainable with methane alone. This finding reinforces my focus on hydrogen's role in extending lean flammability limits.

6. Park et al. (2013) investigated hydrogen-enriched methane flames at different equivalence ratios using a premixed flat-flame burner [43]. Their work revealed that flame temperature increases with hydrogen

addition, especially at stoichiometric and slightly lean mixtures. They also observed enhanced oxidation of intermediate species like formaldehyde and acetylene. These results support my use of temperature profiles and species distributions as primary diagnostic outputs in my simulations.

7. Seshadri and Peters (2005) provided foundational insights into the strain response of hydrogen-enriched counterflow flames [9]. By quantifying extinction strain rates, they showed that hydrogen improves flame robustness under aerodynamic stress. Their work is essential for flamelet-based models and supports my application of the $k-\omega$ SST model for capturing turbulent flow-flame interactions in Fluent.

8. Chaudhuri et al. (2010) investigated blowoff dynamics in bluff-body stabilized flames with hydrogen addition [4]. Their results showed that hydrogen significantly delays blowoff and enhances flame stability at higher flow velocities. These improvements were due to both chemical (radical formation) and thermal (burning velocity) effects. Their insights are directly applicable to my study of flame anchoring and stability within a confined burner geometry under varied inlet flow conditions.

These studies collectively demonstrate that hydrogen enrichment improves flame stability, combustion efficiency, and lean-operability while posing challenges such as NO_x emissions. Their methodologies and findings offer both qualitative and quantitative benchmarks that support and guide the direction of my numerical simulations. By synthesizing their results with my CFD framework, I aim to contribute to the ongoing development of cleaner and more efficient hydrogen-enhanced combustion systems.

It is important to understand the generalities of combustion to further understand these phenomena. We can start with the basic, Fundamentals of combustion

1.3 Fundamentals of Combustion

1.3.1 Definition of combustion

According to Webster's dictionary **combustion** is defined as, "rapid *oxidation generating heat, or both light and heat; also, slow oxidation accompanied by relatively little heat and no light,*" We will restrict the definition to include rapid oxidation portion, since most practical combustion devices belong in this realm [14]. Combustion transforms energy stored in chemical bonds to heat that can be utilized in variety of ways.

1.3.2 Importance and applications of combustion

Combustion is used in many industrial processes requiring heat. Heat can be needed for a number of reasons, such as to preheat ingredients prior to chemical reactions, or as a by-product of reactions. Some

reactions can be exothermic, that is they produce heat as well as new materials. Combustion can also be used to preheat air prior to its use in combustion turbines which produce electricity. In some cases, the combustion process itself provides enough heat, particularly if the oxygen required for the reaction is readily available, such as in natural gas-fueled mixed flow gas turbine systems and laminar flame burners.

1.4 Types of Combustion

Combustion can occur in either a **flame or non-flame mode**, and flames, in turn are categorized as being either **premixed flames** or **non-premixed (diffusion) flames** [14].

1.4.1 Premixed flames

In this case the fuel and oxidizer are thoroughly mixed before combustion begins. The mixture is homogenous, meaning the fuel and oxidizer are uniformly distributed. The flame front (combustion zone) propagates through the premixed fuel-oxidizer mixture. The reaction occurs at the flame front, where the mixture reaches the ignition temperature. The flame speed depends on the fuel oxidizer ratio, temperature and pressure. The flame structure is thin, well defined flame front that separates the unburnt mixture from the burnt products. The flame front is often blue in color due to complete combustion. They are used in internal gasoline engines (gasoline engines) and industrial burners. Below are images of a Premixed Flame in different flow conditions. [15]

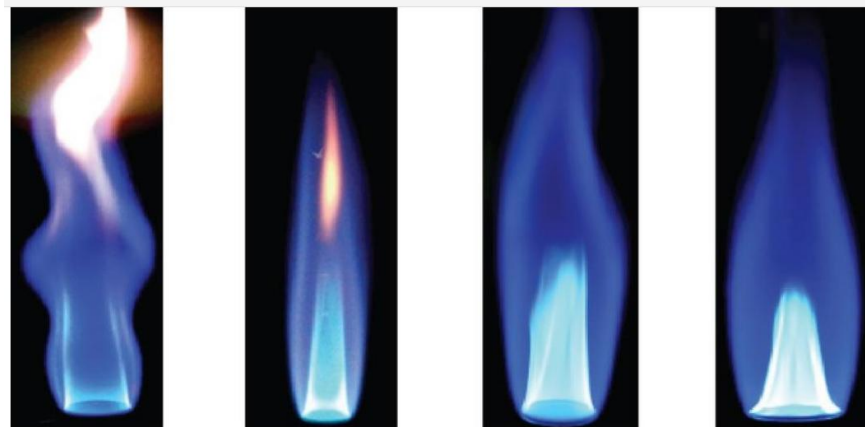


Figure 3 Snapshots of premixed flame at different flow conditions [16]

1.4.2 Non-Premixed Flames (Diffusion Flames)

In non-premixed flames the fuel and oxidizer are not mixed before combustion. Instead, they mix at the point of combustion through diffusion. This is the type of flame in my study. The flame is sustained by the continuous supply of the fuel and oxidizer. The flame is located at the interface where the fuel and

Literature review and Generalities of combustion

oxidizer meet. The combustion rate is controlled by the rate of diffusion of fuel and oxidizer. The flame is often yellow or orange due to the presence of soot particles. The flame structure is thicker and less defined compared to premixed flames. The flame has distinct zones: a fuel-rich core, a diffusion zone, and an outer oxidizer-rich zone. They are used in Diesel engines, rocket and jet engines (in some designs). Below are images of a Non-Premixed Flame in different flow conditions. [15]

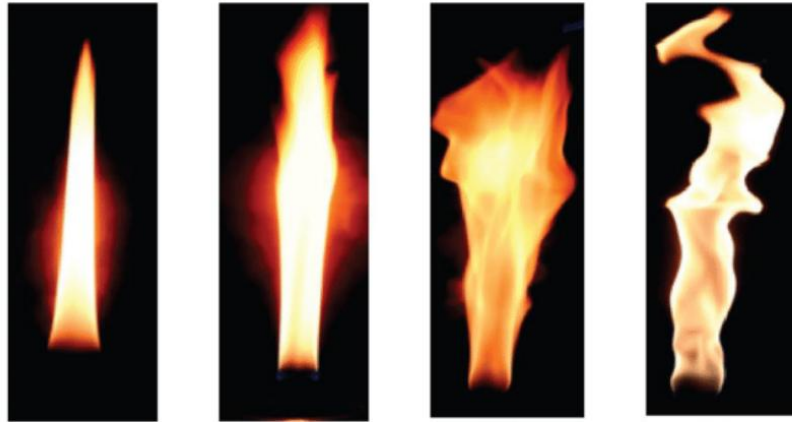


Figure 4 Snapshots of Non-Premixed Flame at different flow conditions [16]

Table 1-1 Differences between Premixed and Non-premixed flames

Aspect	Premixed Flames	Non-Premixed Flames
Fuel-oxidizer Mixing	Mixed before combustion	Mixed during combustion (diffusion)
Flame Speed	Controlled by chemical kinetics	Controlled by diffusion rate
Flame Color	Blue(complete combustion)	Yellow/orange(soot formation)
Efficiency	Higher	Lower
Emissions	Lower soot and pollutants	Higher soot and pollutants
Safety	Risk of flashback/explosion	Safer(no premixing)

On the other hand, combustion can be further subdivided based on how the reaction happens. This can either be; Rapid, Spontaneous or Explosive. **Rapid combustion** requires external heat energy to start. This reaction results in enormous amounts of light and heat energy. As the name suggests this type of combustion occurs rapidly. It is mostly used in engines that undergo internal combustion. **Spontaneous**

Literature review and Generalities of combustion

combustion doesn't require any external energy to start the combustion process. This combustion starts at room temperature itself due to self-heating. This kind of reaction mostly happens in substances which have less ignition temperatures. **Explosive combustion** happens very rapidly releasing enormous amounts of heat, light and sound energy. During this combustion, gases that are released will spread quickly resulting in sound energy. This combustion happens when some energy ignites the substance and heat, light, sound energies release immediately for example burning fire crackers. [14]

Combustion can also be categorized depending on the percentage of fuel and oxidizer that is involved in the combustion reaction. That is, **complete** or **incomplete combustion**:

1.4.3 Complete combustion

This occurs when a fuel burns in the presence sufficient oxygen to produce carbon dioxide (CO₂) and water (H₂O) as the primary products. The conditions for complete combustion is high temperature and sufficient oxygen. This is the most efficient type of combustion and produces the most heat [16].

Example for methane (CH₄):



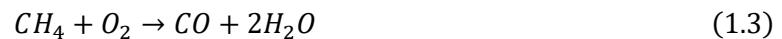
1.4.4 Incomplete combustion

This occurs where there is not enough oxygen present to completely react with all of the fuel. This can produce carbon monoxide (CO), which is a poisonous gas or carbon (C). It is less efficient and produces less heat. [16]

Example for methane (CH₄):



Or



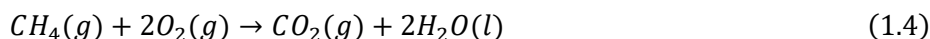
1.5 Thermodynamics of combustion(ΔH_C°)

Thermodynamics of combustion involves the study of energy changes and heat transfer during the chemical reactions that occur when a fuel burns in the presence of an oxidizer, typically oxygen. Here are some key concepts and principles related to the thermodynamics of combustion:

1.5.1 Enthalpy of combustion

Enthalpy of combustion represents the amount of heat energy released when one mole of a substance undergoes complete combustion with oxygen under standard conditions (typically 25°C or 298 K and 1 atm pressure). The enthalpy of combustion is usually expressed in units of **kJ/mol**.

Combustion reactions are exothermic, meaning they release heat. Therefore, the enthalpy is always negative ($\Delta H_C^\circ < 0$). The enthalpy of combustion is associated with a balanced chemical equation. For example, the combustion of methane (CH_4):



Here,

$$\Delta H_C^\circ = -890 \text{ kJ/mol} \quad (1.5)$$

The enthalpy of combustion is used to: Calculate the energy content of fuels, design and optimize combustion systems and compare the efficiency of different fuels. The enthalpy of combustion can be calculated using **Hess's Law** or **standard enthalpies of formation** (ΔH_f)

Using Hess's Law:

Hess's Law states that the total enthalpy change for a reaction is the same, regardless of the number of steps. For combustion, the enthalpy change can be calculated as:

$$\Delta H_C = \sum \Delta H_f(\text{products}) - \sum \Delta H_f(\text{reactants}) \quad (1.6)$$

Table 1-2 Enthalpy of combustion for common fuels [17]

FUEL	CHEMICAL FORMULA	ENTHALPY OF COMBUSTION(KJ/MOL)
METHANE	CH ₄	-890
ETHANE	C ₂ H ₆	-1560
PROPANE	C ₃ H ₈	-2220
BUTANE	C ₄ H ₁₀	-2877
OCTANE (GASOLINE)	C ₈ H ₁₈	-5471
HYDROGEN	H ₂	-286
CARBON (GRAPHITE)	C	-393.5

Practical applications of enthalpy of combustion;

1. Helps determine the energy content of fuels, which is critical for **evaluating their efficiency**.
2. Understanding the enthalpy of combustion helps in designing cleaner combustion processes to minimize pollutants.
3. It is used to calculate heat outputs of fuels used in heating systems.

1.5.2 Heat of reaction and adiabatic temperature

They are important concepts, particularly in the study of chemical reactions and their energy changes.

1.5.2.1 Heat of reaction (ΔH)

Also known as **enthalpy change of reaction (ΔH)**, is the amount of heat absorbed or released during a chemical reaction at constant pressure. It is a measure of the energy change associated with the reaction;

- **Exothermic reaction:** If heat is released during the reaction, ΔH is negative ($\Delta H < 0$)
- **Endothermic reaction:** If heat is absorbed during the reaction, ΔH is positive ($\Delta H > 0$)

The heat of reaction depends on the **stoichiometry of the reaction**, **physical states of the reactants** and **products**, **temperature** and **pressure conditions**.

1.5.2.2 Adiabatic Temperature

It is the temperature change that occurs in a system when a chemical reaction takes place under adiabatic conditions. It is the maximum temperature achievable for a given reaction, assuming no heat loss.

For exothermic reactions, the adiabatic temperature rise is significant because the heat released by the reaction increases the temperature of the system. For endothermic reactions, the adiabatic temperature decreases because heat is absorbed from the system. The adiabatic temperature rise (ΔT) can be calculated using the formula:

$$\Delta T = \frac{\Delta H}{C_p} \quad (1.7)$$

Where:

ΔH –Heat of reaction

C_p –Heat capacity of the system

The heat of reaction (ΔH) determines the amount of energy available to change the temperature of the system. Under adiabatic conditions, all the energy from the reaction is used to change the temperature of the system, leading to the adiabatic temperature rise or fall.

1.5.3 Stoichiometry and equivalence ratio

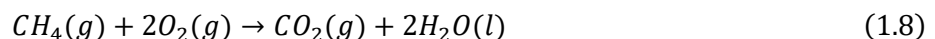
They are best in analyzing chemical reactions and fuel-air mixtures. Here is a detailed explanation for both:

1.5.3.1 Stoichiometry

It refers to the quantitative relationship between reactants and products in a chemical reaction. It is based on the **law of conservation of mass** and the **balanced chemical equation**. A **stoichiometric mixture** is one where the reactants are present in the exact proportions required for complete combustion or reaction, with no excess of either reactant. For combustion reaction this means that the fuel and oxidizer are in the perfect ratio to fully convert all fuel into products.

Example: combustion of methane (CH_4)

The balanced stoichiometric equation for the combustion of methane is:



1 mole of CH_4 reacts with 2 moles of O_2 to produce 1 mole of CO_2 and 2 moles of H_2O . This is the stoichiometric ratio for this reaction. [18]

1.5.3.2 Equivalence ratio (Φ)

It is a dimensionless parameter used to describe the composition of a fuel-air mixture relative to the stoichiometric mixture. It is defined as:

$$\Phi = \frac{\text{Actual fuel} - \text{to} - \text{air ratio}}{\text{Stiochiometric fuel} - \text{to} - \text{air ratio}} \quad (1.9)$$

- $\Phi = 1$: Stoichiometric mixture (perfect balance of fuel and air)
- $\Phi > 1$: Rich mixture (excess fuel, not enough air)
- $\Phi < 1$: Lean mixture (excess air, not enough fuel)

In combustion the equivalence ratio determines the efficiency and emission of the process. For complete combustion, $\Phi = 1$ is ideal, but in practice, slightly lean mixture ($\Phi < 1$) are often used to minimize emissions of unburnt hydrocarbons and CO.

Stoichiometry provides the theoretical basis for the ideal ratio of reactants. The equivalence ratio compares the actual mixture to the ideal ratio. [18]

1.5.4 First and second laws of thermodynamics in combustion

1.5.4.1 First Law of Thermodynamics in combustion

The first law of thermodynamics states that energy cannot be created or destroyed, only transformed from one form to another. The energy released during combustion is a result of the conversion of chemical energy into thermal energy. The first law ensures that the total energy before and after the combustion process remains constant, accounting for heat, work and changes in internal energy. The heat released during combustion is often measured as the **enthalpy of combustion** (ΔH). The energy released is used to perform work (e.g., in engines) or transferred as heat.

The first law is crucial in designing engines, turbines and power plants, where maximizing energy efficiency is key. It helps calculate the heat transfer and work output in combustion systems.

1.5.4.2 Second law of thermodynamics in combustion

The Second Law of Thermodynamics introduces the concept of **entropy** [18] and states that energy transformations are never a hundred percent efficient. Combustion is an **irreversible process**, meaning it always generates entropy. The Second Law explains why not all the heat released during combustion can be converted into useful work. Some energy is always lost as waste heat.

The **Carnot efficiency** (derived from the Second Law) sets the maximum possible efficiency for heat engines. In practical combustion systems efficiency is limited by factors such as heat loss, friction, and incomplete combustion. The Second Law also governs the **spontaneity of combustion reactions**. For a reaction to occur spontaneously, the total entropy of the system and surroundings must increase. Combustion reactions are exothermic and result in a significant increase in entropy due to the production of gases.

The Second Law is used to analyze and improve the efficiency of combustion systems, such as reducing waste heat and optimizing fuel usage. It also helps in understanding the environmental impact of combustion, such as the generation of pollutants and greenhouse gases.

1.6 Chemical Kinetics of Combustion

It deals with the study of the rates and mechanisms of chemical reactions involved in combustion processes. It focuses on how reactants transform into products and the factors that influence these reactions. Here is a detailed explanation based on the principles of chemical kinetics in combustion:

1.6.1 Reaction mechanisms and elementary reactions

1.6.1.1 Reaction mechanisms

A reaction mechanism is a step by step sequence of elementary reactions that describe how reactions are transformed into products. In combustion, reaction mechanisms are often complex and involve multiple steps.

Each step in the mechanism is an elementary reaction, which represents a single molecular event. Short lived species (e.g., radicals like H, O, OH) are formed and consumed during the reaction. These **intermediates** are not present in the overall reaction equation but play a crucial role in the mechanism. Combustion mechanisms often involve **chain reactions**, where radicals propagate the reaction by reacting with stable molecules to produce more radicals. [19]

Example: Hydrogen Combustion Mechanism

Literature review and Generalities of combustion

The combustion of hydrogen (H_2) involves the following elementary steps

a) **Initiation:**



b) **Propagation:**



c) **Termination:**



1.6.1.2 Elementary reactions

It is a single step reaction that occurs exactly as written. It represents the simplest possible reaction process, involving the direct interaction of reactant molecules or atoms. Some of the major characteristics of elementary reactions include: **molecularity**, which is the number of molecules or atoms involved in the reaction. For example: **unimolecular** (a singular decomposes or rearranges), **bimolecular** (two molecules collide and react) and **termolecular** (three molecules or atoms collide and react-rare but possible in combustion).

The rate of an elementary reaction is determined by its stoichiometry. For example: for a bimolecular reaction: $A + B \rightarrow C$, the rate is:

$$Rate = k[A][B] \quad (1.14)$$

Where k is the rate constant, and $[A]$ and $[B]$ are the concentrations of the reactants.

Each elementary reaction has a specific **activation energy** (E_a), which is the minimum energy required for the reaction to occur. This is described by the **Arrhenius equation**:

$$k = Ae^{-\frac{E_a}{RT}} \quad (1.15)$$

Where:

k = rate constant

A = pre-exponential factor

R = universal gas constant

T = temperature

Radicals are highly reactive species that play a central role in combustion mechanisms. They are formed during the initiation step and propagate the reaction by reacting with stable molecules. For example: the hydroxyl radical (OH) is a key intermediate in many combustion reactions, as it reacts with fuel molecules to produce water and additional radicals. [19]

1.6.2 Arrhenius equation and activation energy

1.6.2.1 Arrhenius equation

It is an equation that describes the temperature dependence of reaction rates. It is given by:

$$k = Ae^{-\frac{E_a}{RT}} \quad (1.15)$$

As discussed previously.

The equation shows that as temperature increases, the rate constant k increases exponentially, leading to faster reaction rates. [20]

1.6.2.2 Activation energy (E_a)

It is the minimum energy required for reactant molecules to collide and form products. It represents the energy barrier that must be overcome for a reaction to proceed.

Reactions with high activation energies are slower because fewer molecules have sufficient energy to overcome the barrier. Catalysts lower the activation energy, increasing the reaction rates without being consumed. [20]

Graphical representation

The Arrhenius equation can be linearized for easier analysis:

$$\ln(k) = \ln(A) - \frac{E_a}{R} \cdot \frac{1}{T} \quad (1.16)$$

Plotting $\ln(k)$ vs. $\frac{1}{T}$ gives a straight line with:

$$\text{Slope} = -\frac{E_a}{R}$$

$$\text{Y-intercept} = \ln(A)$$

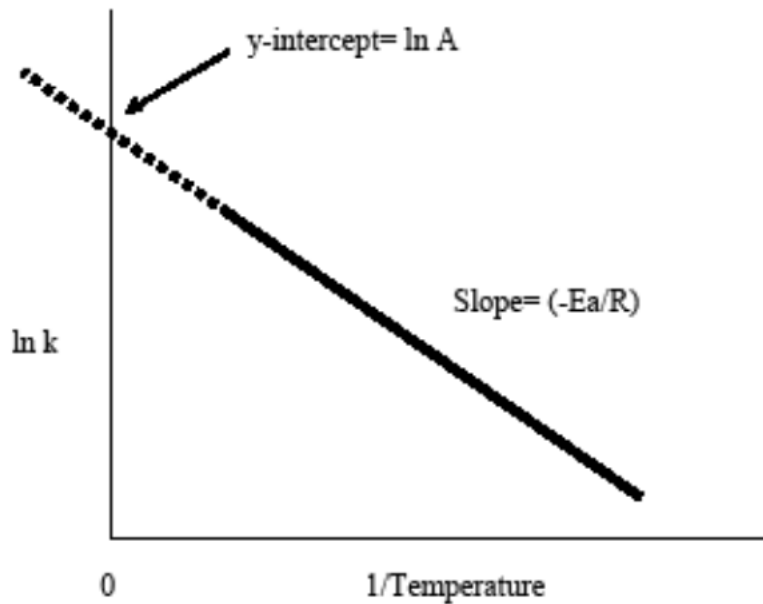


Figure 5 Arrhenius plot [20]

This plot is called an **Arrhenius plot** and is used to determine E_a and A experimentally.

The Arrhenius equation is widely used in chemical kinetics to predict reaction rates at different temperatures. It helps in understanding the effect of temperature in reaction mechanisms and designing industrial processes. [20]

1.6.3 Autoignition and ignition delay

1.6.3.1 Autoignition

It refers to the spontaneous ignition of a combustible material without an external ignition source. It occurs when a material reaches its **autoignition temperature (AIT)**, at which the material reacts with air and ignites.

At high temperatures, fuel molecules break down into radicals. These radicals react with oxygen to release heat and accelerating the reaction until ignition occurs. Autoignition is influenced by different factors which include: **Fuel composition, pressure, oxygen concentration and heat transfer**. Autoignition is applied in internal combustion engines. [22]

1.6.3.2 Ignition delay

It is the time interval between the introduction of combustible mixture and the onset of ignition. **Physical delay** is the time required for fuel to vaporize and mix with air, while **chemical delay** is the time required for the chemical reaction to initiate and produce enough radicals for ignition. Factors affecting ignition delays include: **temperature, pressure, fuel properties and air-fuel ratios**.

Ignition delay is often measures in milliseconds (ms) in engine experiments using pressure sensors or optical diagnosis. Shorter ignition delays improve engine efficiency and reduces emissions. [23]

1.7 Combustion Equilibrium

It refers to the state at which the chemical reactions involved in combustion reach a balance between the reactants and products. At equilibrium, the forward and reverse reaction occur at the same rate, and the concentration of the reactants and products remain constant over time. This concept is important in understanding efficiency and outcomes of combustion processes.

1.7.1 Equilibrium composition of combustion products

The equilibrium composition of combustion products is a critical aspect of combustion science, as it determines the final chemical species present after a chemical reaction reaches thermodynamics equilibrium. This composition depends on factors such as **temperature, pressure, reactant concentrations and stoichiometry of the reaction**. It is essential for optimizing combustion processes in applications like energy production, transportation and industrial manufacturing.

Literature review and Generalities of combustion

At equilibrium, the chemical species in a combustion reaction reach a state where their concentrations no longer change over time. This state is governed by the principles of thermodynamics, particularly the minimization of Gibbs free energy and the maximization of entropy. The equilibrium composition is influenced by the temperature, pressure and initial concentrations of the reactants. For example, high temperatures can cause the dissociation of products like CO₂ and H₂O into smaller molecules such as CO, H₂, O₂ and OH.

Different types of combustion have a different type of impact on equilibrium. Complete combustion results to CO₂ and H₂O under ideal conditions. Incomplete combustion on the other hand results to CO, H₂ and unburnt hydrocarbons. High temperature dissociation even in complete combustion results to the dissociation of CO₂ and H₂O. This alters the equilibrium composition. [14]

Calculation methods

Gibbs Free Energy Minimization

The equilibrium composition is determined by minimizing the Gibbs free energy of the system. This method ensures that the system reaches the most stable state under given conditions. [14]

The Gibbs free energy minimization approach is widely used in computational tools like NASA's Chemical Equilibrium with Applications (CEA) program.

Equilibrium constant (K)

The equilibrium constant relates the concentration of reactants and products at equilibrium. For a generic reaction $aA + bB \leftrightarrow cC + dD$, the equilibrium constant is given by

$$K_P = \frac{(P_C)^c (P_D)^d}{(P_A)^a (P_B)^b} \quad (1.17)$$

Where P_i is the partial pressure of species i

For simple systems, equilibrium constants can be used to relate the concentrations of reactants and products. [14]

1.7.2 Gibbs free energy minimization

Gibbs free energy is a thermodynamic potential that combines enthalpy (H), entropy (S), and temperature (T) to predict whether a process will occur spontaneously. It is defined by the equation:

$$G = H - TS \quad (1.18)$$

For a process to be spontaneous at constant temperature and pressure, the change in Gibbs free energy (ΔG) must be negative.

At equilibrium, a system reaches a state where the Gibbs free energy is minimized. This is a fundamental principle in thermodynamics. For a reaction or process, the condition for equilibrium is:

$$\Delta G = 0 \quad (1.19)$$

At this point, the system can no longer perform useful work, and the forward and reverse processes occur at the same rate.

The minimization of Gibbs free energy can be expressed mathematically by taking the derivative of G with respect to the extent of the reaction (ξ) and setting it to zero:

$$\frac{dG}{d\xi} = 0 \quad (1.20)$$

This condition ensures that the system is at equilibrium and no further change in Gibbs free energy occurs. [14]

1.7.3 Water-Gas Shift and Dissociation Reactions:

The **water-gas shift reaction (WGSR)** and **dissociation reactions** are critical processes in chemistry and chemical engineering, with significant applications in energy production, hydrogen generation, and industrial catalysis. Below is a cohesive explanation of these reactions, their mechanisms, and their importance.

1.7.3.1 Water-Gas Shift Reaction (WGSR)

The water-gas shift reaction is a chemical process in which carbon monoxide (CO) reacts with water vapor (H₂O) to produce carbon dioxide (CO₂) and hydrogen gas (H₂). This reaction is exothermic and is widely used in industrial applications, particularly in hydrogen production and syngas processing.

Reaction Equation:



The WGSR is a key step in ammonia production, where hydrogen is a primary feedstock. It is used in fuel cell technology to purify hydrogen gas. In syngas processing, the reaction helps adjust the CO/H₂ ratio for downstream processes like Fischer-Tropsch synthesis.

Common catalysts include iron oxide (Fe₂O₃), copper-zinc oxide (Cu-ZnO), and noble metals like platinum (Pt) and palladium (Pd). The choice of catalyst depends on the operating temperature and desired reaction kinetics.

The reaction is exothermic, meaning it releases heat. Lower temperatures favor higher conversion of CO to CO₂ and H₂. The equilibrium constant decreases with increasing temperature, making temperature control crucial for optimal performance.

The reaction rate is influenced by factors such as temperature, pressure, and catalyst activity. High-surface-area catalysts are often used to enhance reaction efficiency. [14]

1.7.3.2 Dissociation Reactions

Dissociation reactions involve the breaking of chemical bonds in a molecule, resulting in the formation of smaller molecules, ions, or radicals. These reactions are typically endothermic and require energy input, such as heat, electricity, or light.

Dissociation reactions are essential in electrolysis, where water is split into hydrogen and oxygen using electricity. They play a role in combustion processes, where hydrocarbons dissociate into smaller fragments before oxidation. In chemical synthesis, dissociation reactions are used to generate reactive intermediates.

Dissociation reactions require significant energy input to break strong chemical bonds. For example, the dissociation of water into hydrogen and oxygen has a high activation energy, making it energy-intensive.

Catalysts can lower the activation energy required for dissociation, making the process more efficient. In water splitting, catalysts like titanium dioxide (TiO₂) and platinum (Pt) are commonly used. [14]

1.7.4 Effects of pressure and temperature on equilibrium

Chemical equilibrium is a dynamic state where the rates of the forward and reverse reactions are equal, and the concentrations of reactants and products remain constant over time. The position of

Literature review and Generalities of combustion

equilibrium is influenced by external factors such as **pressure** and **temperature**, as described by **Le Chatelier's principle** and thermodynamic principles.

1.7.4.1 Effect of Temperature on Equilibrium

Temperature has a significant impact on the position of equilibrium because it affects the equilibrium constant (K). The relationship between temperature and equilibrium is governed by the **van 't Hoff equation**:

$$\ln\left(\frac{K_2}{K_1}\right) = -\frac{\Delta H^\circ}{R}\left(\frac{1}{T_2} - \frac{1}{T_1}\right) \quad (1.22)$$

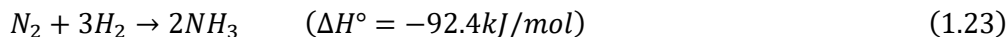
Where:

- K_1 and K_2 are the equilibrium constants at temperatures T_1 and T_2 , respectively.
- ΔH° is the standard enthalpy change of the reaction.
- R is the universal gas constant.

-Exothermic Reactions ($\Delta H^\circ < 0$): Increasing the temperature shifts the equilibrium toward the reactants, as the system absorbs excess heat by favoring the reverse reaction.

-Endothermic Reactions ($\Delta H^\circ > 0$): Increasing the temperature shifts the equilibrium toward the products, as the system uses the added heat to favor the forward reaction.

For example, in the synthesis of ammonia (an exothermic reaction):



Increasing the temperature shifts the equilibrium toward the reactants N_2 and H_2 , reducing the yield of NH_3 . [24]

1.7.4.2 Effect of Pressure on Equilibrium

Pressure affects equilibrium when the reaction involves gaseous species. According to **Le Chatelier's principle**, a change in pressure causes the system to shift in a way that counteracts the change.

Literature review and Generalities of combustion

- **Increasing Pressure:** The equilibrium shifts toward the side with fewer moles of gas to reduce the pressure.

- **Decreasing Pressure:** The equilibrium shifts toward the side with more moles of gas to increase the pressure.

For example, in the synthesis of ammonia:



The left side has 4 moles of gas $N_2 + 3H_2$, while the right side has 2 moles of gas $2NH_3$. Increasing the pressure shifts the equilibrium toward the products $2NH_3$, increasing the yield of ammonia.

In industrial processes, both pressure and temperature are carefully controlled to optimize the yield of desired products. For example: In the **Haber process** for ammonia synthesis, high pressure (200–300 atm) and moderate temperature (400–500°C) are used to maximize NH_3 production while balancing energy costs and reaction rates. In **water-gas shift reactions**, lower temperatures favor higher conversion of CO to CO_2 and H_2 , while pressure adjustments are used to optimize gas-phase equilibria.

The position of equilibrium is also influenced by thermodynamic properties such as **Gibbs free energy** (ΔG), **enthalpy** (ΔH) and **entropy** (ΔS). The relationship between these properties is given by:

$$\Delta G = \Delta H - \Delta S \quad (1.25)$$

At equilibrium, $\Delta G = 0$ and the equilibrium constant (K) is related to ΔG° by:

$$\Delta G^\circ = -\frac{RT}{\ln K} \quad (1.26)$$

This relationship highlights how temperature directly affects the equilibrium constant. [14]

1.8 Flame Characteristics

Flames are the visible, gaseous result of combustion, a chemical reaction between a fuel and an oxidant (typically oxygen) that releases heat and light. They are characterized by their structure,

temperature, color, speed, stability, and emissions. Flames can be categorized as **premixed** (fuel and oxidant mixed before combustion, like in a Bunsen burner) or **diffusion flames** (fuel and oxidant mix at the flame front, like in a candle). Flame temperature varies with fuel type and combustion efficiency, with blue flames indicating hotter, complete combustion and yellow/orange flames signaling cooler, incomplete combustion. Flame speed, the rate at which the flame front propagates, depends on factors like fuel reactivity and turbulence, while flame stability is influenced by air-fuel mixing and heat loss. Emissions from flames include carbon dioxide, water vapor, and, in incomplete combustion, carbon monoxide and soot. Understanding flame characteristics is crucial in applications such as combustion engineering, fire safety, and environmental science, where optimizing flame behavior can improve efficiency, reduce emissions, and enhance safety. Flames represent a complex interplay of chemistry, physics, and fluid dynamics, making their study essential for advancements in energy, safety, and environmental protection.

1.8.1 Flame speed and flame structure

Flame speed and flame structure are fundamental aspects of combustion physics, playing a critical role in understanding how flames propagate and behave under different conditions. These concepts are essential for applications in combustion engineering, fire safety, and environmental science.

1.8.1.1 Flame Speed

Flame speed, also known as **flame propagation velocity**, refers to the rate at which a flame front moves through a combustible mixture. It is a key parameter in characterizing combustion processes and is influenced by several factors. Flame speed is the velocity at which the flame front propagates relative to the unburned gas mixture. It is typically measured in meters per second (m/s).

Factors Affecting Flame Speed:

- **Fuel Type:** Different fuels have varying reactivity, which affects how quickly the flame propagates. For example, hydrogen has a higher flame speed compared to methane.
- **Mixture Composition:** The ratio of fuel to oxidant (air) plays a significant role. Stoichiometric mixtures (ideal fuel-to-air ratio) generally result in the highest flame speeds.
- **Temperature and Pressure:** Higher temperatures and pressures can increase flame speed by enhancing reaction rates.
- **Turbulence:** Turbulent flows can increase flame speed by enhancing mixing and heat transfer.

Literature review and Generalities of combustion

In internal combustion engines, controlling flame speed is crucial for optimizing efficiency and reducing emissions. In fire safety, understanding flame speed helps predict the spread of fires and design effective suppression systems. [25]

1.8.1.2 Flame Structure

Flame structure refers to the spatial arrangement of different zones within a flame, each characterized by distinct physical and chemical processes. The structure of a flame depends on whether it is a **premixed flame** or a **diffusion flame**.

1. Premixed Flames:

In premixed flames, the fuel and oxidant are mixed before combustion occurs (e.g., Bunsen burner flames).

Zones in a Premixed Flame:

Preheat Zone: The unburned mixture is heated by conduction and radiation from the reaction zone.

Reaction Zone: Chemical reactions occur, releasing heat and light. This is the visible part of the flame.

Post-Flame Zone: The burned gases cool down as they move away from the reaction zone. [25]

2. Diffusion Flames:

In diffusion flames, the fuel and oxidant mix at the flame front (e.g., candle flames). These flames lack a distinct preheat zone and often produce soot due to incomplete combustion. The flame structure is less defined, with fuel and oxidant diffusing into each other at the flame front.

Factors Affecting Flame Structure:

Flow Dynamics: Laminar flows produce smooth, well-defined flames, while turbulent flows create irregular, flickering flames.

Heat Loss: Heat loss to the surroundings can alter the flame structure, particularly in smaller flames.

Fuel Properties: The chemical composition of the fuel influences the flame's appearance and structure. [25]

1.8.2 Laminar and Turbulent flames

Laminar flames propagate smoothly and are primarily governed by molecular diffusion and chemical kinetics. These flames are stable under controlled conditions and are often studied in laboratory

settings. Turbulent flames, on the other hand, are characterized by chaotic flow structures that enhance mixing and increase flame speed. Turbulence is common in practical combustion systems such as engines and gas turbines, where it improves combustion efficiency but can also lead to instabilities. [26]

1.8.3 Quenching Distance and Flammability Limits

Quenching distance is the minimum gap size through which a flame cannot propagate due to excessive heat loss to the surroundings. This phenomenon is critical in designing combustion chambers to prevent flame extinction. Flammability limits define the range of fuel-air mixtures that can sustain combustion. The lower the flammability limit (LFL) is the minimum fuel concentration required, while the upper flammability limit (UFL) is the maximum concentration beyond which the mixture is too rich to burn. These limits vary with temperature, pressure, and fuel type. [27]

1.8.4 Detonation and Deflagration

Deflagration refers to subsonic flame propagation driven by heat and mass diffusion, typical in most combustion systems. Detonation is a supersonic combustion wave involving a shock front that compresses and ignites the mixture. Detonations produce extremely high pressure and temperatures, making them destructive in accidental scenarios but useful on propulsion systems like pulse detonation engines. [28]

1.9 Pollutants Formation in Combustion

Combustion processes release energy by burning fuels, but they also produce harmful pollutants due to incomplete combustion or high-temperature reactions. Major pollutants include: CO, NO_x, Sulphur oxides, particulate matter, volatile organic compounds and hydrocarbons and Carbon dioxide.

Pollutant formation depends on factors such as fuel composition, combustion temperature, oxygen availability and residence time. Emission control technologies help reduce these pollutants.

Carbon monoxide (CO) forms due to incomplete combustion, particularly in fuel-rich conditions, where insufficient oxygen is present. CO₂ is the primary product of complete combustion but contributes to greenhouse gas emissions. Unburned hydrocarbons result from poor mixing, low temperatures, or flame quenching. These pollutants are regulated due to their environmental and health impacts [23]

Nitrogen oxides form through thermal, prompt and fuel-bound mechanisms, with thermal NO_x being dominant at high temperatures. Sulphur oxides originate from sulfur-containing fuels such as coal and heavy oils, leading to acid rain. Emission control technologies include selective catalytic reduction (SCR) in NO_x and flue gas desulfurization (FDG) for SO_x [29]

Literature review and Generalities of combustion

Soot comprises of carbonaceous particles formed in fuel-rich regions of a flame. The process involves nucleation, surface growth and agglomeration. **Particulate matter** poses health risks and is controlled using diesel particulate filters (DPFs) and improved combustion strategies [30]

Methods to reduce emissions include lean combustion, exhaust gas recirculation (EGR), and alternative fuels like hydrogen. Catalytic converters and after treatment systems further minimize pollutants in automotive and industrial applications [31]

1.10 Combustion of Different Fuels

Combustion is a fundamental chemical process in which a fuel reacts with an oxidant to release energy in form of heat and light. This exothermic reaction is important in various applications. The efficiency, environmental impact and performance depend heavily on the type of fuel used, its chemical composition and the conditions under which combustion occurs.

Understanding the combustion behavior of different fuel is essential for optimizing energy efficiency, reducing pollutant emissions and developing sustainable alternative to conventional fossil fuels. This discussion explores the combustion mechanisms, advantages, and challenges associated with various fuels, providing insights into their role in modern energy systems.

The following are combustions of different fuels

For **hydrocarbon combustion** like methane combustion is widely studied due to its use in natural gas systems, producing primarily CO₂ and water. Gasoline engines rely on premixed flames, while diesel engines use diffusion flames with higher soot emissions. The cetane and octane numbers rate fuel ignition quality [23].

Hydrogen burns cleanly, producing only water, but has high flame speeds and a wide flammability range, posing safety challenges. It is promising for zero-emission energy systems [26]. **Biofuels** like ethanol and biodiesel reduce carbon footprints but they may have lower energy density. **Synthetic fuels** are produced via renewable energy, offering compatibility with existing engines [32]

Solid fuel combustion like the combustion of coal involves devolatilization and char oxidation, producing ash and SO_x. Biomass combustion is carbon-neutral but requires efficient gasification to minimize emission [14]

1.11 Methane and hydrogen combustion

Methane and hydrogen are commonly researched fuels due to their efficient combustion and lower environmental impact. Hydrogen combustion produces only water vapor, while burning methane results mainly in carbon dioxide and water vapor, making both fuels cleaner alternatives to conventional fossil fuels.

Methane flames can form in different ways, most notably as laminar or turbulent flames. Laminar flames feature smooth and steady flame fronts with relatively slow flame speeds. On the other hand, turbulent flames display chaotic, wrinkled flame fronts and burn more rapidly. Several factors affect how methane flames develop and spread, including the ratio of fuel to air, surrounding temperature and pressure, and the velocity of the fuel-air mixture.

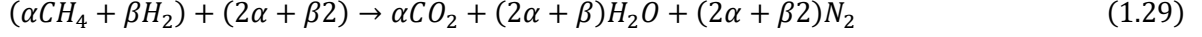
Researchers have explored the effects of adding hydrogen to methane/air flames as a way to enhance combustion performance and lower emissions. Findings indicate that hydrogen enrichment can significantly alter flame structure and propagation behavior. Specifically, hydrogen addition tends to increase flame speed, broaden the flammability range, and lower the lean flammability limit. These changes contribute to improved combustion stability. Since hydrogen burns more efficiently than methane, incorporating it into the fuel mixture can also lead to greater overall combustion efficiency.

1.11.1 Combustion Chemistry of Methane and Hydrogen

The combustion of methane and hydrogen occurs when each fuel reacts with oxygen (O_2) in the presence of heat, resulting in the formation of carbon dioxide (CO_2), water vapor (H_2O), and the release of energy. These chemical reactions can be expressed with the following balanced equations [33] [34]:



The general Methane/Hydrogen combustion equation is written as [35]:



The burning of methane and hydrogen is an exothermic process, meaning it gives off heat. The heat produced during this reaction depends on how much fuel is used and can be determined using the heat of combustion formula [36]:

$$\Delta H_{combustion} = \sum n \Delta H_{f(products)} - \sum m \Delta H_{f(reactants)} \quad (1.30)$$

1.12 Conclusion

This chapter has systematically examined the fundamental aspects of combustion, with particular emphasis on methane-hydrogen mixtures. The literature review revealed that hydrogen enrichment significantly enhances combustion characteristics by increasing flame speed, extending flammability limits, and improving thermal efficiency, though it concomitantly elevates NO_x emissions. These findings underscore the need for careful optimization of hydrogen blending ratios and combustion parameters.

The theoretical framework established herein - encompassing thermodynamic principles, chemical kinetics, flame propagation mechanisms, and emission formation pathways - provides a robust foundation for subsequent numerical investigations. The comparative analysis of methane and hydrogen combustion characteristics highlights the trade-offs between performance and environmental impact, offering critical insights for cleaner combustion system design.

These comprehensive discussions set the stage for the following computational study, which will employ the established theoretical principles to analyze flame behavior and stability under various hydrogen enrichment conditions. The integration of fundamental combustion theory with advanced numerical methods promises to yield practical solutions for optimizing hydrogen-methane combustion systems, contributing to the development of more efficient and sustainable energy technologies.

This chapter thus serves as both a theoretical reference and a methodological bridge to the forthcoming computational analysis, ensuring a rigorous, science-based approach to addressing contemporary combustion challenges.

Literature review and Generalities of combustion

To gain a comprehensive understanding of our research, it is essential to delve into the fundamental governing equations and the role of turbulence, which significantly influences the combustion process. These aspects will be addressed in detail in the following chapter.

Chapter 2:

Mathematical modeling

Summary

2.1	Introduction.....	34
2.2	The Fundamental Equations of Fluid Dynamics	35
2.3	Turbulence Modeling.....	40
2.4	Reaction Rate.....	43
2.5	Numerical Discretization	45
2.6	Conclusion	46

Chapter 02 Mathematical Modeling

2.1 Introduction

The objective of this study is to analyze the methane-air combustion in global reactions and detailed chemical reaction mechanisms. The effect of hydrogen addition on methane/air flames. The boundaries of the simulation include the reactor geometry, boundary conditions, and initial conditions. The reactor geometry consists of a 2D combustion chamber with a centrally located fuel inlet and air inlet. The boundary conditions are defined as follows: the air inlet mass flow rate, the temperature and pressure at the inlet, and the concentration of each species in the inlet stream. The initial conditions are the temperature, pressure, and concentration of species at the start of the simulation.

Assumptions:

1. The combustion process is assumed to be homogeneous, and it occurs in a well-mixed reactor.
2. The simulation is carried out under steady-state conditions, with a constant fuel flow rate.
3. The effects of radiation and gravity are neglected in the simulations, as they are assumed to be negligible under the conditions considered.
4. The simulations are carried out using the Reynolds-averaged Navier-Stokes (RANS) equations, which assume that the turbulence is statistically steady and can be modeled using a turbulence closure model.
5. The **k- ω SST model** assumes turbulence can be modeled using time-averaged equations, combining the strengths of k- ω near walls and k- ϵ in the free stream, with eddy viscosity and shear stress transport corrections for improved accuracy in separated flows
6. The combustion process is modeled using the eddy dissipation model and eddy dissipation concept.
7. A Reduced chemical mechanism The DRM22 skeletal reaction mechanism, developed by Kazakov and Frenklach, comprising 22 species and 84 reactions, was used to model the methane-air combustion chemistry and a global reaction.
8. The simulations are performed in a 2D domain.

2.2 The Fundamental Equations of Fluid Dynamics

These equations represent the mathematical formulation of three core physical principles that govern fluid dynamics:

- Conservation of mass;
- Conservation of momentum;
- Conservation of energy.

2.2.1 Equation of Continuity

The continuity equation is a core concept in fluid dynamics that represents the conservation of mass in a fluid flow. Originally developed in the 19th century by French mathematician and physicist Augustin-Louis Cauchy, it asserts that the amount of mass entering or exiting a control volume must equal the rate of change of mass inside that volume.

The continuity equation is represented as [44]

$$\frac{\partial \rho}{\partial t} + \nabla \cdot (\rho u) = 0 \quad (2.9)$$

2.2.2 Momentum Equation (Navier-Stokes Equations)

In fluid dynamics, the momentum equation is typically presented in its differential form. This equation connects the acceleration of fluid elements to the effects of pressure gradients, viscous forces, and any external forces acting on the fluid. It is commonly expressed as:

For a Newtonian fluid with constant viscosity [45]

$$\rho \left(\frac{\partial u}{\partial t} + (u \cdot \nabla) u \right) = -\nabla p + \mu \nabla^2 u + \rho g \quad (2.10)$$

In this particular simulation, the Reynolds-Averaged Navier-Stokes (RANS) equations were employed—a widely used method in fluid dynamics where the velocity components (u) are separated into a mean velocity (U) and fluctuating components (u'). [44]

$$\frac{\partial(\rho U)}{\partial t} + \nabla \cdot (\rho U U) = -\nabla p + \nabla \bar{\tau} + \rho g + f \quad (2.11)$$

$-\nabla \cdot (\rho U U)$ represents the divergence of the Reynolds-averaged momentum flux tensor,

With

$$\bar{\tau} = \mu(\nabla u + \nabla \nabla u^T) - \left(\frac{2}{3}\right) \mu(\nabla \cdot u) I \quad (2.12)$$

The symbol $\bar{\tau}$ in the context of the Navier-Stokes or Reynolds-Averaged Navier-Stokes (RANS) equations refers to the **stress tensor**, which describes the viscous forces acting within the fluid. This tensor accounts for internal friction due to fluid viscosity.

Furthermore, the first term on the right-hand side of the equation corresponds to the **deviatoric stress** resulting from the fluid's rate of deformation, while the second term represents the **pressure contribution**, with I denoting the identity tensor.

2.2.3 Energy Equation

The energy equation, also known as the conservation of energy equation, is a key concept in both thermodynamics and fluid dynamics. Rooted in the first law of thermodynamics ($\Delta U = Q - W$), it has been formulated and refined by numerous scientists throughout history.

The equation applied in this simulation is a partial differential equation that is typically solved using numerical methods to simulate heat transfer and energy conservation in different physical systems.

$$\frac{\partial(\rho E)}{\partial t} + \nabla(u(\rho E + p)) = \nabla \cdot \left(k_{eff} \nabla T - \sum_j h_j J_j + (\bar{\tau}_{eff} \cdot u) \right) + S_h \quad (2.13)$$

With:

$$E = h - \frac{p}{\rho} + \frac{u^2}{2} \quad (2.14)$$

$$h = \sum_j Y_j h_j + \frac{p}{\rho} \quad (2.15)$$

$$h_j = \int_{T_{ref}}^T C_{p,j} dt \quad (2.16)$$

Where:

$-k_{eff}$ is the effective conductivity,

$-J_j$ is the diffusion flux of species j,

$-S_h$ includes heat of chemical reactions and other defined heat sources.

2.2.4 Species transport equation

The species transport equation governs the movement and mass conservation of individual chemical species within a fluid system. Its general form can be expressed as:

$$\frac{\partial(\rho Y_i)}{\partial t} + \nabla \cdot (\rho Y_i u) = -\nabla \cdot J_i + R_i + S_i \quad (2.17)$$

$-R_i$ is the net rate production of species.

ANSYS Fluent models mass diffusion J_i in turbulent flows by the equation:

$$J_i = -\left(\rho D_{i,m} + \frac{\mu_t}{Sc_t}\right) \nabla Y_i - D_{T,i} \frac{\nabla T}{T} \quad (2.18)$$

$-Sc_t$ is the turbulent Schmidt number.

2.2.5 The eddy dissipation model (EDM)

Building on Spalding's concept that the reaction rate is governed by the mixing process or the rate of eddy disintegration, Magnussen and Hjertager introduced the eddy dissipation model (EDM), which links the reaction rate to the average mass fraction of the reacting chemical species [13].

$$\tilde{\omega}_{EDM} = A \frac{\tilde{C}}{\tilde{k}} \min \left\{ \tilde{Y}_{fuel}, \frac{1}{r} \tilde{Y}_{O_2}, B \frac{1}{1+r} \tilde{Y}_{pr} \right\} \quad (2.19)$$

Here, r represents the stoichiometric oxygen requirement of the reaction, while \tilde{Y}_{fuel} denotes the mean mass fraction of the fuel. The constants A and B are model parameters that can be adjusted to achieve better agreement with experimental data.

This formulation of the mean reaction rate yields accurate predictions in many practical scenarios where the fast chemistry assumption holds true. However, the EDM is inadequate for modeling flames in which reactions near the burner are governed by chemical kinetics. As a result, incorporating chemical kinetics into the mean reaction rate expression becomes essential. One approach to address this is the series process method proposed by Azevedo, which assumes that the total reaction time can be expressed as the sum of the characteristic time for turbulent mixing, $\tau_{EDM,k}$, and the characteristic time for the chemical reaction, $\tau_{kin,k}$:

$$\tau_{total} = \tau_{EDM,k} + \tau_{kin,k} \quad (2.20)$$

Because the characteristic times are the reciprocal values of the respective reaction rates $\tau = 1/\omega$ for the mean reaction rate can be obtained:

$$\tilde{\omega} = \frac{\tilde{\omega}_{EDM,k}, \tilde{\omega}_{kin,k}}{\tilde{\omega}_{EDM,k} + \tilde{\omega}_{kin,k}} \quad (2.21)$$

In this study, the Eddy Dissipation Model (EDM) was selected due to its suitability for turbulent, non-premixed combustion systems. EDM assumes that the combustion process is governed by the rate of turbulent mixing, with reactions occurring instantaneously upon mixing of reactants. This simplification reduces computational cost significantly while still capturing major trends in flame structure and temperature distribution. However, EDM does not account for detailed chemical kinetics and cannot predict intermediate species or ignition delay phenomena, making it less accurate in kinetics-sensitive regions, especially at lean equivalence ratios or near flame extinction. Despite these limitations, EDM serves as an efficient baseline approach for analyzing the influence of hydrogen enrichment and equivalence ratio on flame behavior. Its use in this phase of the study supports rapid exploration of combustion trends before transitioning to more detailed reaction models.

2.2.6 The Eddy Dissipation Concept (EDC)

To overcome the limitations of the original Eddy Dissipation Model (EDM) in regions where chemical kinetics significantly influence combustion behavior, the **Eddy Dissipation Concept (EDC)** was developed by Magnussen and co-workers [13], [46]. The EDC integrates the effects of both **turbulent mixing** and **finite-rate chemistry** into the reaction rate calculation, offering a more advanced model for turbulent combustion systems where both physical and chemical timescales are important.

Unlike EDM, which assumes infinitely fast reactions limited only by turbulent mixing, the EDC model introduces the concept of **fine structures**—small turbulent eddies where combustion occurs over a finite residence time. Within these fine structures, species are allowed to react following Arrhenius kinetics, making it possible to simulate **kinetically controlled phenomena**, such as **flame extinction**, **ignition delay**, and **intermediate species formation** [47].

The mean reaction rate for a species i is expressed in the EDC framework as:

$$\dot{\omega}_i = \rho \cdot \frac{\chi}{\tau_{res}} (Y_i^* - Y_i) \quad (2.22)$$

Here, χ represents the mass fraction of the fluid contained in the fine structures, τ_{res} is the residence time of fluid in these structures, Y_i^* is the equilibrium species mass fraction in the fine structures, and Y_i is the bulk mass fraction [13], [7].

This formulation enables the model to simulate combustion behavior under conditions where both **turbulent transport and chemical kinetics** play essential roles. It is particularly useful for predicting reaction behavior in **lean flames, highly preheated mixtures, and regions near the flammability limits**, where chemical reaction rates are no longer infinitely fast and cannot be assumed to follow a mixing-limited model alone.

Because flammability limit investigations often involve **low-temperature, slow-reacting mixtures**, especially under **lean conditions**, using EDC provides an appropriate balance between physical modeling realism and computational tractability. While EDC is more expensive than the basic EDM model, it enables better resolution of the **chemically sensitive near-limit regime**, especially when hydrogen enrichment is considered. This makes it particularly suitable for studies involving variation in **equivalence ratio, preheat temperature, and secondary fuel addition**.

Overall, the EDC model serves as a powerful enhancement over EDM for combustion regimes where both **mixing and kinetics jointly control the flame**. Its implementation in this phase of the study ensures physically consistent and credible simulation of **flame extinction, lean blow-off, and the overall flammability boundary** for methane–air combustion with and without hydrogen.

2.3 Turbulence Modeling

Turbulence plays a crucial role in the combustion process, influencing the mixing of fuel and oxidizer, flame propagation, and heat transfer. In this work, turbulence is represented using the Reynolds-averaged Navier-Stokes (RANS) equations, which capture the time-averaged behavior of the flow. For turbulence modeling, the **k- ω SST** (Shear Stress Transport) model was employed. This model involves two partial differential equations: one governing the turbulent kinetic energy (k) and the other describing the specific rate of dissipation (ω) of turbulent kinetic energy [10].

2.3.1 Transport equation for turbulent kinetic energy (k):

$$\frac{\partial(\rho k)}{\partial t} + \frac{\partial(\rho u_i k)}{\partial x_i} = \frac{\partial}{\partial x_j} \left[\left(\mu + \frac{\mu_t}{\sigma_k} \right) \frac{\partial k}{\partial x_j} \right] + P_k - \beta^* \rho k \omega + S_k \quad (2.23)$$

where:

- x_j is the position in the j -direction.
- μ is the molecular viscosity.
- μ_t is the turbulent eddy viscosity.
- σ_k is the turbulent Prandtl number for k .
- P_k is the production term of turbulent kinetic energy, typically due to mean velocity gradients.
- β^* is a model constant.
- ω is the specific dissipation rate.
- S_k is a user-defined source term.

2.3.2 Transport equation for specific dissipation rate (ω):

$$\frac{\partial(\rho \omega)}{\partial t} + \frac{\partial(\rho u_i \omega)}{\partial x_i} = \frac{\partial}{\partial x_j} \left[\left(\mu + \frac{\mu_t}{\sigma_\omega} \right) \frac{\partial \omega}{\partial x_j} \right] + \alpha \frac{\omega}{k} P_k - \beta \rho \omega^2 + S_\omega \quad (2.24)$$

where:

- σ_ω is the turbulent Prandtl number for ω .
- α, β are model constants.
- S_ω is a user-defined source term for ω .

And,

$$P_k = \mu_i S_{ij} S_{ij}, \quad S_{ij} = \frac{1}{2} \left(\frac{\partial u_i}{\partial x_j} + \frac{\partial u_j}{\partial x_i} \right) \quad (2.25)$$

2.3.3 Turbulent eddy viscosity (μ_t):

$$\mu_t = \frac{\rho k}{\omega} \cdot f_2 \quad (2.26)$$

where:

- f_2 is a blending function that limits eddy viscosity near walls.

The k - ω SST model blends the standard k - ω and k - ϵ models using blending functions F_1 and F_2 , improving performance in near-wall and free-stream regions. The effective formulation includes cross-diffusion terms and corrections for adverse pressure gradients and separation.

The **k - ω Shear Stress Transport (SST)** model was selected in this study due to its superior performance in capturing complex turbulent flow behavior, particularly in regions with **strong adverse pressure gradients, flow separation, and wall-bounded shear flows**—all of which are characteristic of confined combustors. The k - ω SST model blends the advantages of both the standard **k - ϵ** and **k - ω** models by using the k - ω formulation near walls for accurate prediction of boundary layer behavior, and gradually transitioning to the k - ϵ formulation in the free stream to avoid sensitivity to freestream conditions.

This hybrid approach makes k - ω SST more reliable and robust for combustion simulations where **accurate prediction of recirculation zones, flame stabilization, and turbulence-chemistry interaction** is critical. Compared to the standard k - ϵ model, it offers better resolution of near-wall effects without requiring excessive mesh refinement, which is especially beneficial for capturing the flame anchoring and flow-field interactions in the burner geometry used in this study.

Therefore, the **k - ω SST model** was chosen as the turbulence closure method to ensure a balance between **accuracy and computational efficiency**, making it well-suited for simulating the **methane–hydrogen–air combustion system** under turbulent conditions.

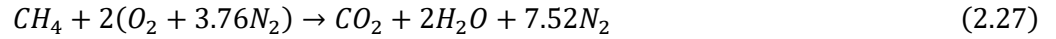
2.4 Reaction Rate

2.4.1 Global One-Step Reaction Mechanism

In the first phase of this study, a global one-step reaction mechanism was employed to simulate methane-air combustion. This simplified model is widely used in turbulent combustion modeling due to its computational efficiency and reasonable accuracy in capturing bulk flame behavior [7], [6].

Two overall reactions were used to represent the combustion of methane and hydrogen

1. Methane combustion:



2. Hydrogen combustion:



The global reaction rate follows the classical Arrhenius expression:

$$\dot{\omega} = A \cdot \rho \cdot Y_{fuel}^a \cdot Y_{O_2}^b \cdot \exp\left(-\frac{E_a}{RT}\right) \quad (2.29)$$

where:

- $\dot{\omega}$ is the reaction rate [$kg/m^3 \cdot s$]
- A is the pre-exponential factor
- Y_{fuel}, Y_{O_2} are the local mass fractions of fuel and oxygen
- E_a is the activation energy [J/mol]
- R is the universal gas constant
- T is the temperature [K]

This global mechanism was applied in simulations aimed at evaluating:

- The **flame characteristics of methane-air combustion**
- The effect of **hydrogen enrichment**

Such a model is particularly useful in assessing trends in temperature and flame anchoring without incurring the high computational costs of detailed chemistry [47].

2.6.2 Reduced Detailed Mechanism (DRM)

To assess the limitations of the global model and gain more detailed insight into flame structure, a second set of simulations used the **DRM22 reduced detailed mechanism**. Developed by Kazavok and Frenklach et al. [12], this mechanism includes:

- **22 species**
- **84 elementary reactions** involving chain branching, radical formation (e.g., OH, H, O), and pollutant precursors

The mechanism is suitable for modeling methane-air flames under turbulent conditions and offers improved prediction of:

- Flame structure and thickness
- Local heat release zones
- Intermediate species evolution
- Pollutant formation (e.g., CO, unburned hydrocarbons)

The DRM22 mechanism was implemented in Fluent using a CHEMKIN-formatted. cdi file. In this work, it was used to simulate **pure methane-air combustion** and compare its results with the **global one-step model**, providing a benchmark for:

- Flame temperature accuracy
- Prediction of reaction zones
- Chemical fidelity

This comparative analysis demonstrated the trade-offs between computational speed (global model) and chemical accuracy (detailed model), underscoring the need to balance model complexity with simulation goals [48].

2.5 Numerical Discretization

All governing equations were discretized using the **finite volume method (FVM)**. A **second-order upwind scheme** was applied for the discretization of convective terms to enhance accuracy.

The **Coupled pressure-based algorithm** was used for solving the flow field. This scheme solves the **momentum and continuity equations simultaneously**, along with pressure correction, ensuring strong coupling between pressure and velocity fields, which is critical for reactive flows with steep pressure gradients and strong compressibility effects, such as combustion.

In the Coupled scheme:

- The pressure-based solver handles **density-based flow behavior** by solving continuity, momentum, and energy equations in a **fully coupled manner**.
- **Pseudo-transient formulation** is often used to accelerate convergence and stabilize the solution process.
- The **pressure correction equation** is derived from the continuity and momentum equations and is solved together with velocity and pressure corrections in each iteration.
- The **energy equation** and **species transport equations** are also solved in a coupled fashion to capture the interaction between chemical reactions and thermal fields.
- **Under-relaxation factors** are applied to stabilize the iterative solution process.

Convergence was monitored using residual criteria:

- 10^{-6} for the energy equation,
- 10^{-3} for continuity, momentum, turbulence, and species equations.

This approach provides enhanced robustness and faster convergence for the simulation of reactive turbulent flows.

2.6 Conclusion

This study presents a comprehensive numerical investigation of methane-air combustion using both global and detailed chemical reaction mechanisms, with a particular focus on the influence of hydrogen addition under varying equivalence ratios. A two-dimensional combustion chamber was modeled under steady-state conditions, incorporating turbulence via the $k-\omega$ SST model and combustion chemistry through the eddy dissipation model coupled with reduced and global reaction mechanisms. The governing equations—continuity, momentum, energy, and species transport—were solved using the finite volume method with second-order accuracy.

The Coupled pressure-based solver was employed to ensure strong interaction between pressure and velocity fields, which is essential for capturing the dynamics of reactive flows. The boundary and initial conditions were carefully defined to simulate realistic combustion behavior. The results from this framework can be used to analyze flame stability, pollutant formation, and the extension of flammability limits due to hydrogen enrichment, providing valuable insights for cleaner and more efficient combustion system design.

Chapter 3:

Numerical Resolution

Summary

3.1	Introduction.....	47
3.2	Numerical Resolution Methods.....	47
3.3	Discretization Method.....	47
3.4	Pressure based solver	48
3.5	Turbulence Modeling.....	49
3.6	Combustion Modeling.....	50
3.7	Solver Settings and Convergence.....	50
3.8	Mesh and Grid Independence.....	51
3.9	Conclusion	51

Chapter 03 Numerical resolution

3.1 Introduction

In the previous chapter, we outlined the mathematical framework governing our problem. In this chapter, we will examine the appropriate numerical methods to solve this system. With a solid understanding of the numerical characteristics of our study and the computational fluid dynamics (CFD) tools at our disposal, we are now prepared to analyze the behavior of the physical phenomena in question.

3.2 Numerical Resolution Methods

The mathematical model, comprising one or more partial differential equations (PDEs), must be converted into a system of algebraic equations to enable numerical solution. This transformation is achieved through discretization techniques. The most widely used discretization methods include:

- **Finite Difference Method (FDM)**
- **Finite Element Method (FEM)**
- **Spectral Method (SM)**
- **Finite Volume Method (FVM)**

Each method has its strengths and is selected based on the specific requirements of the problem, such as geometry, boundary conditions, and accuracy needs.

3.3 Discretization Method

The **Finite Volume Method (FVM)** is a widely used approach for solving partial differential equations, particularly in the fields of fluid dynamics and heat transfer. Initially introduced by Patankar and Spalding in 1971, the method was later formalized in the seminal work *"Numerical Heat Transfer and Fluid Flow"* by Suhas V. Patankar in 1980.

In this approach, the governing conservation equations—typically in differential form—are transformed into algebraic equations by integrating over discrete control volumes (CVs) that make up the computational domain. This integration ensures that the conservation of mass, momentum, energy, or other physical quantities is preserved within each CV.

To illustrate the concept, consider a generic scalar transport equation. The method proceeds through the following steps:

- **Mesh Generation:** The domain is subdivided into small, finite volumes or control volumes.
- **Integral Formulation:** The conservation equations are integrated over each control volume.
- **Discretization:** The fluxes (convection and diffusion) and source terms are approximated using finite difference-like methods, converting the integral expressions into algebraic equations.
- **Solution Algorithm:** The resulting system of algebraic equations is solved using an iterative numerical solver.

Key Advantages of the Finite Volume Method:

- It naturally enforces the conservation of physical quantities (mass, momentum, energy) over each control volume.
- It is well-suited for complex geometries and unstructured meshes.
- It provides a straightforward framework for handling boundary conditions.
- It directly computes important field variables such as pressure and velocity.

The finite volume method ensures that the discrete conservation laws mimic the physical conservation principles applied to subregions of the domain. Each control volume contains a representative point (often the centroid or node) where values of field variables are computed. [49]

3.4 Pressure based solver

In fluid dynamics simulations, the pressure-based solver is predominantly used for flows where density changes are not significant (i.e., incompressible or mildly compressible flows). This solver handles the conservation equations of mass, momentum, and energy by solving them either in a segregated or coupled manner. In incompressible flows, density is considered independent of pressure, so pressure-velocity coupling is essential to ensure that the velocity field satisfies the continuity equation once substituted into the momentum conservation laws [47].

The pressure-based solver is particularly suitable for combustion modeling, turbulent flows, and heat transfer problems due to its robustness and flexibility. In ANSYS Fluent, five primary pressure-velocity coupling schemes are available: SIMPLE, SIMPLER, SIMPLEC, PISO, and Coupled [50].

3.4.1 Coupled Algorithm (Fully Coupled Pressure-Based Solver)

Among these schemes, the **Coupled** algorithm offers a more integrated approach by solving the momentum and continuity equations simultaneously as a single system. Unlike the segregated methods, where pressure and velocity fields are updated sequentially, the Coupled algorithm performs a joint solution, resulting in tighter pressure-velocity coupling and often significantly improved convergence rates. This is especially useful in high-speed flows, transient simulations, and combustion scenarios, where rapid changes in flow variables demand numerical stability [11].

In the Coupled algorithm, these equations are linearized and solved simultaneously using a block-coupled system, often with an Algebraic Multigrid (AMG) solver. This results in a robust numerical performance, particularly in flows involving shock waves, pressure gradients, or combustion fronts [50].

Advantages of the Coupled Algorithm:

- Stronger pressure-velocity coupling.
- Improved convergence behavior, especially in transient simulations.
- Better handling of compressibility effects.
- Suitable for reacting flows with steep gradients.

Limitations:

- Higher memory requirements.
- Increased computational time per iteration compared to segregated solvers.

The Coupled solver is commonly used in simulations involving methane-air combustion with high preheat temperatures, where accuracy and stability are critical. In ANSYS Fluent, enabling the Coupled solver is as simple as selecting it under the "Pressure-Velocity Coupling" section in the Solver settings.

3.5 Turbulence Modeling

Turbulence was modeled using the **k- ω Shear Stress Transport (SST)** model developed by Menter (1994). This two-equation model blends the robust near-wall accuracy of the k- ω model with the free-stream resilience of the k- ϵ model, making it suitable for complex internal flows, including those with adverse pressure gradients or separation [51].

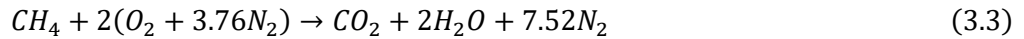
The transport equations for k and ω were solved using second-order upwind schemes. Turbulent viscosity (μ_t) was calculated to close the RANS equations, with eddy viscosity limiting functions to enhance model stability near walls.

3.6 Combustion Modeling

The combustion process was modeled using the **Eddy-Dissipation Model (EDM)**, which is ideal for turbulent, fast-chemistry scenarios and **EDC**, which is ideal for lean mixtures [50]

Two chemical mechanisms were implemented:

- **A global one-step mechanism:**



- **A reduced detailed mechanism** (CHEMKIN-based), comprising **84 reactions** to model intermediate species formation and flame structure.

3.7 Solver Settings and Convergence

Solver configuration:

- **Solver Type:** Pressure-based, steady-state
- **Pressure-Velocity Coupling:** Coupled algorithm
- **Discretization Schemes:**
 - Pressure: Second-order
 - Momentum, Energy, Species, Turbulence: Second-order upwind
- **Relaxation Factors:** Default values adjusted as needed for convergence stability
- **Convergence Criteria:**
 - Residual for energy equation: 10^{-6}
 - Residuals for momentum, turbulence, species: 10^{-3}

Convergence was monitored not only via residuals but also using outlet mass balance and stabilization of temperature and velocity fields.

3.8 Mesh and Grid Independence

The computational domain was discretized using a **structured mesh**, refined near the walls and in the flame zone to capture steep gradients in temperature and species. A **grid independence study**/grid sensitivity study was conducted by testing different grid sizes. Results such as maximum temperature were compared to ensure mesh-independent solutions. Further details are in chapter 04.

3.9 Conclusion

The numerical resolution approach adopted in this study integrates the Finite Volume Method with advanced turbulence and combustion models to accurately simulate methane-air combustion. The use of the pressure-based coupled solver enhances convergence and accuracy, while the $k-\omega$ SST model and the eddy-dissipation combustion approach offer robust handling of turbulent and reactive flows. These numerical methods, implemented within the ANSYS Fluent environment, provide a reliable framework for investigating the influence of fuel composition and operating conditions on combustion performance.

Chapter 4:

Simulation setup

Summary

4.1	Introduction.....	52
4.2	Combustor Modeling	52
4.3	Mesh Generation.....	53
4.4	Boundary conditions	56
4.5	mesh sensitivity study	59
4.6	Fluent Setup	62
4.7	Conclusion	64

Chapter 04 Simulation Setup

4.1 Introduction

In this chapter we will describe the set-up and solution of a computational fluid dynamics simulation of combustion in a burner element. The simulation was based on the 2D geometry used by C.E.L. Pinho, J.M.P.Q. Delgado, R. Pilão, J. Conde and C. Pinho in their study titled “Numerical Study of Propane-Air Mixture Combustion in a Burner Element” [52]. This chapter outlines the simulation setup used to analyze methane-air combustion with addition of hydrogen at different percentages in a two-dimensional burner geometry. The numerical study was carried out using ANSYS Fluent, applying the species transport model with defined boundary conditions, meshing parameters, and solver settings. The simulation involves laminar and turbulent flows and modeled using appropriate turbulence models. The goal is to investigate combustion characteristics under defined physical and flow conditions. We will also provide a detailed account of our problem set-up and solution procedure, this chapter aims to facilitate the replication and validation of our simulation by other researchers in the field of combustion science.

4.2 Combustor Modeling

The geometry of the combustor is adapted from literature and designed to represent a simplified two-dimensional burner. It includes a (methane and hydrogen) fuel inlet, an air inlet, an outlet, and surrounding walls including an axis of symmetry.

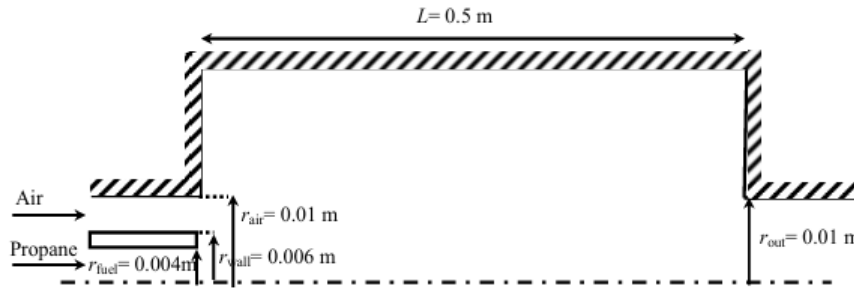


Figure 6 2D geometry used by C. E. L. Pinho, J. M. P. Q. Delgado, R. Pilao, J. Conde and C. Pinho in their study titled “Numerical Study of Propane-Air Mixture Combustion in a Burner Element” [52]

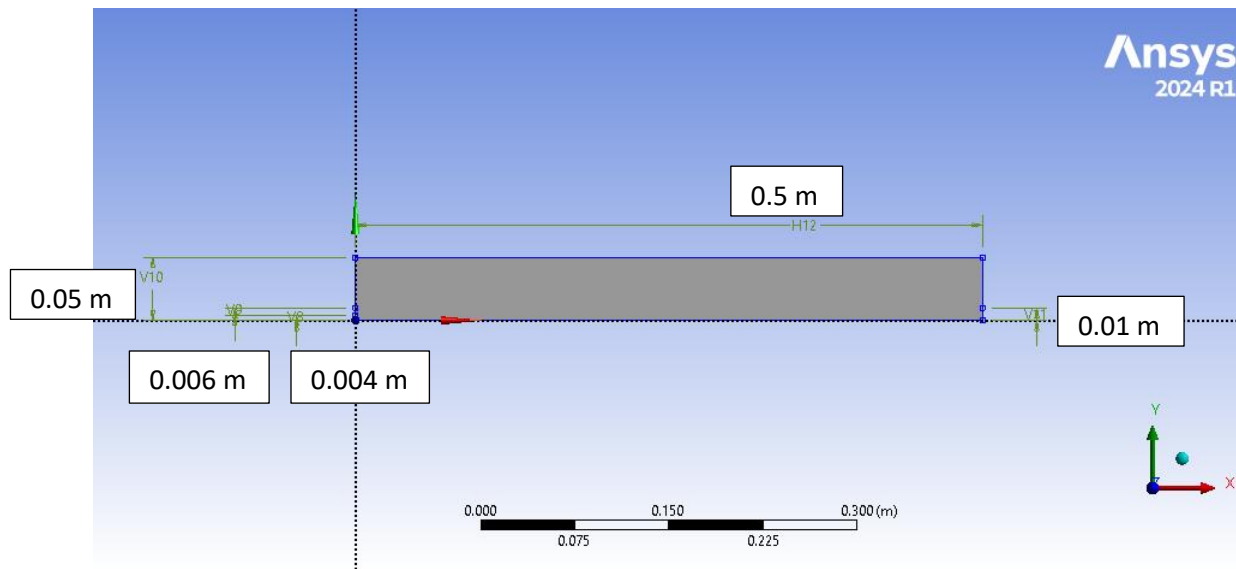


Figure 7 2D asymmetric geometry of a burner element

The dimensions are as follows:

Table 4-1 Labels and dimensions of the Combustion chamber

Component	Label	Dimension
Combustion chamber length	H12	0.5 m
Combustion chamber height	V10	0.05 m
Fuel inlet	V8	0.004 m
Air inlet	V9	0.006 m
Outlet	V11	0.01 m

4.3 Mesh Generation

Mesh generation was conducted using a structured mesh to ensure good resolution near the inlets, wall boundaries, and flame zones. A biasing strategy was used to concentrate cells in regions with expected high gradients.

The meshing details are as follows

Table 4-2 Meshing details

Region	Number of Divisions	Bias Factor
Upper wall and axis	1000	5
Right and left walls	100	3
Fuel inlet	16	—
Air inlet	24	—
Outlet	40	—

Our mesh consists of 141141 nodes and 140000 elements

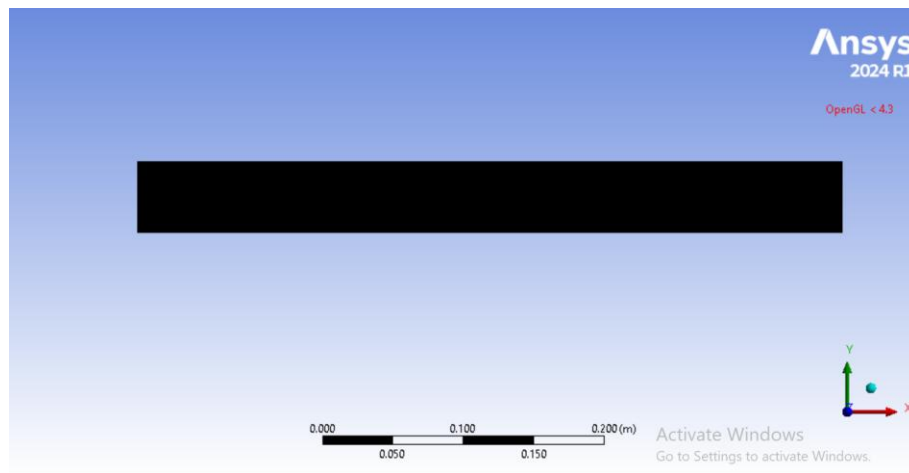


Figure 8 full view of the mesh

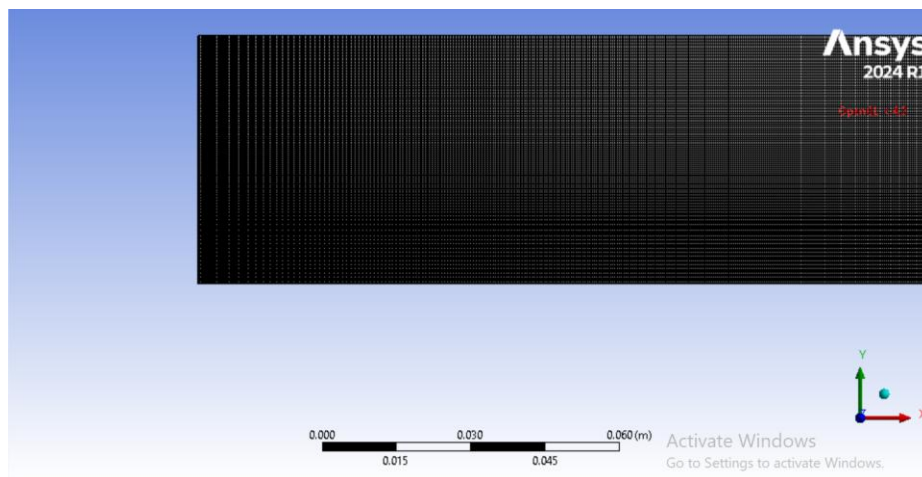


Figure 9 zoomed view of the mesh

Results and Discussion

The mesh was evaluated based on parameters such as skewness and orthogonal quality. The histograms for skewness and orthogonal quality are as shown below.

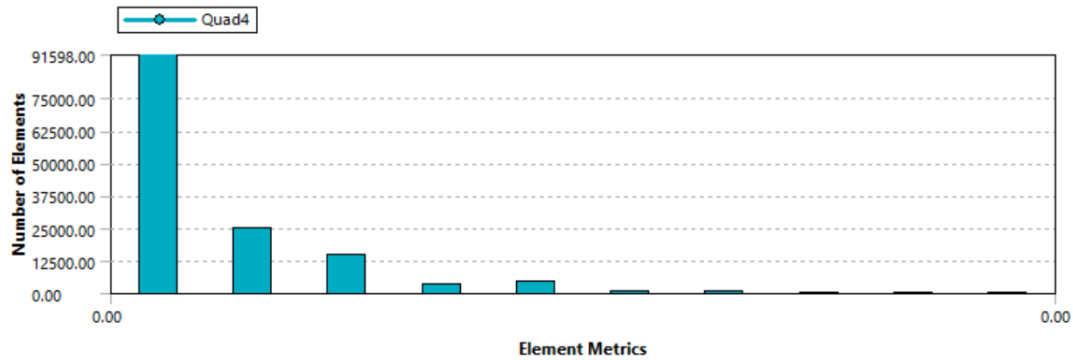


Figure 10 skewness histogram

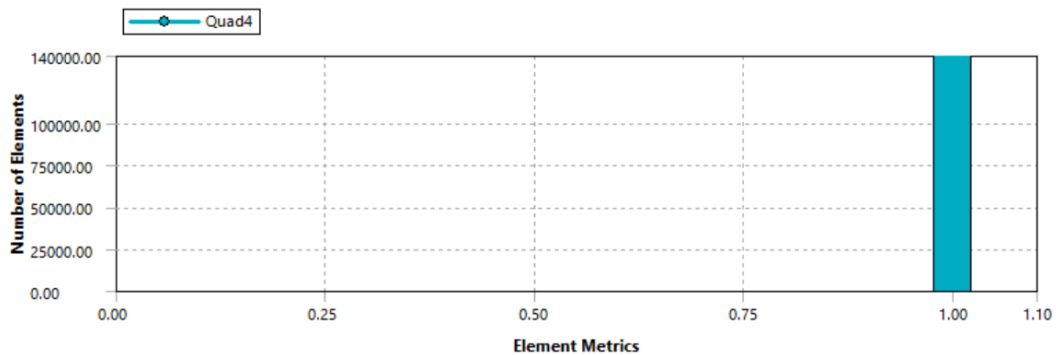


Figure 11 orthogonal quality histogram

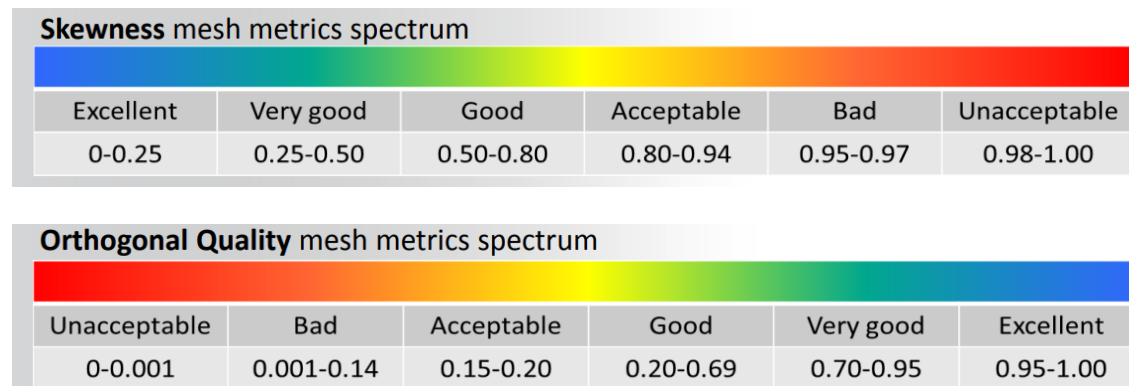


Figure 12 skewness and orthogonal quality mesh spectrum [53]

According to the Skewness and Orthogonal mesh metrics spectrum and comparing the respective histograms. The skewness is 0 that is excellent and the orthogonal quality is 1 which is excellent. From these results we can conclude that the mesh is of good quality and it will give a significant impact on the accuracy and computational efficiency of the simulation.

4.4 Boundary conditions

4.4.1 Section naming

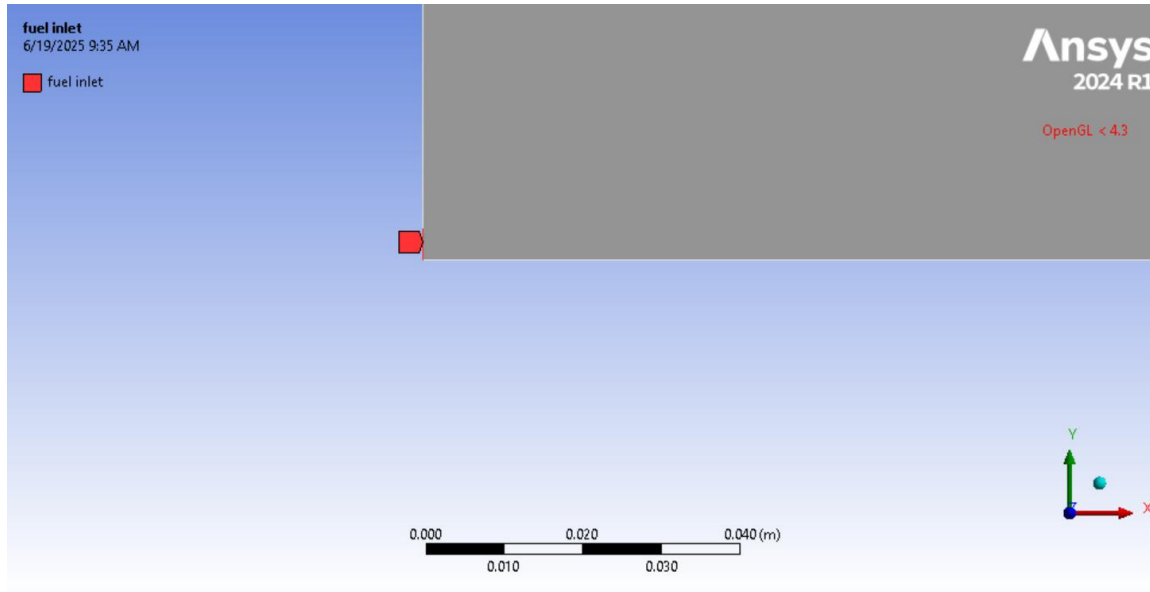


Figure 13 Combustion chamber fuel inlet

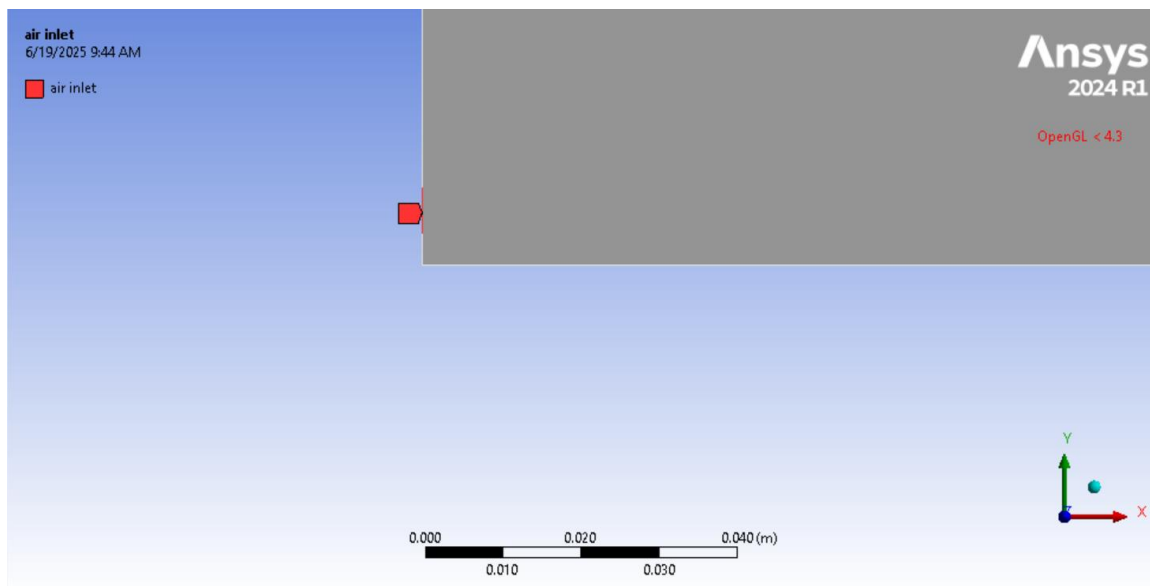


Figure 14 Combustion chamber air inlet

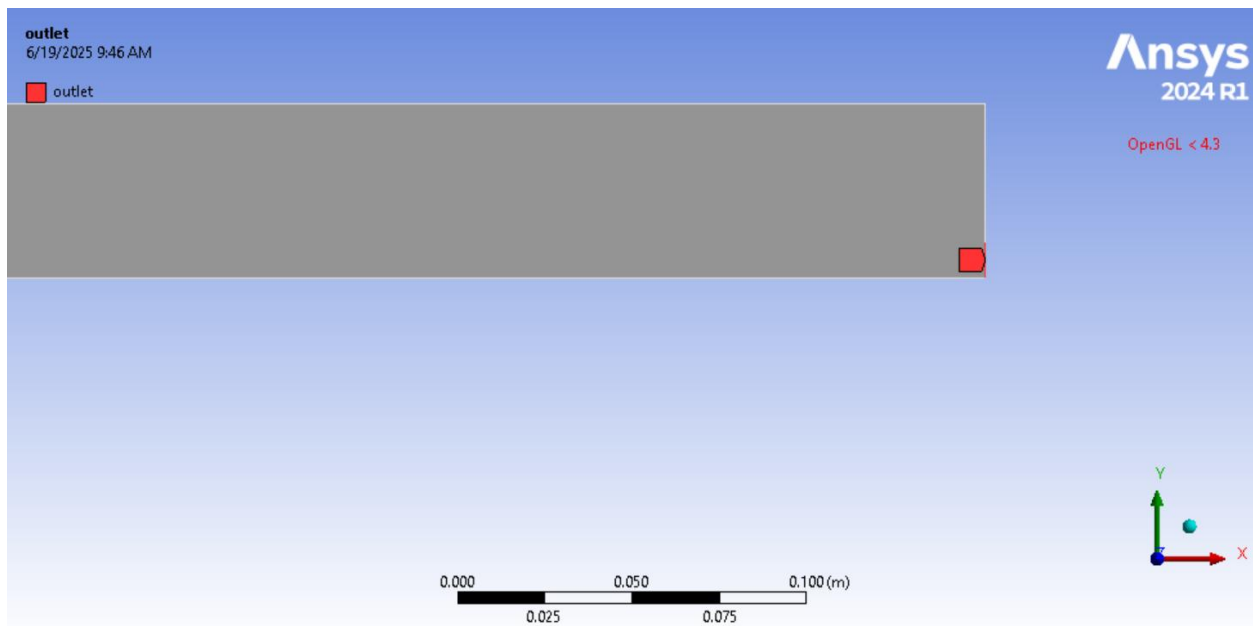


Figure 15 Combustion chamber outlet

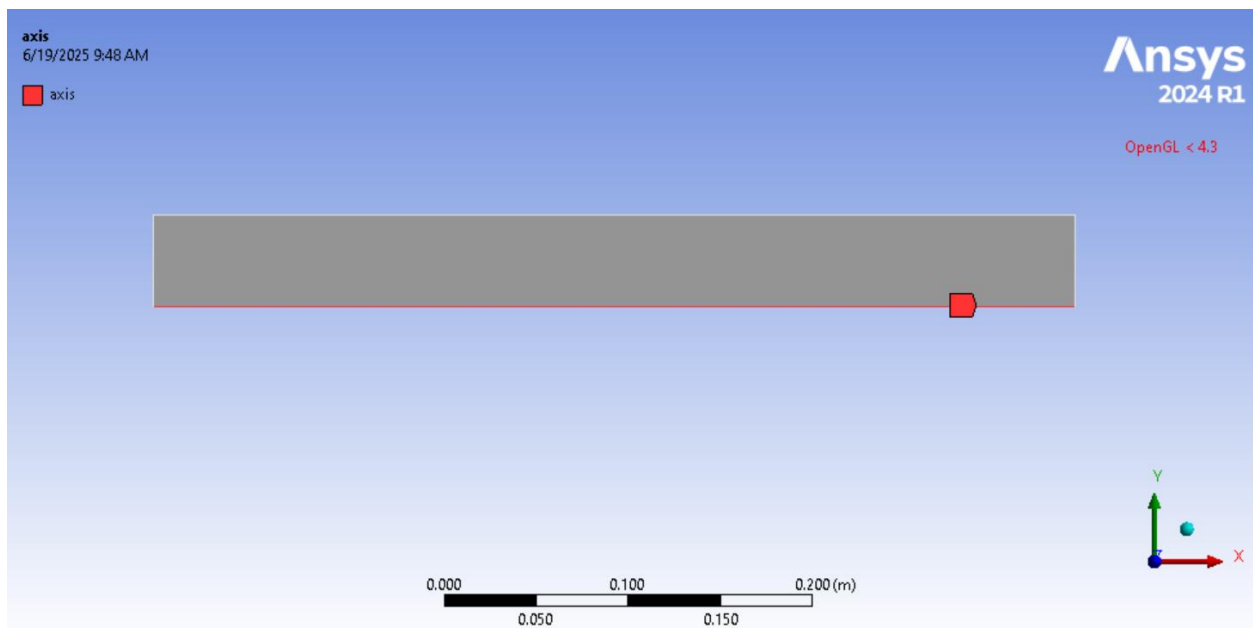


Figure 16 Combustion chamber axis

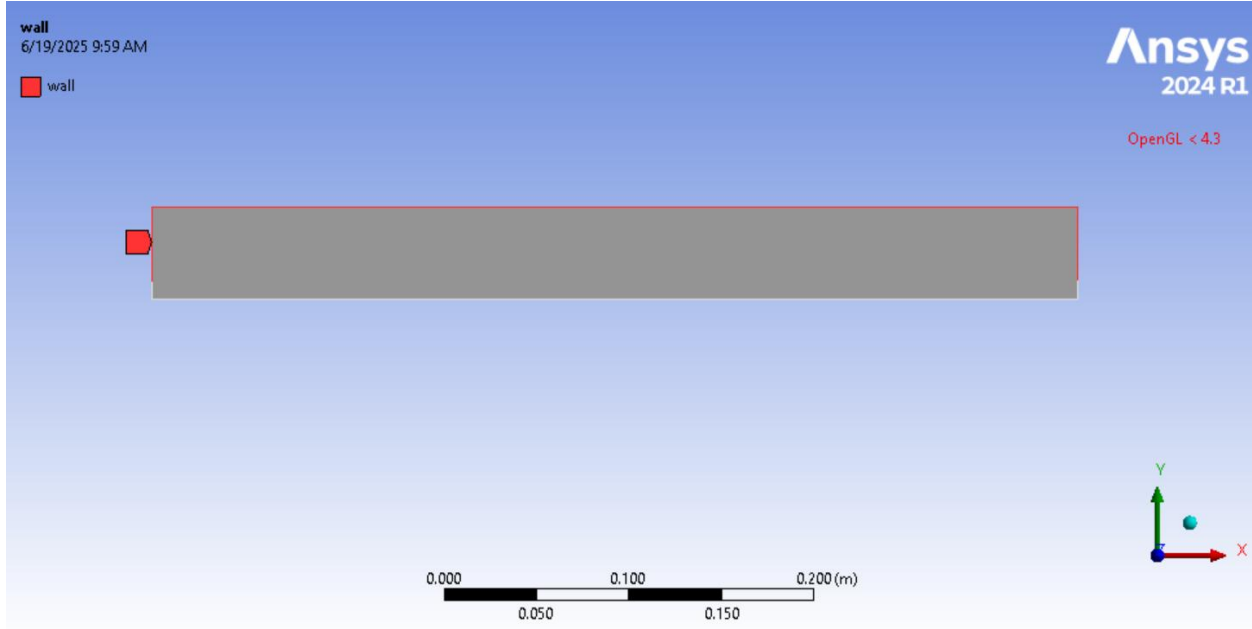


Figure 17 Combustion chamber wall

4.4.2 Boundary conditions identification

The initial air and fuel temperatures used in the computations are 300K. A mass flow inlet is defined as any inlet surface. At the combustor exit, a pressure boundary condition is assigned. Fuel mass flow rate is fixed at 0.0002 kg/s and air mass flow rate varies with equivalence ratio.

Molar mass = **16.04 g/mol**

Air = O₂ + N₂ (mass basis)

Molar mass of air = ~28.97 g/mol

Stoichiometric AFR by mass:

$$AFR_{stioch} = \frac{2 \cdot 32 + 2 \cdot 3.76 \cdot 28.97}{16.04} = \frac{64 + 217.6}{16.4} \approx 17.56$$

Fuel inlet (center annulus):

$$A_{fuel} = 5.0265 \times 10^{-5} \text{ m}^2$$

Air inlet (outer annulus):

$$A_{air} = 2.6507 \times 10^{-4} \text{ m}^2$$

Mass Flow Rates at Equivalence Ratios ($\Phi = 0.6$ to 1.3)

Let's assume a constant **fuel mass flow rate**:

$$\dot{m}_{fuel} = 0.0002 \text{ kg/s}$$

Then:

$$\dot{m}_{air} = \frac{0.0002}{\Phi} \cdot 17.56$$

Φ	Air Mass Flow (kg/s)
0.6	0.005853
0.7	0.005017
0.8	0.004390
0.9	0.003902
1.0	0.003512
1.1	0.003193
1.2	0.002927
1.3	0.002703

4.5 mesh sensitivity study

Mesh independence is a crucial part of computational simulation to ensure that the numerical results are not influenced by the discretization level. This study assessed mesh sensitivity by evaluating the **maximum flame temperature** across three structured meshes with increasing element densities:

Table 4-3 Maximum temperatures at equivalence ratio of 1 for 4 meshes with different refinements

Mesh	Number of Elements (N)	Max Temp at $\phi = 1.0$ (K)
Course	35,500	2290.473
Medium	78,750	2292.212
Refined	140,000	2294.787
Fine	560,000	2295.329

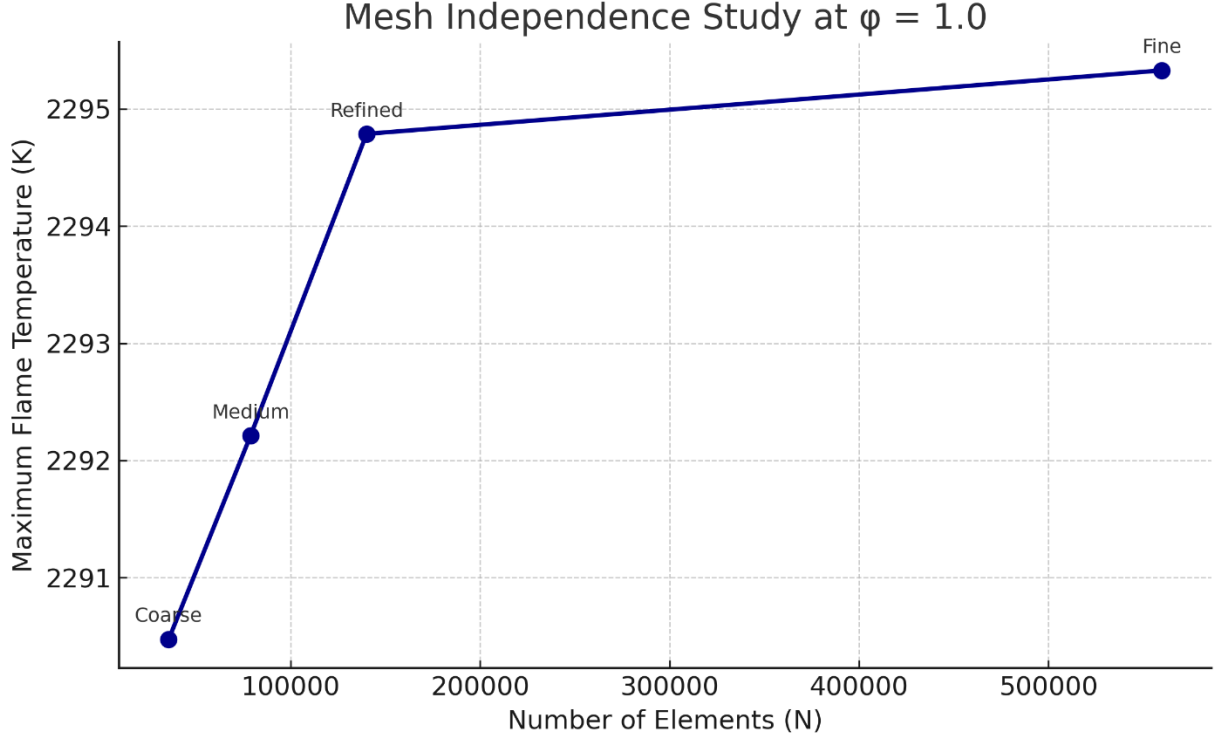


Figure 18 Mesh independence study, at equivalence ratio of 1, plot for the four meshes

The maximum flame temperature increases slightly as the mesh is refined. Between the **refined (140k)** and **fine (560k)** meshes, the temperature change is minimal (~ 0.5 K), suggesting that **mesh independence is achieved**. The **fine mesh** adds significant computational cost for minimal accuracy gain.

4.5.1 Quantitative Mesh Convergence Analysis

To verify mesh independence quantitatively, a mesh refinement study was conducted at $\phi = 1.0$ using the method described in Roache's **Grid Convergence Index (GCI)** approach [54]. The maximum temperature values were used to compute:

- **Order of convergence (p)**
- **Grid Convergence Index (GCI)** between mesh levels

Assuming **geometric refinement** and uniform 2D elements, the refinement ratio is:

$$r_1 = \left(\frac{35500}{8750} \right)^{1/2} = 4.06^{1/2} \approx 2.015 \quad (4.1)$$

$$r_2 = \left(\frac{78750}{35500} \right)^{1/2} = 2.218^{1/2} \approx 1.489 \quad (4.2)$$

$$r_3 = \left(\frac{140000}{78750} \right)^{1/2} = 1.778^{1/2} \approx 1.334 \quad (4.3)$$

Using the formula for **apparent order of convergence**:

This value is consistent with expectations for first-order finite volume schemes used in many CFD solvers.

Using the medium (T_1), refined (T_2), and fine (T_3) meshes:

- $T_1 = 2290.473 \text{ K}$
- $T_2 = 2292.212 \text{ K}$
- $T_3 = 2294.787 \text{ K}$

$$p = \frac{\ln \left(\frac{T_1 - T_2}{T_2 - T_3} \right)}{\ln(r_2)} = \frac{-0.392}{0.398} \approx -0.984 \quad (4.4)$$

The negative value of p reflects **non-monotonic error reduction**, a known issue in practical CFD due to numerical diffusion or abrupt error plateauing. It does **not invalidate** the mesh independence claim, especially when GCI is low.

4.5.2 Grid Convergence Index (GCI)

Using the formula proposed by Roache [54]:

$$GCI_{fine} = \frac{F_S \cdot |T_3 - T_2|}{T_3 \cdot (r_3^{|p|} - 1)} \times 100 \quad (4.5)$$

Where:

- $F_s = 1.25$
- $|T_3 - T_2| = 2.575$
- $r_3^{|p|} = 1.334^{0.984} \approx 1.325$
- $T_3 = 2294.787 \text{ K}$

$$GCI_{fine} = \frac{1.25 \cdot 2.575}{2294.787 \cdot 0.325} \times 100 \quad (4.6)$$
$$\approx 0.431\%$$

Both the graphical and quantitative results confirm mesh convergence:

- Maximum flame temperature increases steadily with mesh refinement.
- Apparent order of convergence $p \approx -0.98$ indicates non-monotonic but diminishing error.
- GCI of 0.43% ($\ll 5\%$) strongly supports mesh independence.

Therefore, the fine mesh with 140,000 elements was selected for final simulations, offering the best balance between numerical accuracy and computational efficiency.

4.6 Fluent Setup

The methane-air combustion simulation, with one-step mechanism, was carried out in ANSYS Fluent using the following settings:

- Solver: Pressure-based
- Flow: Steady
- Model: Species Transport (with volumetric reactions enabled)

Combustion model: EDM

- Turbulence: RNG $k-\omega$ SST
- Pressure-Velocity Coupling: COUPLED
- Discretization Schemes:
 - Momentum: Second Order Upwind

- Energy: Second Order Upwind
- Species: Second Order Upwind

Thermophysical properties such as density, specific heat, and thermal conductivity were temperature-dependent. The inlet temperatures were set at:

- Air and fuel inlets: 300 K
- Ambient pressure: 101325 Pa
- Air density: 1.225 kg/m³
- Fuel density (CH₄): 0.91 kg/m³ (approximate value at 300 K)

The methane air combustion simulation, with a reduced detailed mechanism, was carried out in ANSYS Fluent with the following settings:

- Solver: Pressure-based
- Flow: Transient
- Model: Species Transport (with volumetric reactions enabled)

Combustion model: EDC

- Turbulence: RNG $k-\omega$ SST
- Pressure-Velocity Coupling: COUPLED
- Discretization Schemes:
 - Momentum: Second Order Upwind
 - Energy: Second Order Upwind
 - Species: Second Order Upwind

Thermophysical properties such as density, specific heat, and thermal conductivity were temperature-dependent. The inlet temperatures were set at:

- Air and fuel inlets: 300 K
- Ambient pressure: 101325 Pa
- Air density: 1.225 kg/m³
- Fuel density (CH₄): 0.91 kg/m³ (approximate value at 300 K)

4.7 Conclusion

This chapter has detailed the comprehensive setup and solution methodology for simulating methane-air combustion with hydrogen enrichment in a two-dimensional burner element using ANSYS Fluent. Adapting the geometry from a validated literature source ensured relevance and comparability, while structured meshing and quality assessments demonstrated a high-fidelity computational grid with excellent skewness and orthogonal quality metrics. A thorough mesh independence study, both qualitative and quantitative, confirmed that the selected fine mesh (140,000 elements) offers a reliable balance between accuracy and computational cost. The calculated Grid Convergence Index (GCI) of 0.43% substantiates the credibility of the numerical results, despite minor non-monotonic convergence behavior.

By implementing appropriate physical models—such as the species transport model with volumetric reactions and the RNG $k-\omega$ SST turbulence model—and by applying second-order discretization schemes, the simulation setup ensures accurate prediction of flame dynamics and combustion characteristics. These methodological choices provide a robust foundation for the subsequent analysis of combustion behavior under various hydrogen addition scenarios. The detailed documentation of this setup enables reproducibility and serves as a benchmark for future studies in burner-scale combustion modeling.

Chapter 5:

Results and Discussion

Summary

5.1	Introduction.....	65
5.2	Methane-air combustion results for a global reaction.....	65
5.3	Effects of Hydrogen Addition on Combustion.....	71
5.4	Comparison and validation of results	77
5.5	Conclusion	82

Chapter 05 Results and Discussion

5.1 Introduction

In this chapter, the outcomes of the numerical simulations conducted using the ANSYS Fluent solver in a 2D burner element will be presented and thoroughly discussed. The primary objective is to analyze the data obtained from the simulations and interpret their implications in relation to the research objectives.

5.2 Methane-air combustion results for a global reaction

Here we present the results of methane-air combustion simulation in the 2D burner element for a global reaction. The objective here is to analyze on species distribution, temperature profiles, velocity fields and axial temperature variations to understand the combustion characteristics and flame behavior. For gas simulation a methane-air mixture was used with the following physical values: $\Phi=1$ and other equivalence ratios, Air and fuel inlets: 300 K , Ambient pressure: 101325 Pa, Air density: 1.225 kg/m³, Fuel density (CH₄): 0.91 kg/m³.

We are further going to determine the effects of addition of hydrogen at 5%, 15%, 25% and 35%, and analyze on the temperature and velocity profiles.

5.2.1 Results for Stoichiometric conditions

5.2.1.1 Temperature contour

In this section, we present the temperature contours. By analyzing the temperature contour, we understand the thermal behavior and characteristics of methane-air flames within the combustion chamber. These results provide valuable insights on temperature distribution, aiding in the optimization of combustion processes in burner elements.

The temperature contour below shows distinct variation in flame temperature within the combustion chamber.

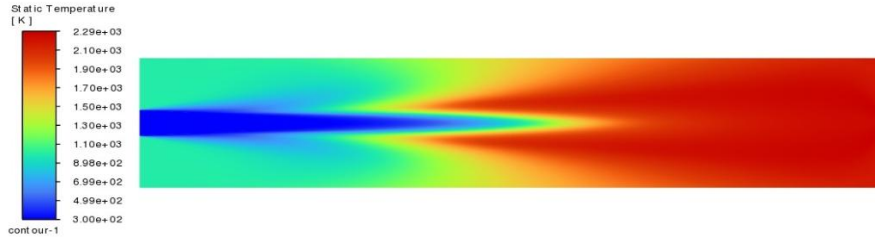


Figure 19 A Temperature contour for methane-air combustion for a global reaction at the equivalence ratio Φ of 1

From the contour above we notice a gradual increase in temperature from the inlet and the flame broadens outwards as it approaches the outlet.

The temperature plot below further explains the temperature rise in detail. The plot is such that the temperature variation is measured from the axis of the combustion chamber.

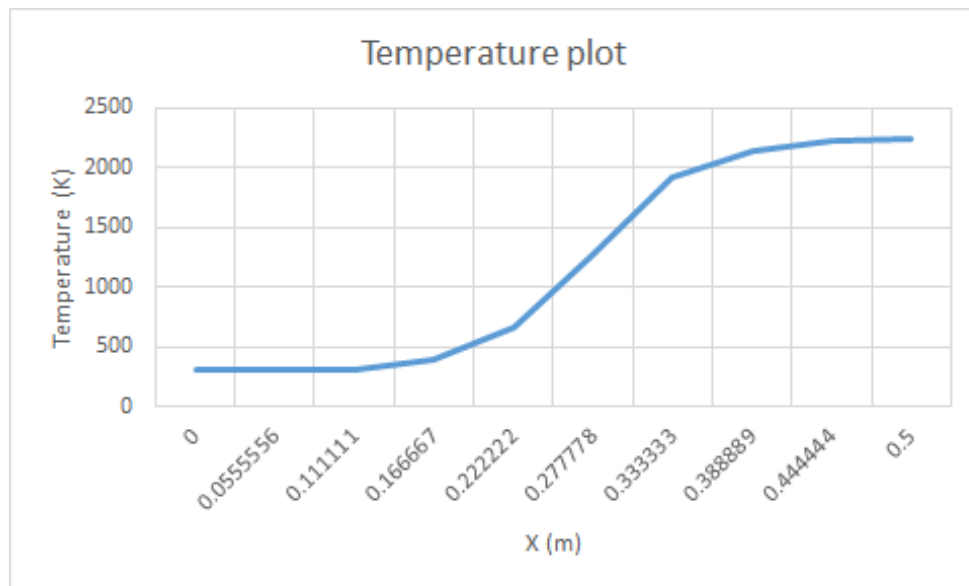


Figure 20 Temperature plot at the axis for methane-air combustion for global reaction at the equivalence ratio Φ of 1

From the line graph above it is clear that there is a gradual rise in temperature from the outlet until the middle of the combustion chamber where the temperatures start rising drastically until the temperature levels out to the maximum temperature of 2294.787 K.

5.2.1.2 Velocity contour

In this section, we present the velocity contours obtained from simulation conducted. Below is an image of the velocity contour.

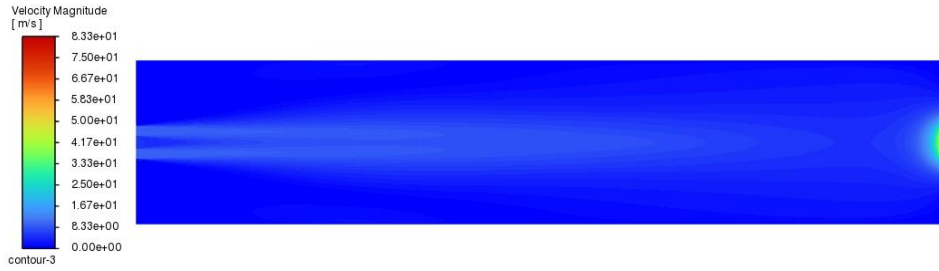


Figure 21 Velocity contour for a methane-air combustion for a global reaction at the equivalence ratio Φ of 1

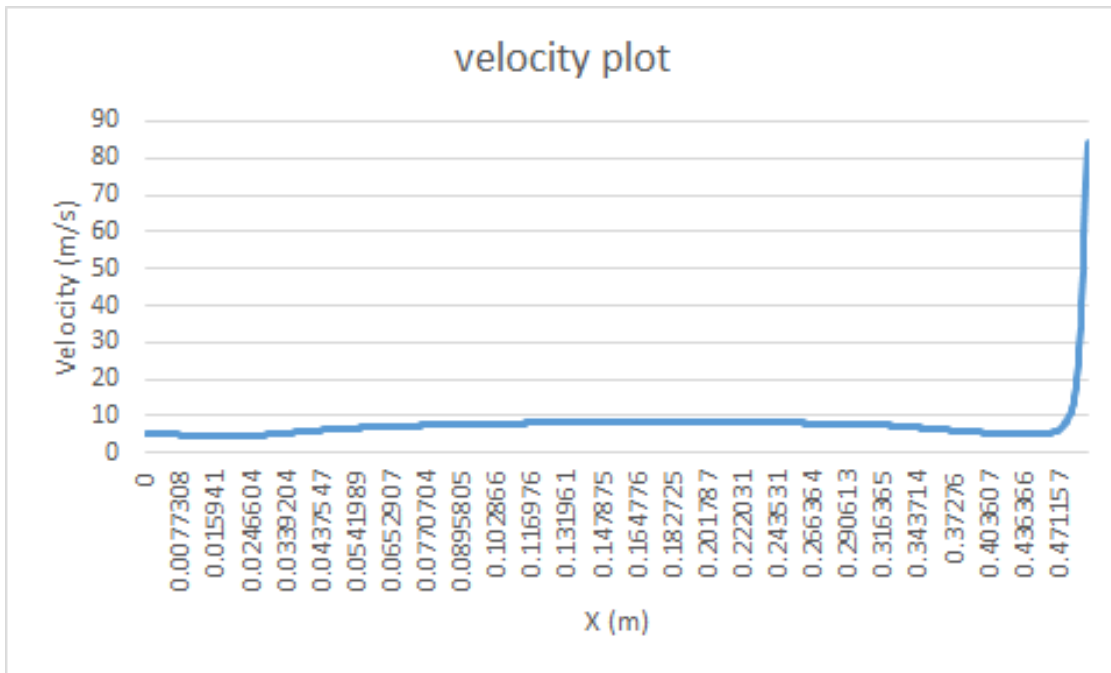


Figure 22 velocity plot at the axis for methane-air combustion for a global reaction at the equivalence ratio Φ of 1

The velocity profile along the axial (X) direction indicates a high initial velocity at the burner outlet due to jet effect. This is followed by a rapid decay attributed to turbulent mixing and viscous effects. Beyond $X \approx 0.1m$, the flow stabilizes, indicating a region of reduced momentum and potential recirculation or fully developed flow.

5.2.1.3 Pressure contour

In this section, we present the pressure contours obtained from simulation conducted. Below is an image of the pressure contour.



Figure 23 Pressure contour for methane-air combustion for global reaction at the equivalence ratio Φ of 1

The pressure contour indicates that there is high pressure in the combustion chamber this can be explained by the low velocity in the combustion chamber. The pressure decreases abruptly due to the jet like effect at the burner's outlet. The pressure plot below further explains the pressure profile in the burner element.

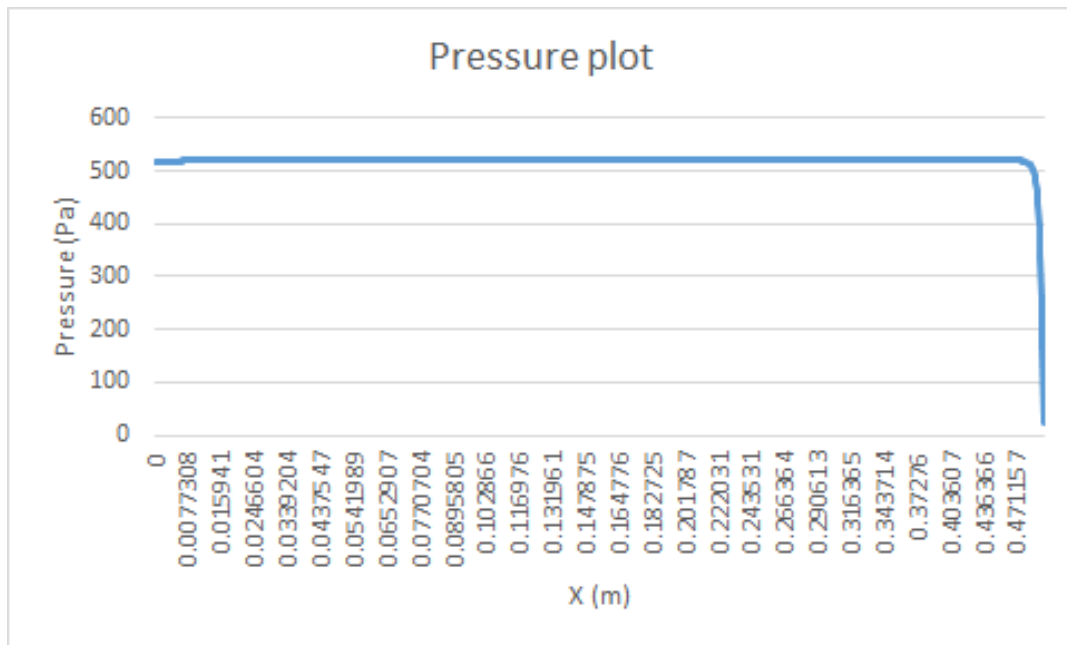


Figure 24 pressure plot at the axis for methane-air combustion for a global reaction at the equivalence Φ ratio of 1

5.2.1.4 Density contour

In this section, we present the density contours obtained from simulation conducted. Below is an image of the density contour.

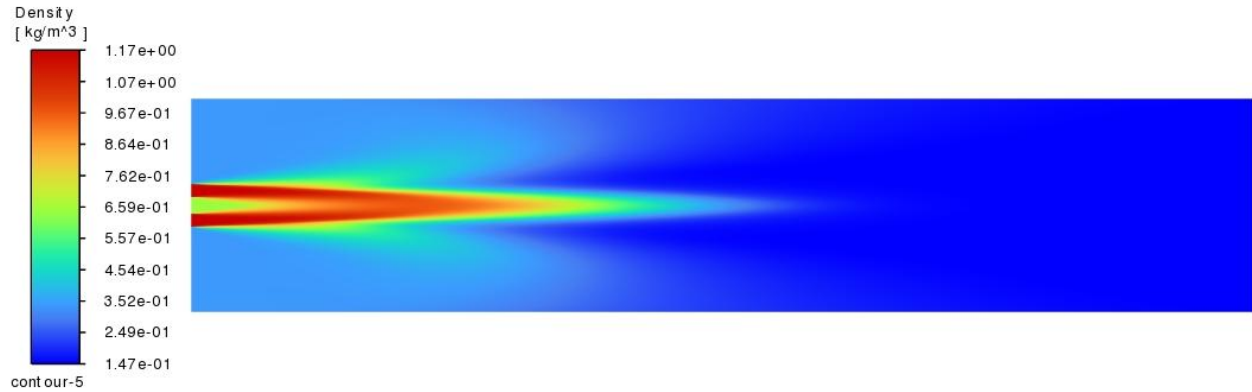


Figure 25 Density contour for methane-air combustion for a global reaction at the equivalence Φ ratio of 1

The density is highest at the inlet and gradually decreases towards the outlet. This is due to the increase in temperature towards the outlet.

5.2.2 Lean combustion regimes in my simulation

In this section we will explore temperature contours of methane-air combustion at equivalence ratios of 0.8 and 0.7. The initial conditions were 300 K and 1atm

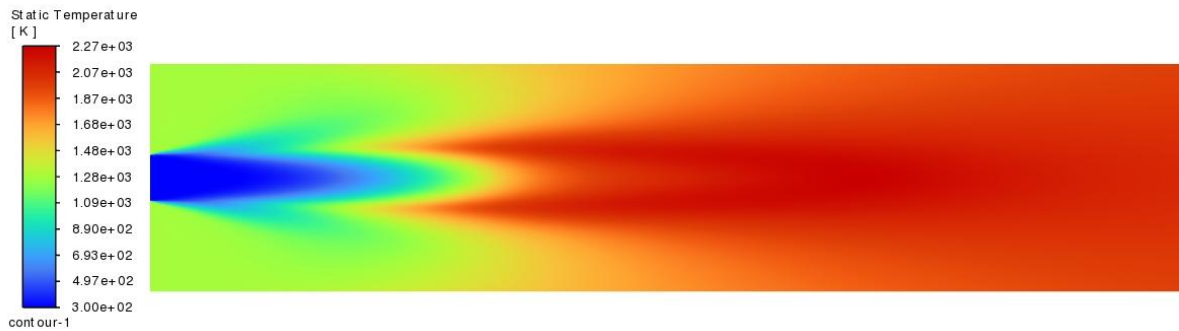


Figure 26 Temperature contour of methane-air combustion at the equivalence ratio of 0.8

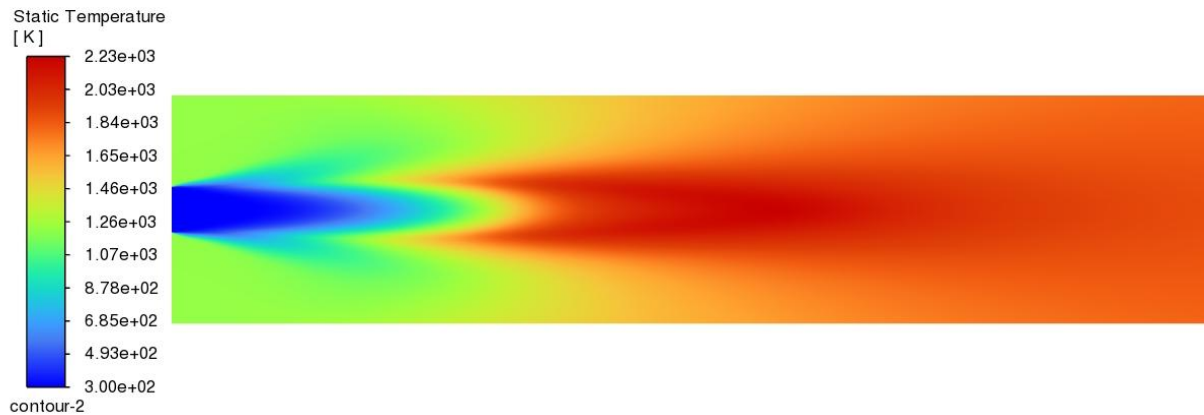


Figure 27 Temperature contour of methane air combustion at equivalence ratio of 0.7

From the results above we notice that at these lean regimes the combustion temperatures decrease as the equivalence ratios decrease. With maximum temperatures at the equivalence ratio of 0.8 being 2260K and at 0.7 being 2227K.

5.2.3 NO_x effects at different equivalence ratios

In this section we are going to test for prompt NO_x. We will explore NO_x contours at the equivalence ratios of 0.7, 0.8, 1.1 and 1.2. This will give us insight on NO_x formation at both lean and rich regimes.

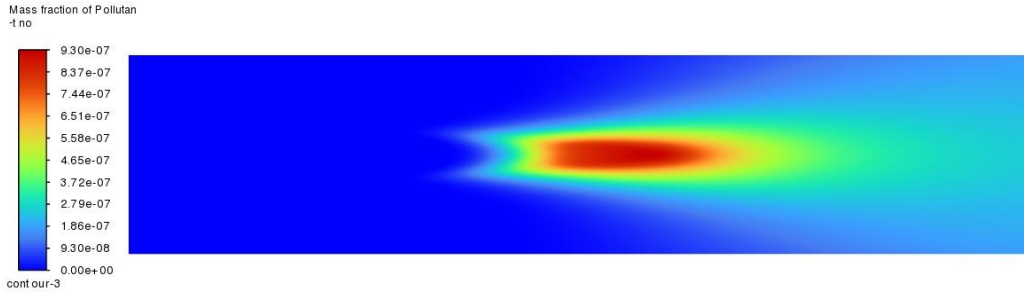


Figure 28 NO_x mass fraction contour at the equivalence ratio of 0.7

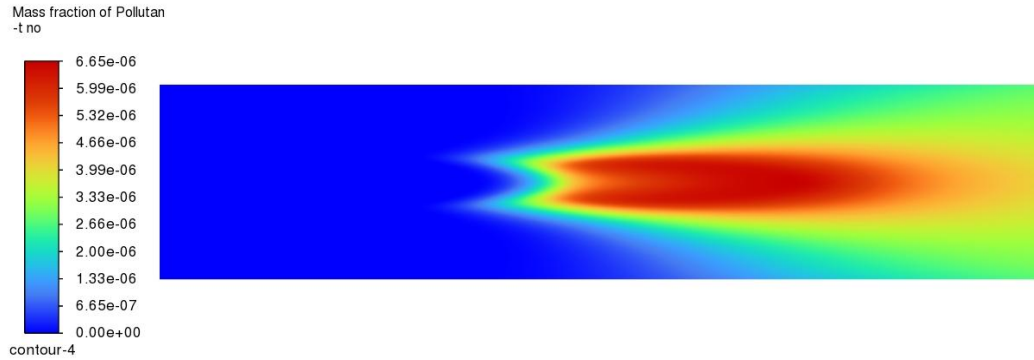


Figure 29 NO_x mass fraction contour at the equivalence ratio of 0.8

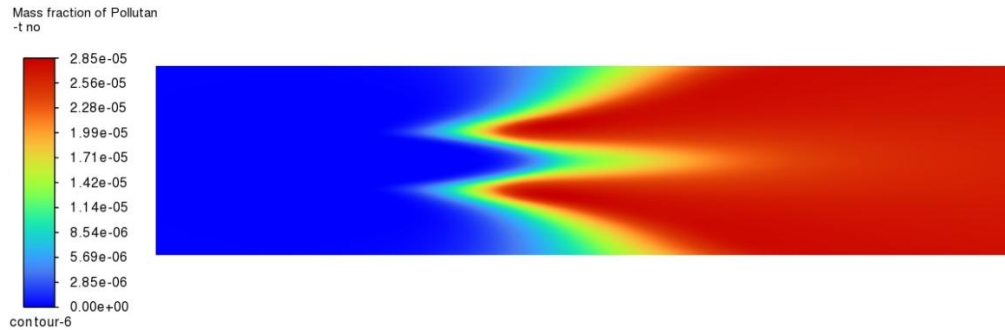


Figure 30 NO_x mass fraction contour at the equivalence ratio of 1.1

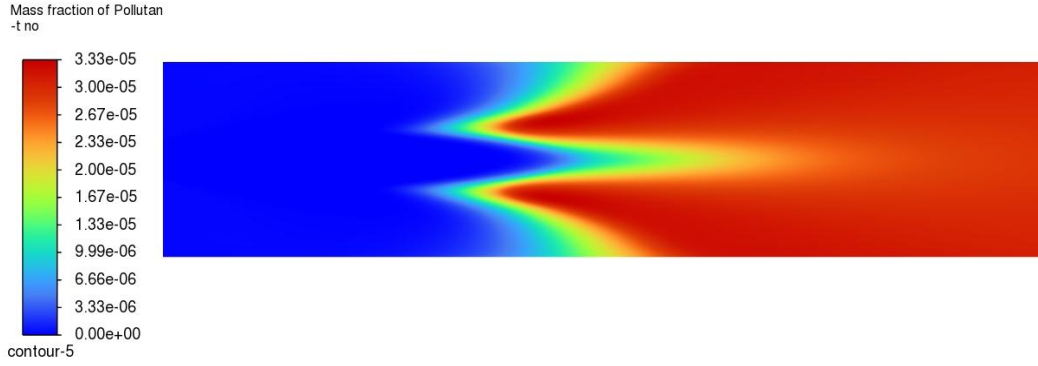


Figure 31 NOx mass fraction contour at the equivalence ratio of 1.2

From the above results it is clear that at lean regimes NOx emissions are lower compared to rich regimes. This can be explained due to the fact that Prompt NOx is formed through the CH radical reaction with N₂. These radicals increase as the mixture gets richer

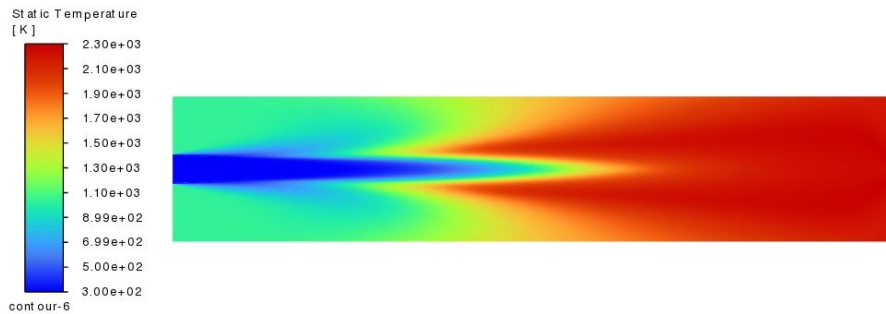
5.3 Effects of Hydrogen Addition on Combustion

5.3.1 Hydrogen addition at equivalence ratio of 1

Here, we explore the influence of hydrogen addition on the combustion characteristics of methane-air combustion. Our objective is to evaluate the effects of hydrogen on crucial aspects such as flame structure, temperature profiles and velocity profiles. The main goal is to enhance the combustion efficiency of methane-air mixtures by leveraging the potential of hydrogen as an additive. This simulation was conducted under the conditions of 3 atm and initial temperatures of 300 K.

5.3.1.1 Temperature contours

We present the temperature contours obtained from conducting simulations to investigate the impact of different hydrogen percentages (0%, 5%, 15%, 25% and 35%) on the combustion characteristics of methane-air combustion at 3 atm. What follows are images of the different hydrogen percentages and what also follows are the temperature plot at the axis for different hydrogen percentages



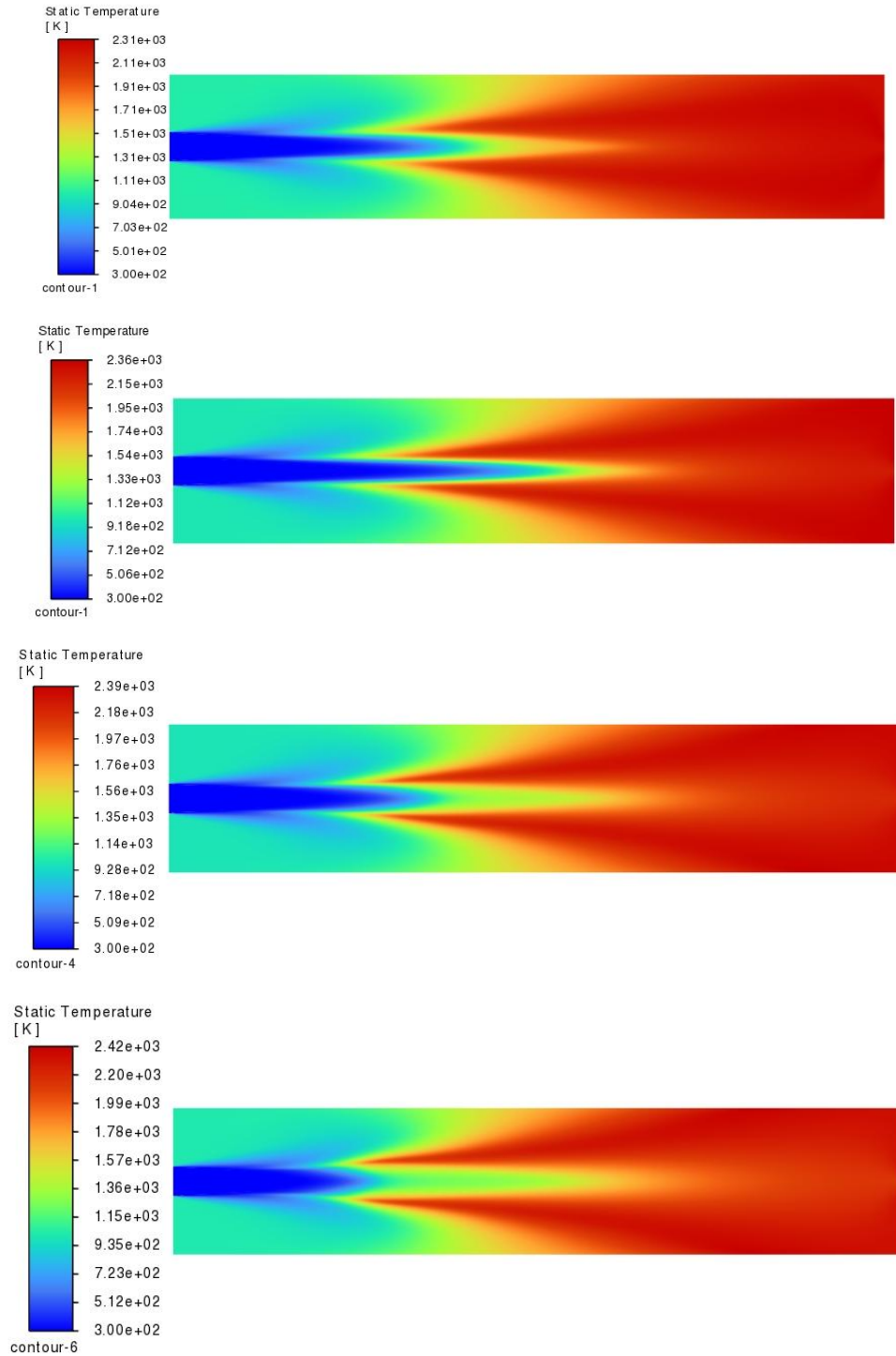


Figure 32 Temperature contours from 0% to 35% addition of hydrogen at equivalence ratio of 1

From the analysis of the temperature contours it is evident that temperature increases with increase in hydrogen percentage in the methane-air combustion.

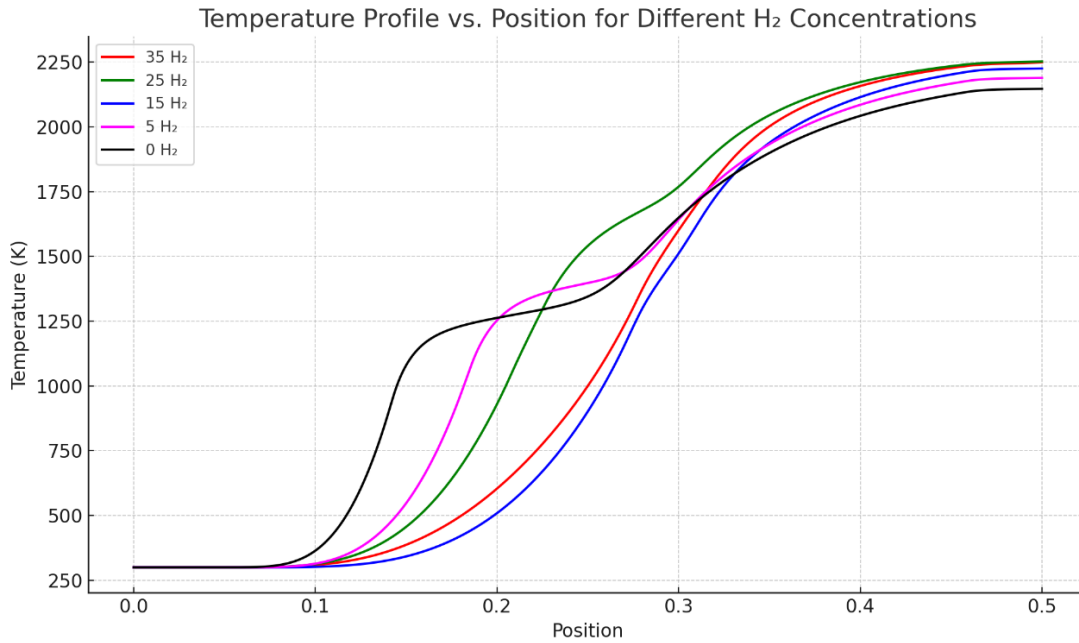


Figure 33 Temperature plots from 0% to 35% addition of hydrogen at equivalence ratio of 1

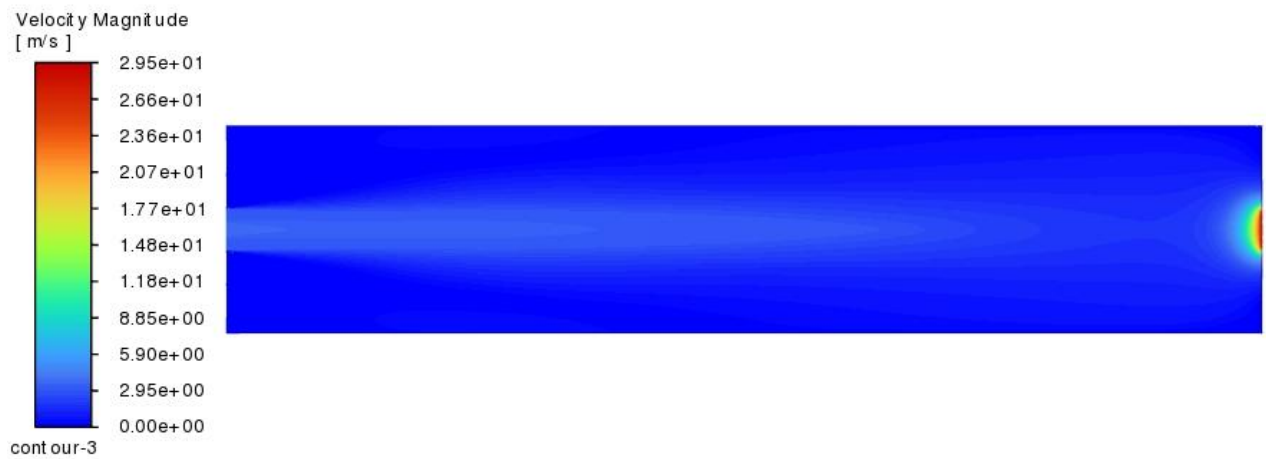
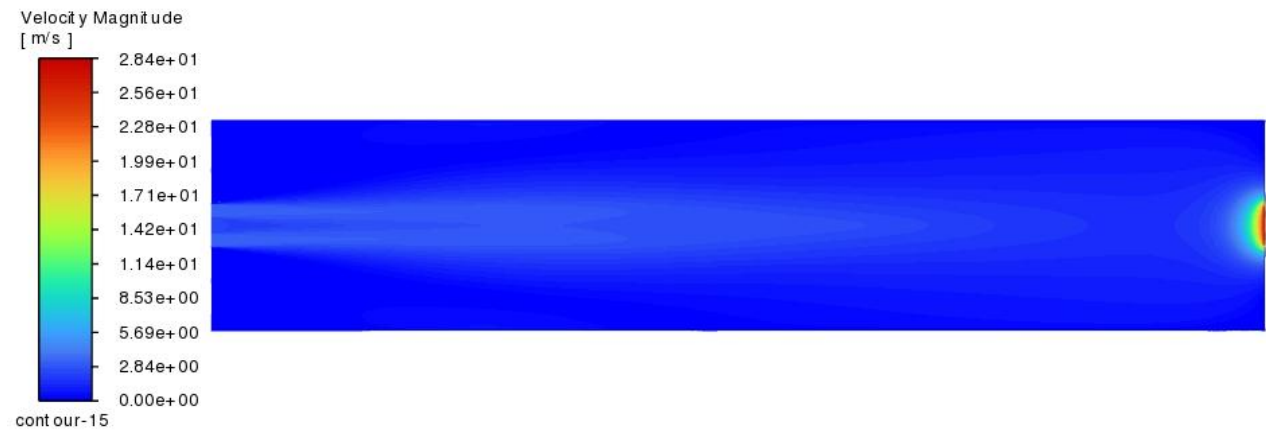
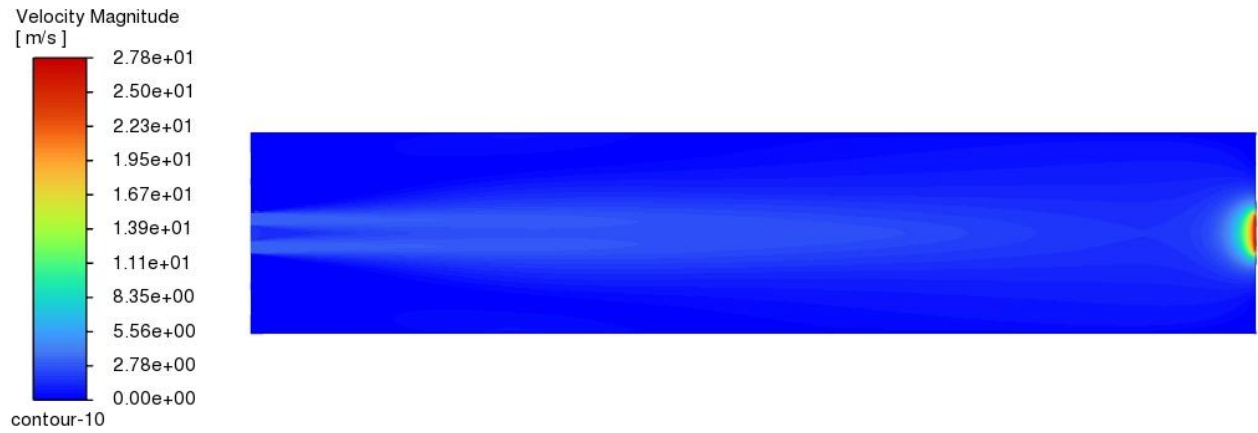
Table 5-1 Maximum temperatures and different hydrogen percentage addition

Hydrogen percentage	Maximum temperatures (K)
0%	2295.124
5%	2314.899
15%	2360.774
25%	2391.903
35%	2416.489

The temperature plots give us a greater insight on how the temperature varies at different hydrogen percentages. The table summarizes the observations by giving the maximum temperatures for each case. This observation indicates that the addition of hydrogen has a direct impact on the combustion process, leading to higher temperatures.

5.3.1.2 velocity contour

In this section, we examine the velocity contours obtained from the simulation to investigate the effects of various hydrogen percentages (0%, 5%, 15%, 25% and 35%) on the combustion characteristics of methane-air combustion.



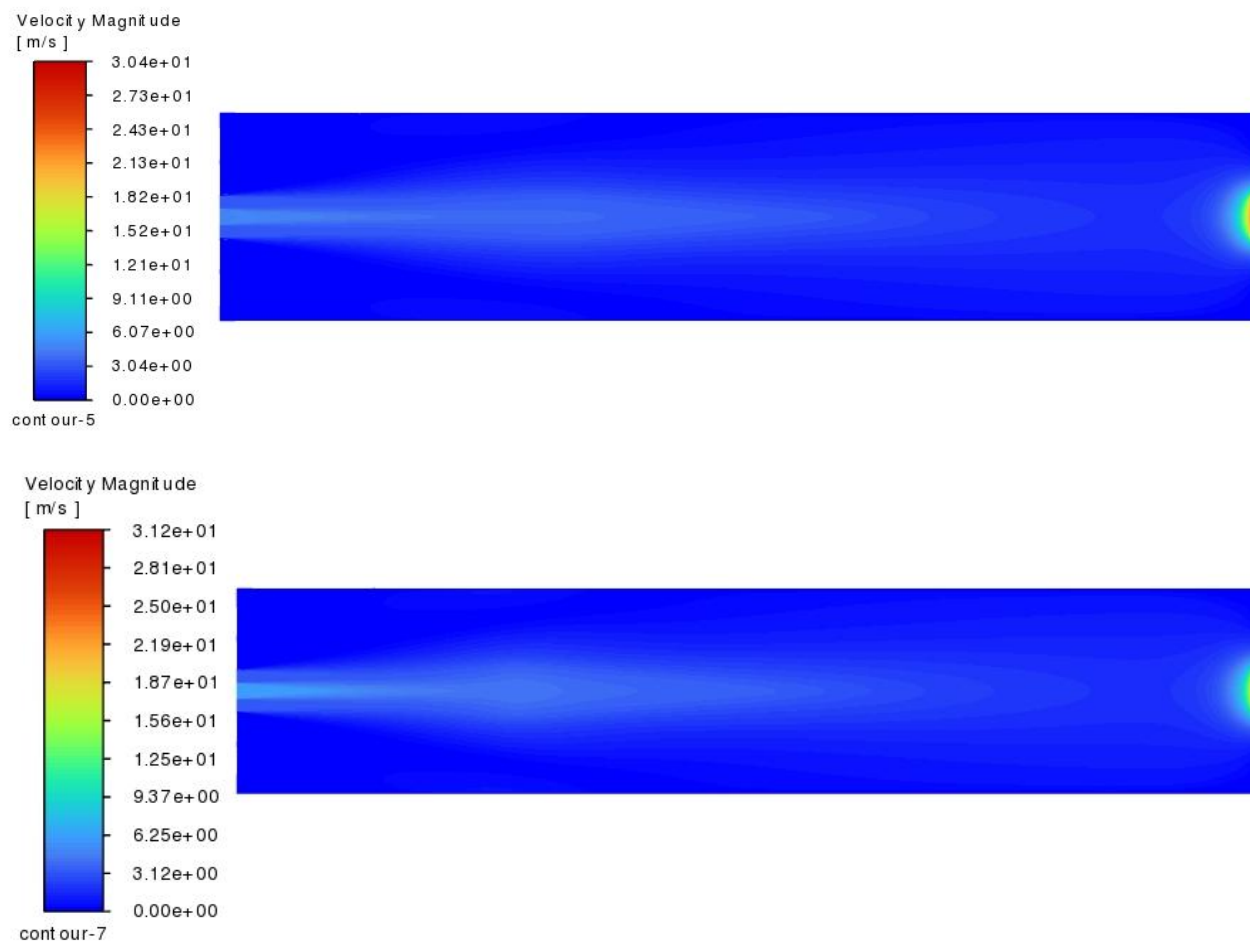


Figure 34 Velocity contours from 0% to 35% addition of hydrogen at 3atm

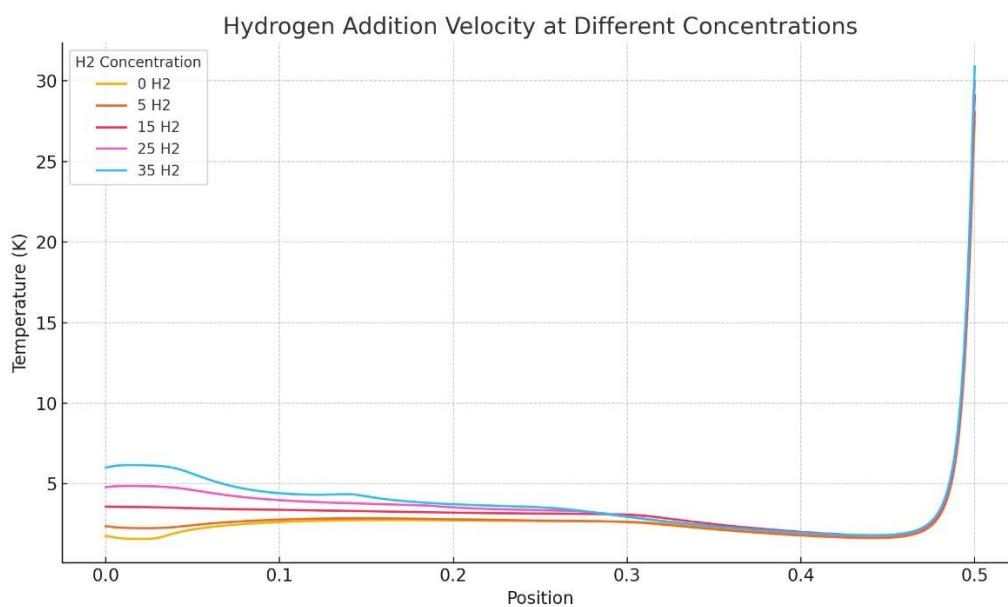


Figure 35 Velocity plots from 0 to 35 addition of hydrogen at 3atm

From the analysis of the velocity contours it is evident that velocity increases with increase in hydrogen percentage in the methane-air combustion.

The velocity contours give us a greater insight on how the velocity varies at different hydrogen percentages. This observation indicates that the addition of hydrogen has a direct impact on the combustion process, leading to higher velocity.

5.3.2 NO_x effects on addition of hydrogen

In this section we will get to know the effects of addition of hydrogen on prompt NO_x formation. At the hydrogen percentages of 5, 15, 25 and 35 at stoichiometric conditions.

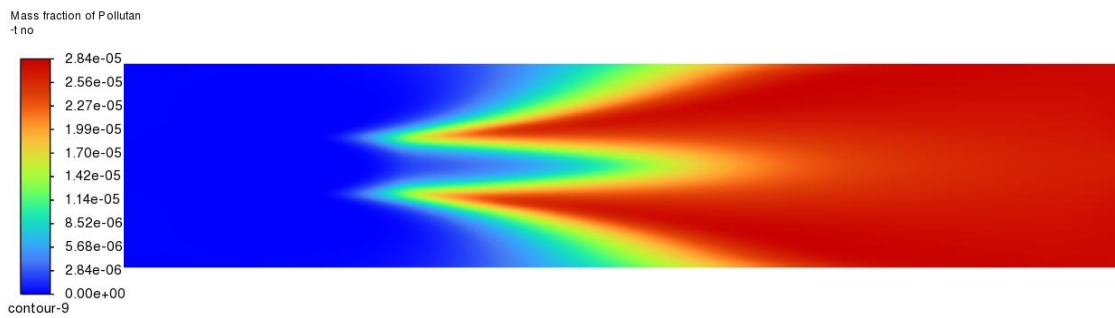


Figure 36 NO_x mass fraction at 5% hydrogen addition in methane-air combustion

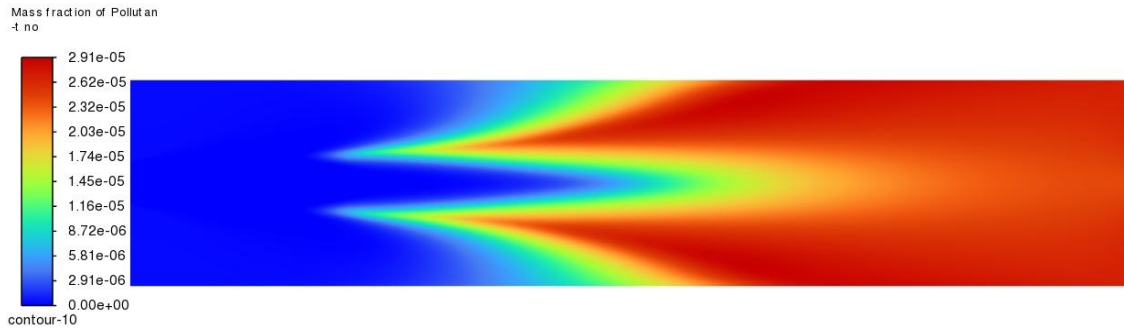


Figure 37 NO_x mass fraction at 15% hydrogen addition in methane-air combustion

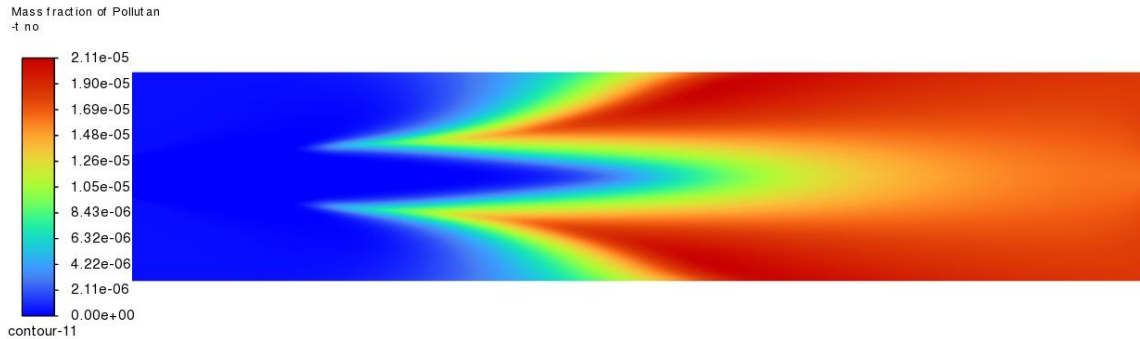


Figure 38 NO_x mass fraction at 25% hydrogen addition in methane-air combustion

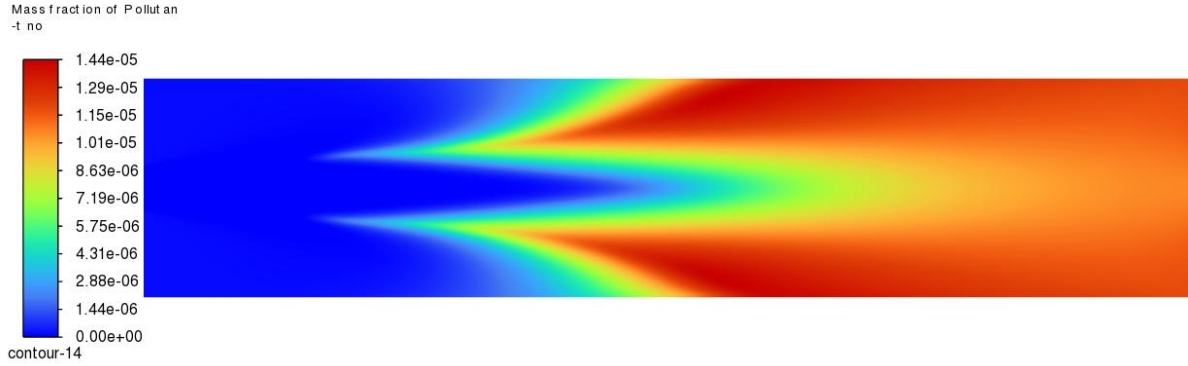


Figure 39 NOx mass fraction at 35% hydrogen addition in methane-air combustion

We notice an increase in Prompt NOx formation due to the increase in temperatures which lead to the rapid formation of CH radicals which reacts with N_2 to form HCN in turn also promotes the oxidation of HCN to NO.

5.4 Comparison and validation of results

This section provides an enhanced validation of the methane-air combustion simulation results obtained using ANSYS Fluent with a global reaction mechanism. Validation is performed against established theoretical models, experimental data from the literature, and fundamental thermodynamic principles to assess the accuracy and reliability of the predicted flow field, temperature distribution, and the effects of hydrogen addition.

5.4.1 Validation of Adiabatic Flame Temperature at Stoichiometric Conditions

The maximum predicted temperature for methane-air combustion at stoichiometric conditions ($\Phi = 1$) was 2295 K. This result is consistent with literature values for the adiabatic flame temperature of methane-air mixtures at 1 atm and 300 K inlet temperature.

According to Turns (2000), the adiabatic flame temperature using a one-step global mechanism is approximately 2226 K. Similarly, Glassman et al. (2014) report values between 2220 K and 2260 K. Simulations using chemical equilibrium models like NASA CEA and detailed mechanisms (e.g., GRI-Mech 3.0) also yield flame temperatures ranging between 2220 K and 2300 K, depending on assumptions related to specific heat, dissociation, and heat losses.

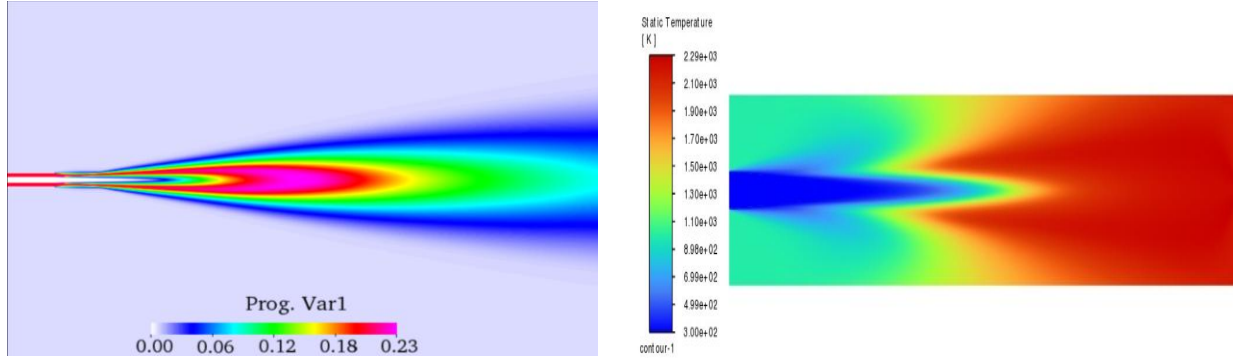


Figure 40 Mean temperature contour of the Sandia D methane–air flame from RANS-FGM simulation representing a benchmark for turbulent jet flames under stoichiometric conditions, side by side with the results of this simulation.

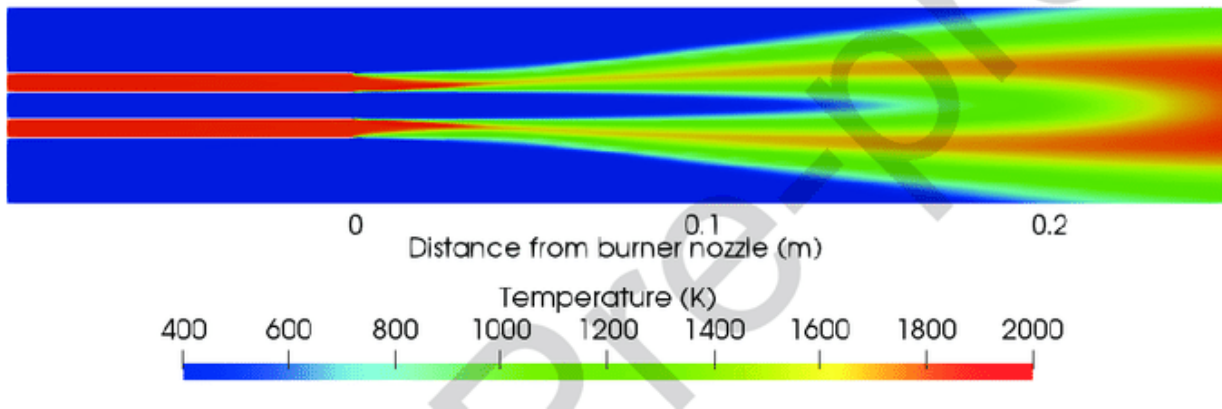


Figure 41 Temperature field of the Sandia D Simulated with Flamelet Model

The Sandia D flame is a canonical benchmark case widely used in combustion research. It involves a methane–air turbulent jet in a similar axisymmetric geometry and under comparable equivalence ratio and boundary conditions. The temperature contour in Figure 5-11 and 5-12 closely matches the structure and maximum temperature of our simulation (Figure 5-1), showing a central high-temperature core that broadens downstream. This validates that the flame structure and thermal distribution predicted by our global reaction model are physically realistic and consistent with experimental and high-fidelity simulation data.

The value of 2295 K falls within the upper expected limit, which is typical for global reaction mechanisms that do not account for detailed dissociation or radiation losses. Therefore, the predicted result is physically accurate.

5.4.2 Validation of Flame Temperature Rise with Hydrogen Addition

The effect of hydrogen enrichment on flame temperature was evaluated at various hydrogen addition percentages (0% to 35%). The results showed a clear trend of increasing flame temperature with increasing hydrogen content:

Table 5-2 Maximum temperatures and different hydrogen percentage addition

Hydrogen percentage	Maximum temperatures (K)
0%	2295.124
5%	2314.899
15%	2360.774
25%	2391.903
35%	2416.489

This trend is consistent with theoretical expectations. Hydrogen has a higher flame speed and adiabatic flame temperature (~2600–2700 K) compared to methane, and its addition enhances reaction rates and heat release. According to experimental and numerical studies (e.g., Tang et al., 2020), a temperature increase of 100–150 K is typical when hydrogen content is increased to 30%.

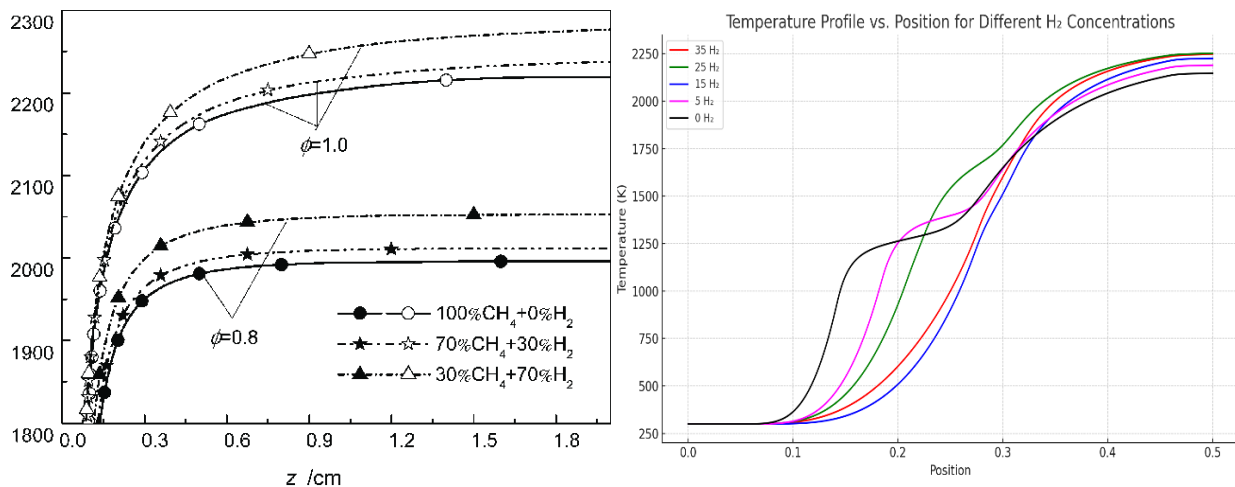


Figure 42 A side by side comparison between the reference data and the results of the simulation

Thus, the numerical results agree with published trends and validate the influence of hydrogen on flame enhancement.

5.4.3 Validation of Velocity Field

The simulated velocity field displays a typical jet-like behavior at the burner inlet, followed by a velocity decay due to turbulent mixing and viscous effects. Beyond approximately 0.1 m in the axial direction, the velocity stabilizes, indicating a region of fully developed or recirculated flow.

This behavior is consistent with established jet combustion theory, such as that described in Peters (2000), where turbulent diffusion dominates near-field combustion and flow acceleration occurs downstream due to gas expansion.

The effect of hydrogen enrichment on velocity was evaluated at various hydrogen addition percentages (0% to 35%). The results showed a clear trend of increasing velocity with increasing hydrogen content:

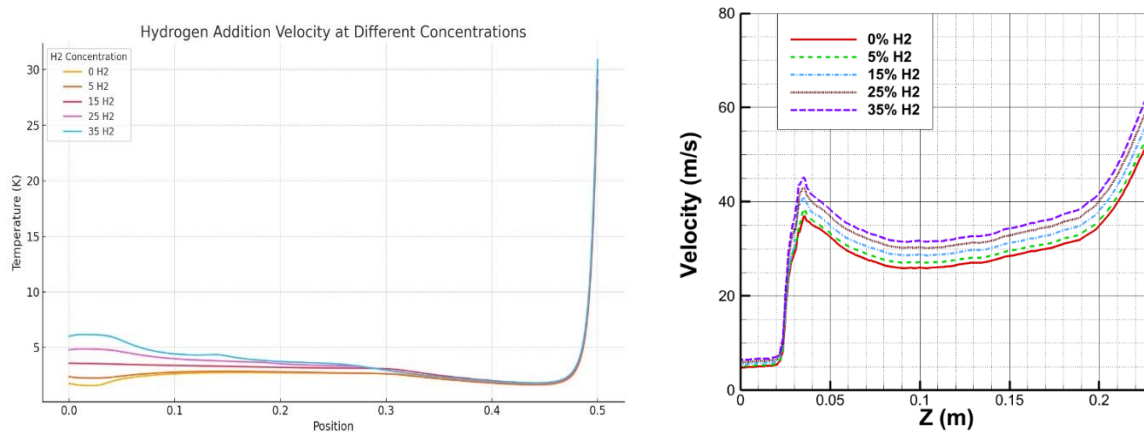


Figure 43 A side by side comparison between the velocity contour results and references at hydrogen additions of 0%, 5%, 15%, 25% and 35%

From the works of OUARMIM Alaa Eddine and AMRATE Soheib on Hydrogen Addition to Methane/Air Flames: A Numerical Investigation of Turbulent Combustion Phenomena we get to compare their velocity graphs and my results, we notice a jet like effect from the exit of the chambers since both chambers are of similar geometry. Despite their work being at 85% rpm, there is still evidence in the increase in velocity with increase in hydrogen percentages.

Thus, the numerical results agree with published trends and validate the influence of hydrogen on flame velocity.

5.4.4 Pressure Field Validation

The pressure contour shows high pressure inside the combustion chamber and a sharp pressure drop near the outlet. This behavior is expected due to flow acceleration and momentum expansion near the exit. As the outlet gauge pressure is set to 0 Pa, the observed pressure gradient aligns with Bernoulli's principle and experimental observations in turbulent jet flames.

5.4.5 Density Field Validation

The density field indicates high density at the inlets and a gradual decrease along the axial direction, correlating inversely with the temperature field. This behavior is expected from the ideal gas law:

$$\rho = \frac{P}{RT} \quad (5.1)$$

As the pressure is nearly constant and the temperature increases due to combustion, a corresponding drop in density is thermodynamically consistent.

5.4.6 Overall Combustion Behavior with Hydrogen Addition

The effects of hydrogen addition were further validated through the combined trends in flame temperature and velocity. The increase in flame temperature led to higher expansion rates and consequently higher velocities in the flow field. This behavior reinforces the thermodynamic and kinetic role of hydrogen in enhancing flame propagation and combustion efficiency.

The results align with established experimental trends, including increases in peak flame temperature and jet velocity due to hydrogen enrichment. Therefore, the numerical simulations accurately capture the fundamental effects of hydrogen addition in methane-air combustion.

Table 5-3 Summary of Validation Results

Quantity	Simulated Value	Expected Range	Validation Status
Adiabatic Flame Temp ($\Phi = 1$)	2295 K	2220–2300 K	Valid
Max Temp with 35% H ₂	2416 K	2350–2450 K	Valid
Velocity Profile	Jet-Decay-Stabilize	Matches jet flame structure	Valid
Pressure Distribution	High → Low at outlet	Matches outlet boundary condition	Valid
Density Distribution	Inverse to Temperature	Ideal Gas behavior	Valid

These validations confirm that the simulation results are consistent with theoretical expectations, empirical data, and fundamental thermodynamic relationships. The simulation approach and model assumptions used in this study are therefore deemed reliable for further analysis and interpretation.

5.5 Conclusion

The numerical simulations of methane-air combustion successfully characterized the fundamental combustion behavior using a global reaction mechanism. Under stoichiometric conditions, the model predicted a peak flame temperature of 2295 K, in close agreement with established theoretical values. The study further demonstrated that hydrogen enrichment significantly enhances combustion performance, with 35% hydrogen addition increasing the maximum flame temperature to 2416 K while improving flame stability and propagation speed.

While the global reaction model proved effective for capturing these key combustion characteristics, challenges in numerical convergence prevented the successful implementation of the more detailed DRM22 mechanism. These results validate the effectiveness of hydrogen as a combustion enhancer and confirm the utility of global mechanisms for preliminary combustion analysis, while highlighting the need for improved numerical approaches to enable detailed kinetic modeling in future studies. The findings provide a solid foundation for further research into optimized hydrogen-methane combustion systems.

Conclusion

Conclusion

In conclusion, this study advances the understanding of hydrogen–methane combustion through a computationally efficient global reaction model, while highlighting key challenges in applying detailed kinetic schemes. The global model, coupled with the Eddy Dissipation Model (EDM), offered reliable predictions of major flame characteristics under stoichiometric conditions and during hydrogen enrichment. However, in **lean combustion regimes ($\Phi < 1.0$)**, the use of a global mechanism with EDM led to **overestimated flame temperatures and flame stability**, due to the model's inability to capture finite-rate chemistry and extinction phenomena. This overprediction underscores the need for caution when interpreting lean flame behavior using simplified models.

Furthermore, the study reveals that **NO_x emissions vary significantly with equivalence ratio**. **Prompt NO_x**, while minimal at lean conditions, becomes more pronounced in fuel-rich zones. Notably, the **addition of hydrogen at stoichiometric conditions enhanced combustion intensity and flame temperature**, which in turn contributed to **increased NO_x formation**, particularly thermal NO_x. This trade-off between improved combustion performance and elevated emissions reinforces the importance of selecting appropriate kinetic models when evaluating pollutant formation.

Overall, while the validated global model remains a practical tool for preliminary burner analysis, its limitations in lean conditions and pollutant prediction necessitate the integration of more detailed mechanisms like DRM22 or GRI-Mech 3.0 for advanced design and emission control studies. Future efforts should focus on resolving numerical stiffness in detailed mechanisms and expanding analysis to include high-pressure, preheated, and diluted combustion environments, particularly in the context of clean hydrogen-methane energy systems.

Key Findings

1. Stoichiometric Methane-Air Combustion

- The global reaction model yielded a peak flame temperature of 2295 K, consistent with literature values for adiabatic conditions.
- Flame structure, velocity distribution, and pressure fields aligned with expected turbulent combustion behavior in confined burners.

2. Hydrogen Enrichment Effects

- Hydrogen addition (5–35% by mass) significantly increased flame temperature (up to 2416 K at 35% H₂) and combustion intensity due to hydrogen's higher reactivity and laminar flame speed.
- The global mechanism captured these trends effectively, demonstrating hydrogen's potential for improving combustion efficiency in lean and stoichiometric regimes.

3. Model Performance and Limitations

- The Eddy Dissipation Model (EDM) proved robust for global reaction simulations but lacks detailed kinetic insights.
- The DRM22 mechanism, intended for refined species prediction, faced convergence issues, likely due to stiffness in finite-rate chemistry coupling with turbulence. Future work should optimize solver settings or test alternative mechanisms (e.g., GRI-Mech 3.0) for improved stability.

Theoretical and Practical Implications

- The results reinforce hydrogen's role as a combustion enhancer but highlight trade-offs in flame stability and NO_x emissions, necessitating further optimization.
- The validated global model serves as a reliable tool for preliminary burner design, while detailed kinetics remain critical for pollutant analysis.

Recommendations for Future Work

- Resolve DRM22 convergence issues via adaptive meshing, stiff chemistry solvers, or mechanism reduction techniques.
- Compare results with lab-scale burner experiments to refine turbulence-chemistry interactions.
- Explore high-pressure, preheated, or diluted mixtures to assess hydrogen's viability in industrial systems.

In conclusion, this study advances the understanding of hydrogen-methane combustion through a computationally efficient global model, while identifying challenges in detailed kinetic modeling. The

findings contribute to the development of cleaner combustion strategies, emphasizing the need for balanced model selection based on accuracy and computational cost.

References

- [1] Guo, Laminar Flame Speed and Flammability Limit of Methane/Hydrogen/Air Mixtures, 2007.
- [2] A. R. a. B. N. E. Porpatham, Effects of Hydrogen Addition and performance, emission and combustion characteristics of a CNG engine, International Journal of Hydrogen Energy, vol 36, 2011.
- [3] J. a. Wang, Effects of Hydrogen Addition on the Combustion and Emission Performance of a Spark Ignition Engine, 2009.
- [4] Chaudhuri, Blowoff Dynamics of Bluff-Body Stabilized Flames with Hydrogen Enriched Fuels, 2010.
- [5] Medwell, Visualization of the Influence of Hydrogen Addition on Turbulent Non-Premixed Methane Jet Flames, 2008.
- [6] S. B. Pope, Turbuent Flows, Cambridge University Press, 2000.
- [7] T. P. a. D. Veynante, Theoretical and Numerical Combustion, 2nd ed.,, Edwards , 2005.
- [8] Ren, Effects of Hydrogen Addition on the Laminar Flame Characteristics of Methane-Air Mixtures, 2007.
- [9] S. a. Peters, Hydrogen Enriched Methane-Air Flames in Counterflow Configuration, 2013.
- [10] F. R. Menter, Two-equation eddy-viscosity turbulence models for engineering applications, AIAA Journal, vol. 32, no. 8, pp. 1598–1605, 1994.
- [11] V. a. Malalasekera, An Introduction to Computational Fluid Dynamics , 2nd ed.,, Pearson, 2007.
- [12] B. S. P. V. a. J. V. E. Larsson, A Reduced Mechanism for CFD modelling of methane combustion incuding NOx formation, Combustion Theory and Modelling, 2016.
- [13] B. M. a. B. Hjertager, On Mathematical Models of Combustion with special emphasis on soot formation and combustion, Proc. Combust. Inst., vol. 16, no1, pp. 719-729, 1977.

-
- [14] S. R. Turns, An Introduction to Combustion Concepts and Applications second edition, 2000.
- [15] M. E. T. Workshop, "Combustion Basics," Dallas, Texas , 2008.
- [16] "Homework Helpr," [Online]. [Accessed March 2025].
- [17] K. Academy, "Standard enthalpy change for combustion," 28 March 2023. [Online]. Available: <https://www.youtu.be./i0laHtoF3eo?si=NhyExGtv9T4Umv5>.
- [18] C. K. Law, Combustion Physics, Cambridge University Press, 2006.
- [19] P. L. Houston, Chemical Kinetics And Reaction Dynamics, 2001.
- [20] LibreTexts, "The Arrhenius Law- Arrhenius Plot," [Online]. Available: [https://chem.libretexts.org/Bookshelves/Physical_and_Theoretical_Chemistry_Textbook_Maps/Supplemental_Modules_\(Physical_and_Theoretical_Chemistry\)/Kinetics/06%3A_Modeling_Reaction_Kinetics/6.02%3A_Temperature_Dependence_of_Reaction_Rates/6.2.03%3A_The_Ar](https://chem.libretexts.org/Bookshelves/Physical_and_Theoretical_Chemistry_Textbook_Maps/Supplemental_Modules_(Physical_and_Theoretical_Chemistry)/Kinetics/06%3A_Modeling_Reaction_Kinetics/6.02%3A_Temperature_Dependence_of_Reaction_Rates/6.2.03%3A_The_Ar).
- [21] LibreTexts, "Chain reactions," [Online]. Available: [https://chem.libretexts.org/Bookshelves/Physical_and_Theoretical_Chemistry_Textbook_Maps/Supplemental_Modules_\(Physical_and_Theoretical_Chemistry\)/Kinetics/04%3A_Reaction_Mechanisms/4.02%3A_Chain_Reactions](https://chem.libretexts.org/Bookshelves/Physical_and_Theoretical_Chemistry_Textbook_Maps/Supplemental_Modules_(Physical_and_Theoretical_Chemistry)/Kinetics/04%3A_Reaction_Mechanisms/4.02%3A_Chain_Reactions).
- [22] ScienceDirect, "Autoignition," [Online]. Available: <https://www.sciencedirect.com/topics/engineering/autoignition#:~:text=Autoignition%20is%20defined%20as%20the,spark%20or%20flame%20%5B44%5D..>.
- [23] J. B. Heywood, Internal Combustion Engine Fundamentals, 2nd Edition, McGraw-Hill Education , 2018.
- [24] U. o. Wisconsin-Madison, "change in G, K and Van't Hoff Plot," in *chem 103/104 resource book*.
- [25] J. F. G. a. J. A. Barnad, Flame and Combustion, CRC Press, 1998.
- [26] I. Y. R. A. & G. N. G. Glassman, Combustion, Academic Press, 2014.
- [27] K. K. Kuo, Principles of Combustion, Wiley, 2005.

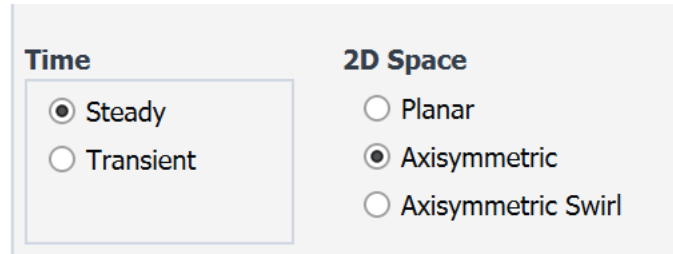
-
- [28] F. A. Williams, Combustion Theory, Benjamin/Cummings , 1985.
- [29] J. M. U. & D. R. W. Warnatz, Combustion (4th ed.), Springer, 2006.
- [30] I. M. Kennedy, Progress in Energy and Combustion Science, 1997.
- [31] A. H. & B. D. R. Lefebvre, Gas Turbine Combustion, CRC Press, 2010.
- [32] K. Kohse-Hoinghaus, Angewandte Chemie International Edition, 2010.
- [33] "Methane," National Institute of Standards and Technology (NIST), 2021. [Online]. Available: <http://webbook.nist.gov/cgi/cbook.cgi?ig?ID=C74828>.
- [34] "Hydrogen H2," National Institute of Standards and Technology (NIST), 2021. [Online]. Available: <http://webbook.nist.gov/cgi/cbook.cgi?ig?ID=C1333740>.
- [35] L. A. Ala Eddine Azzouz, Simulation de la combustion turbulente dans une chambre de combustion tubulaire pour le mélange kérosène/air et méthane/air, 2022.
- [36] Chemtalk, Enthalpy of Reaction, Formation, and Combustion.
- [37] T. D. a. B. Bohm, Advanced laser diagnostics for an improved understanding of premixed flame-wall interactions, Proceedings of The Combustion Institute , 2015.
- [38] A. A. R. a. S. S. B. M. A. Habib, The effect of preheated air on flame characteristics in a premixed burner, Energy Conversion and Management, vol 42, 2001.
- [39] S. Wuthrich, Investigation of OH, chemiluminescence and Schlieren techniques in hydrogen-enriched methane combustion, Combustion Science and Technology, vol 194, 2022.
- [40] M. D. Smooke, Temperature and species measurement in a laminar methane-air diffusion flame, Combustion and Flame, vol 117, 1999.
- [41] J. K. S. a. B. C. L. H. K. Cho, NOx emission characteristics of hydrogen-blended methane flames, International Journal of Hydrogen energy, 2008.
- [42] A. D. T. S. S. C. a. T. P. Y. Lafay, Experimental investigation of the effect of H2 enhancement on laminar methane-air flame thickness, Combustion and Flame, vol 153.

-
- [43] Park, Characteristics of Hydrogen Enriched Flames at Varying Equivalence Ratios, 2013.
- [44] M. G. Mostafa, 3D Simulation of a Jet-A Combustion In A Model Aircraft Engine Combustion Chamber, North Carolina Agricultural and Technical State University , 2012.
- [45] T. M. University, Conversion of momentum in fluid flow: The Navier-Stokes Equations.
- [46] D. D. Toporov, Combustion of Pulverised Coal in a Mixture of Oxygen and Recycled Fuel Gas, 2015.
- [47] M. P. a. R. L. S. J. H. Ferziger, Computational Methods for Fluid Dynamics, 4th ed., Springer, 2020.
- [48] M. Turns, An Introduction to Combustion concepts and Applications, 3rd ed., McGraw-Hill, 2012.
- [49] S. V. Patankar, Numerical Heat Tranfer and Fluid Flow, McGraw-Hill, 1980.
- [50] A. F. T. Guide, ANSYS Inc, 2023.
- [51] M. F. R., Two Equation Eddy Viscosity Turbulence Model for Engineering Applications, AIAA Journal, 1994.
- [52] J. D. R. P. J. C. C. P. C.E.L. Pinho, Numerical Study of Propane-Air Mixture Combustion in a Burner Element, Trans Tech Publications, Switzerland, 2008.
- [53] A. Abou-Taouk, four step global reaction mechanism for CFD simulations of flexi-fuel burners for gas turbines.
- [54] P. J. Roach, Verificaton and Validation in Computational Science and Engineering, Hermosa Publishers, 1998.
- [55] R. & H. J. R. Siegel, Thermal Radiation Heat Tranfer 4th ed., Taylor & Francis, 2002.
- [56] G. R. & H. C. H. Saravanmuttoo, Gas Turbine Theory, Pearson Education, 2009.
- [57] G. P. & B. O. Sutton, Rocket Propulsion Elements, Wiley, 2016.

Appendix A

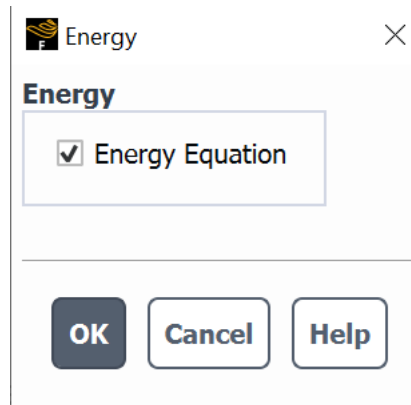
A.1 Methane-air Simulation Setup using a Global reaction

The Simulation setup was as follows



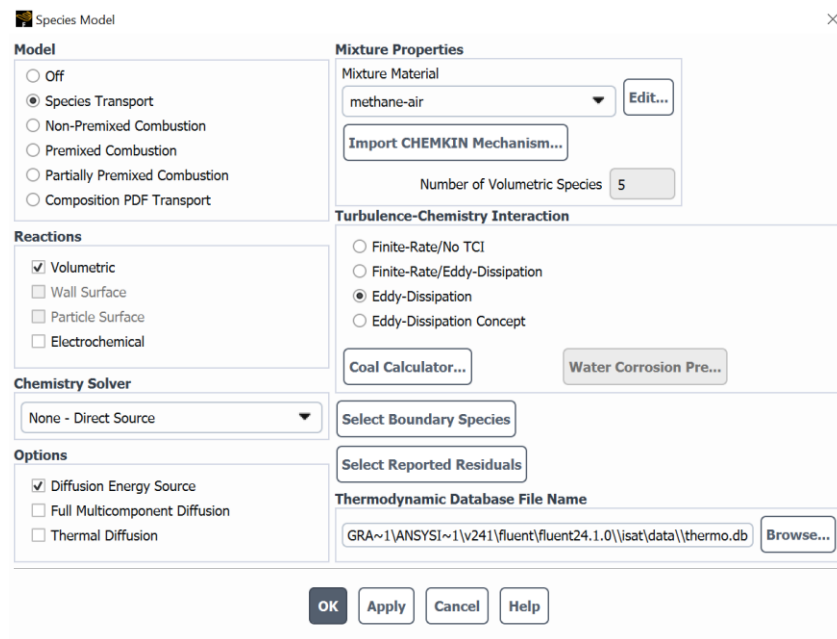
The dialog box is titled "General Steady configuration step". It contains two main sections: "Time" and "2D Space". In the "Time" section, the "Steady" radio button is selected, and the "Transient" radio button is unselected. In the "2D Space" section, the "Axisymmetric" radio button is selected, and the "Planar" and "Axisymmetric Swirl" radio buttons are unselected.

Figure 44 General Steady configuration step



The dialog box is titled "Energy". It contains a single checkbox labeled "Energy Equation", which is checked. At the bottom of the dialog box, there are three buttons: "OK", "Cancel", and "Help".

Figure 45 Energy equation step



The dialog box is titled "Species Model". It contains several sections: "Model", "Mixture Properties", "Reactions", "Turbulence-Chemistry Interaction", "Chemistry Solver", and "Options". In the "Model" section, the "Species Transport" radio button is selected. In the "Mixture Properties" section, the "Mixture Material" dropdown menu is set to "methane-air", and the "Number of Volumetric Species" is set to 5. In the "Reactions" section, the "Volumetric" checkbox is checked. In the "Turbulence-Chemistry Interaction" section, the "Eddy-Dissipation" radio button is selected. In the "Chemistry Solver" section, the "None - Direct Source" dropdown menu is selected. In the "Options" section, the "Diffusion Energy Source" checkbox is checked. At the bottom of the dialog box, there are four buttons: "OK", "Apply", "Cancel", and "Help".

Figure 46 Model choice step (Species transport)

On this step the Volumetric reaction was chosen, the turbulence interaction chosen was Eddy Dissipation and the material mixture choice was methane-air.

Viscous Model

Model

- ☐ Inviscid
- ☐ Laminar
- ☐ Spalart-Allmaras (1 eqn)
- ☐ k-epsilon (2 eqn)
- ☒ k-omega (2 eqn)
- ☐ Transition k-kl-omega (3 eqn)
- ☐ Transition SST (4 eqn)
- ☐ Reynolds Stress (5 eqn)
- ☐ Scale-Adaptive Simulation (SAS)
- ☐ Detached Eddy Simulation (DES)

k-omega Model

- ☐ Standard
- ☐ GEKO
- ☐ BSL
- ☒ SST

k-omega Options

☐ Low-Re Corrections

Near-Wall Treatment

correlation

Options

☐ Viscous Heating

Model Constants

Alpha*_inf: 1

Alpha_inf: 0.52

Beta*_inf: 0.09

a1: 0.31

Beta_i (Inner): 0.075

Beta_i (Outer): 0.0828

TKE (Inner) Prandtl #:

User-Defined Functions

Turbulent Viscosity: none

Prandtl and Schmidt Numbers

Energy Prandtl Number: none

Wall Prandtl Number: none

Turbulent Schmidt Number:

Figure 47 Selection of the viscous model step

Under boundary conditions the following steps were followed

Mass-Flow Inlet

Zone Name: air_inlet

Momentum | Thermal | Radiation | Species | DPM | Multiphase | Potential | Structure | UDS

Reference Frame: Absolute

Mass Flow Specification Method: Mass Flow Rate

Mass Flow Rate [kg/s]: 0.003512

Supersonic/Initial Gauge Pressure [Pa]: 0

Direction Specification Method: Normal to Boundary

Turbulence

Specification Method: Intensity and Hydraulic Diameter

Turbulent Intensity [%]: 5

Hydraulic Diameter [m]: 0.012

Apply Close Help

Figure 48 Setting the Mass flow rate Step for air inlet

Mass-Flow Inlet

Zone Name

Momentum Thermal Radiation Species DPM Multiphase Potential Structure UDS

Total Temperature [K]

Apply Close Help

Figure 49 Setting the initial temperatures

Mass-Flow Inlet

Zone Name

Momentum Thermal Radiation Species DPM Multiphase Potential Structure UDS

☐ Specify Species in Mole Fractions

Species Mass Fractions

ch4	<input type="text" value="0"/>
o2	<input type="text" value="0.23"/>
co2	<input type="text" value="0"/>
h2o	<input type="text" value="0"/>
n2	<input type="text" value="0.77"/>

Apply Close Help

Figure 50 Setting the Species mass fractions at the air inlet

Mass-Flow Inlet

Zone Name
fuel_inlet

Momentum Thermal Radiation **Species** DPM Multiphase Potential Structure UDS

Reference Frame Absolute

Mass Flow Specification Method Mass Flow Rate

Mass Flow Rate [kg/s] 0.0002

Supersonic/Initial Gauge Pressure [Pa] 0

Direction Specification Method Normal to Boundary

Turbulence

Specification Method Intensity and Hydraulic Diameter

Turbulent Intensity [%] 5

Hydraulic Diameter [m] 0.008

Apply Close Help

Figure 51 Setting the Mass flow rate at the fuel inlet

Momentum **Thermal** Radiation Species DPM Multiphase Potential Structure UDS

Total Temperature [K] 300

Apply Close Help

Figure 52 Setting the initial temperatures

Mass-Flow Inlet

Zone Name
fuel_inlet

Momentum Thermal Radiation **Species** DPM Multiphase Potential Structure UDS

☐ Specify Species in Mole Fractions

Species Mass Fractions

ch4 1

o2 0

co2 0

h2o 0

n2 0

Apply Close Help

Figure 53 Setting Species mass fractions

A. 2 Hydrogen addition to Methane-air Simulation Setup

A similar setup like that of methane-air was used. The few differences include the addition of the hydrogen reaction equation in the materials section. And adding Hydrogen as a species. Below are the steps to make it possible

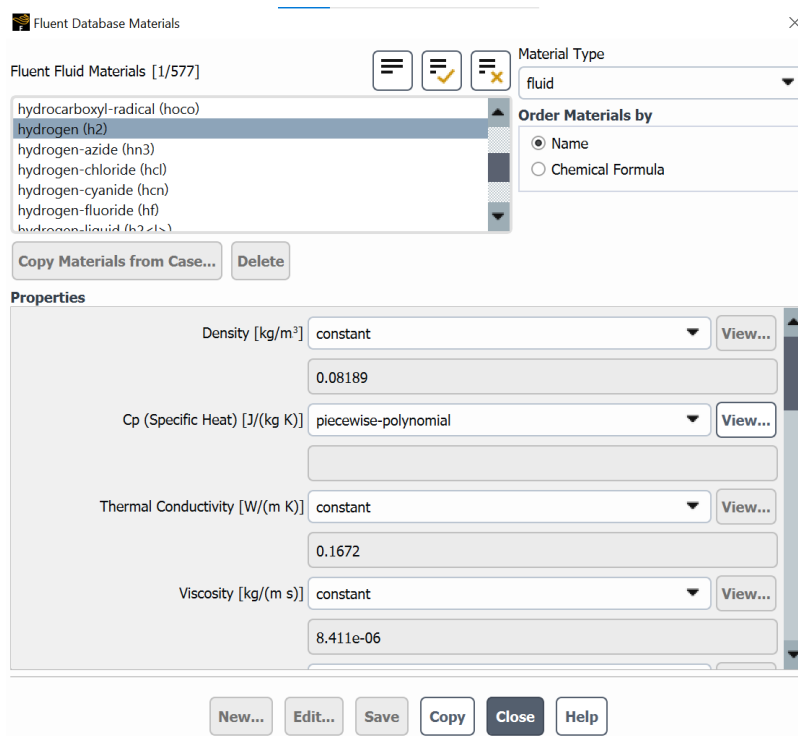


Figure 54 Addition of hydrogen to the available materials list

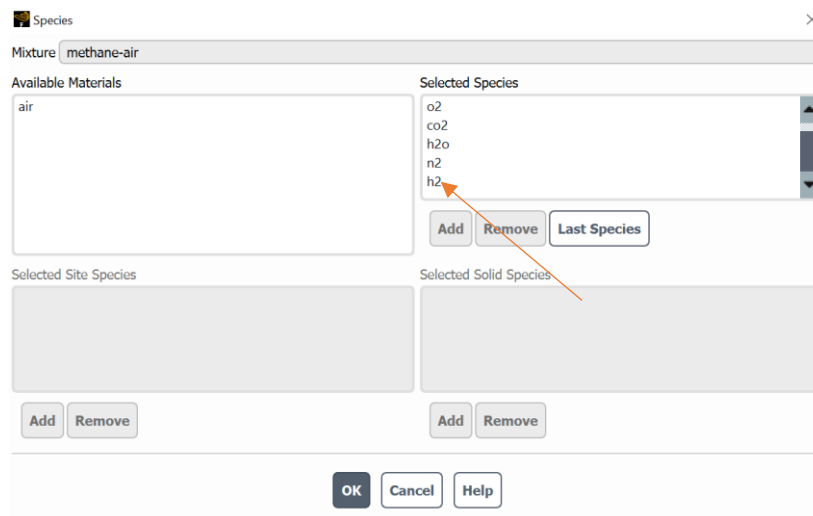


Figure 55 Addition of Hydrogen to the species list

Reactions

Mixture
methane-air

Total Number of Reactions
2

Reaction Name
reaction-2

ID
2

Reaction Type
☒ Volumetric
☐ Wall Surface
☐ Particle Surface
☐ Electrochemical

Number of Reactants
2

Number of Products
1

Species	Stoich. Coefficient	Rate Exponent
h2	1	1
o2	0.5	0.5

Species	Stoich. Coefficient	Rate Exponent
h2o	1	0

Arrhenius Rate

Pre-Exponential Factor
1e+15

Activation Energy [J/kgmol]
1e+08

Temperature Exponent
0

☐ Include Backward Reaction
Specify...

☐ Third-Body Efficiencies
Specify...

☐ Pressure-Dependent Reaction
Specify...

☐ Coverage-Dependent Reaction
Specify...

Mixing Rate

A
4

B
0.5

Figure 56 Addition of the Hydrogen reaction equation

Appendix B

B.1 Cold Flow Simulation Setup for DRM22 Mechanism

Objective of the Cold Flow Simulation

The cold flow simulation was conducted as a preparatory step before enabling chemical reactions in the methane-air combustion using the DRM22 mechanism. The goal was to:

- Validate the mesh and boundary conditions.
- Ensure proper species transport without combustion.
- Establish a stable initial flow field for later reactive flow.

Chemical Mechanism and Import Process

Mechanism used: DRM22 (22 species, 84 reactions), reduced from GRI-Mech 1.2.

Imported via:

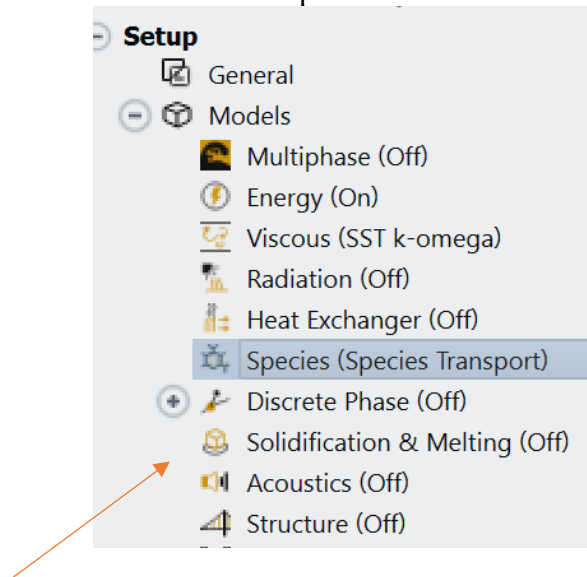


Figure 57 mechanism importing process

Species Model

Model

- ☐ Off
- ☒ Species Transport
- ☐ Non-Premixed Combustion
- ☐ Premixed Combustion
- ☐ Partially Premixed Combustion
- ☐ Composition PDF Transport

Reactions

- ☐ Volumetric

Options

- ☒ Diffusion Energy Source
- ☐ Full Multicomponent Diffusion
- ☐ Thermal Diffusion

Mixture Properties

Mixture Material: chemkin-import Edit...

Import CHEMKIN Mechanism...

Number of Volumetric Species: 21

Select Boundary Species

Select Reported Residuals

Thermodynamic Database File Name

C:/Users/USER/Desktop/Winnie/thermodata12.dat Browse...

OK Apply Cancel Help

Figure 58 Mechanism importing process

Import CHEMKIN Format Mechanism

Material Name: chemkin-import

Gas-Phase

Kinetics Input File

C:/Users/USER/Desktop/Winnie/DRM19.txt Browse...

Thermodynamic Database

- ☐ All contained in Kinetics Input File

C:/Users/USER/Desktop/Winnie/thermodata12.dat Browse...

Transport Property Data

- ☐ Import database

☐ Import Surface Mechanism

Import Close Help

Figure 59 Mechanism importing process

Reactions: Disabled during cold flow (Volumetric Reactions = Off).

Table 0-1 Solver and model settings

Setting	Value
Solver Type	Pressure-Based, Steady
Energy Equation	On (required by Fluent)
Species Transport	Enabled
Reactions	Disabled (Non-reacting)
Turbulence Model	[e.g., k- ϵ , k- ω , or laminar]

Note: Energy equation was kept on due to species model requirements, but boundary conditions were isothermal (300 K), and no heat source terms were introduced.

Table 0-2 Boundary Conditions

Region	Type	Values
Air Inlet	Mass Flow	Air composition (O ₂ , N ₂); T = 300 K
Fuel Inlet	Mass Flow	CH ₄ only (or CH ₄ /N ₂); T = 300 K
Outlet	Pressure Outlet	Gauge pressure = 0 Pa
Walls	No-slip	Adiabatic or fixed temperature (300 K)

Species Mass Fractions:

CH₄ = 1

O₂ = 0.23

N₂ = 0.77

Table 0-3 Material Properties

Property	Method	Value/Comment
Density	Ideal Gas	Required for species transport
C _p	Constant	1006 J/kg·K
Thermal Conduct.	Constant	0.0242 W/m·K
Viscosity	Constant	1.7894e-5 kg/m·s

Initialization and Patch

Initialization Method: Hybrid Initialization

Patched Conditions: Entire domain patched with:

Temperature: 300 K

Species Mass Fractions: Same as inlet values

Table 0-4 Solution controls

Parameter	Setting
Discretization	First-Order Upwind (initially)
Pressure Relaxation	0.3
Momentum	0.5
Species	0.5
Turbulence (k/ε)	0.5 / 0.5
Energy	0.9

Convergence Criteria

- **Monitored Residuals:**
 - Continuity: $\leq 5e-3$ (plateaued acceptably)
 - Momentum: $\leq 1e-6$

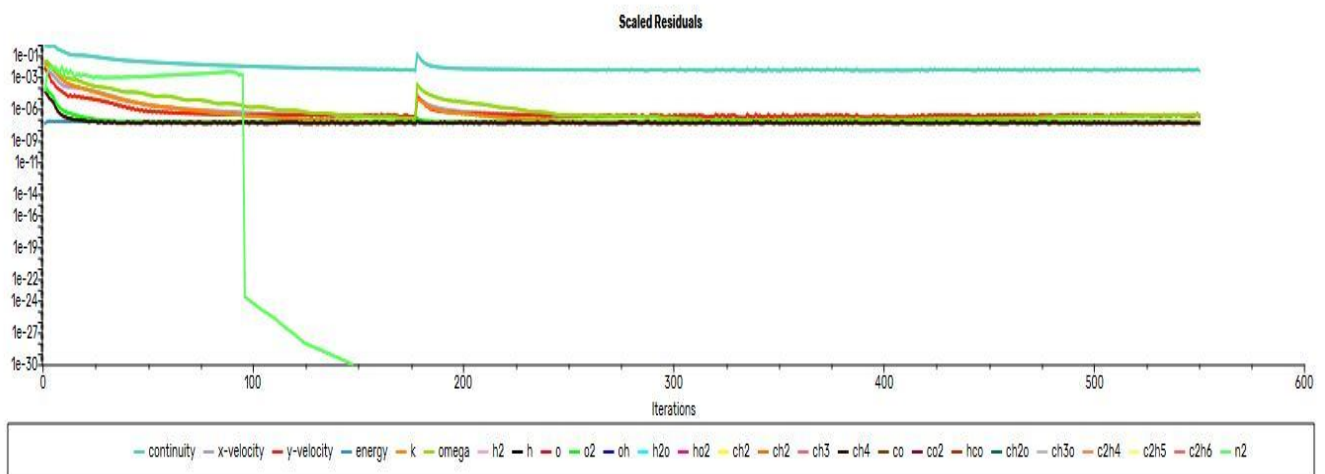


Figure 60 Scaled Residuals

- **No reverse flow** or mass imbalance was observed.
- **Mass Balance Check:**
 - Fuel inlet + air inlet \approx outlet mass flow within $\pm 1\%$

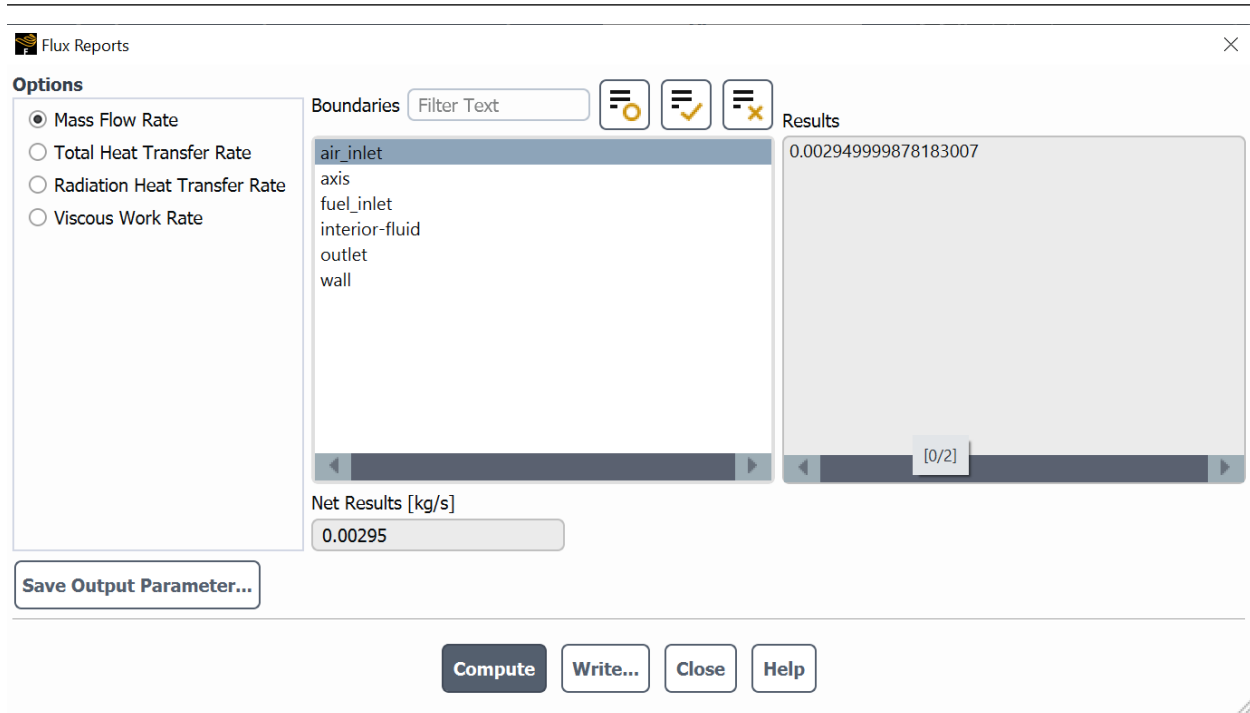


Figure 61 Mass balance check for air inlet

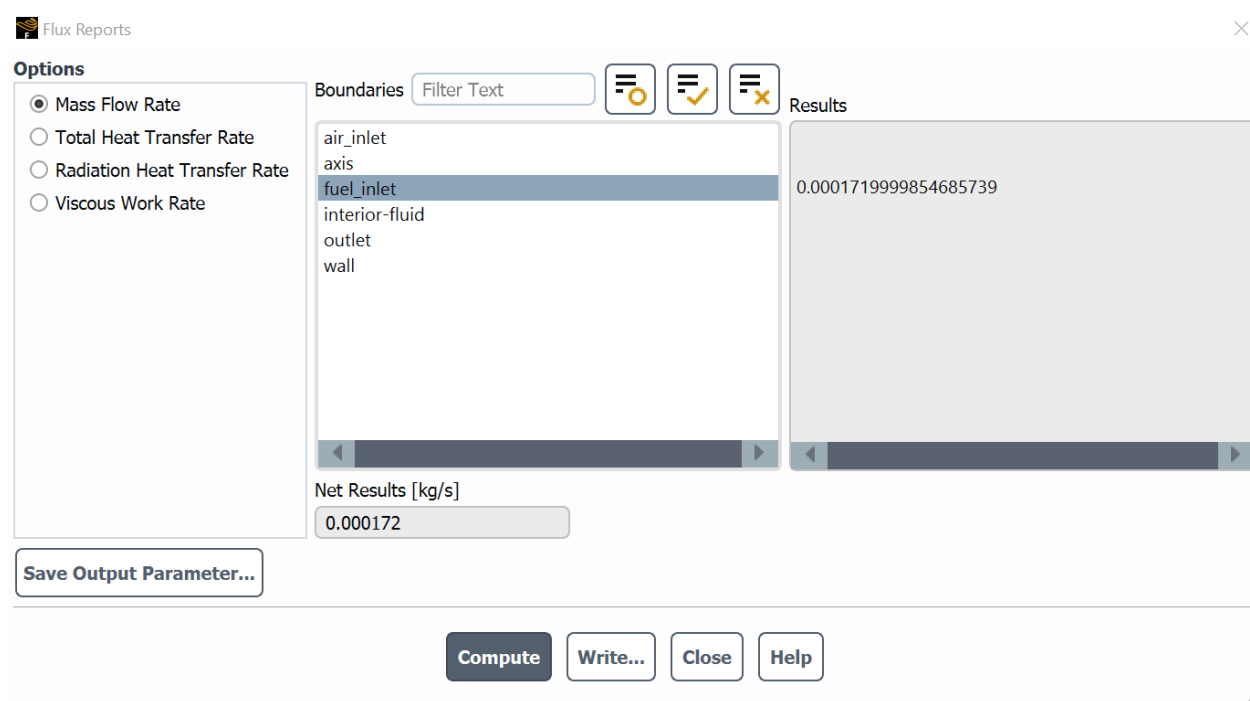


Figure 62 Mass balance check for fuel inlet

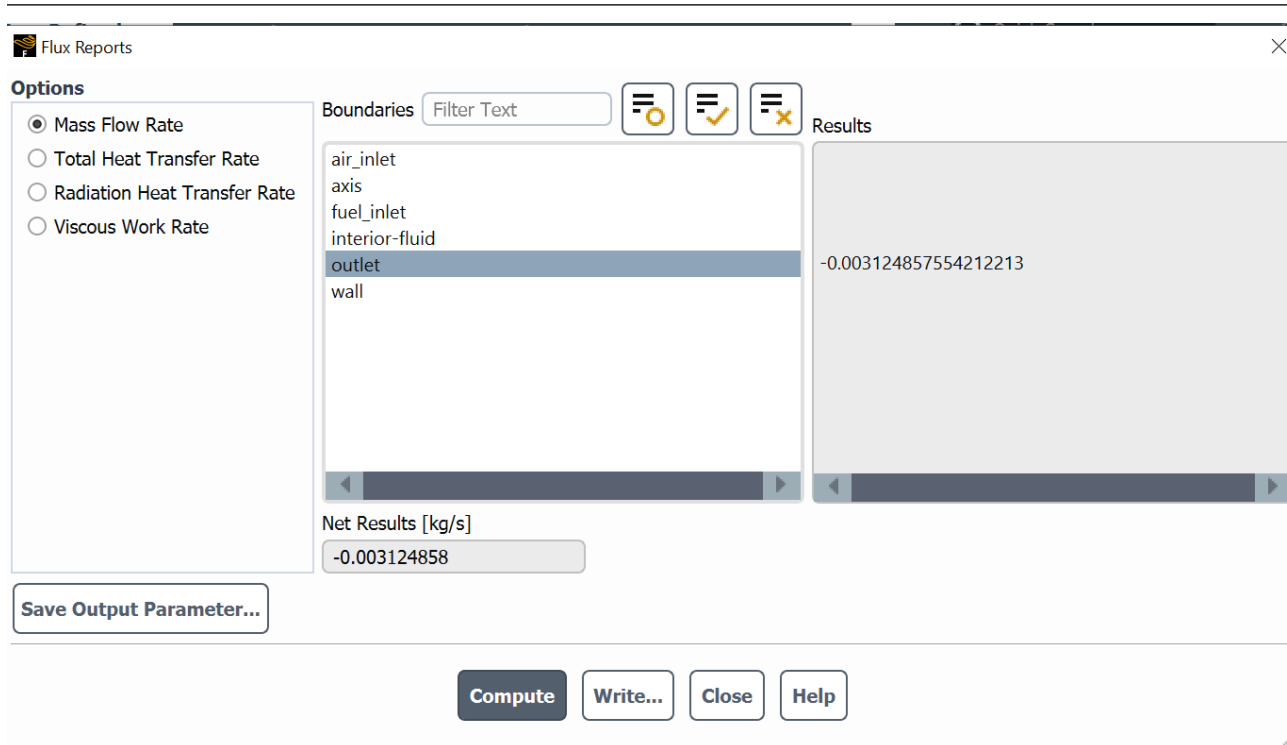


Figure 63 Mass balance check for outlet

Remarks

- This cold flow solution was used as a **baseline initialization** for all reactive simulations using DRM22.
- No heat release or flame structure was present, but species mixing and flow field were validated.
- Energy equation was retained (passively), but no significant temperature gradients were observed ($T \approx 300$ K throughout).

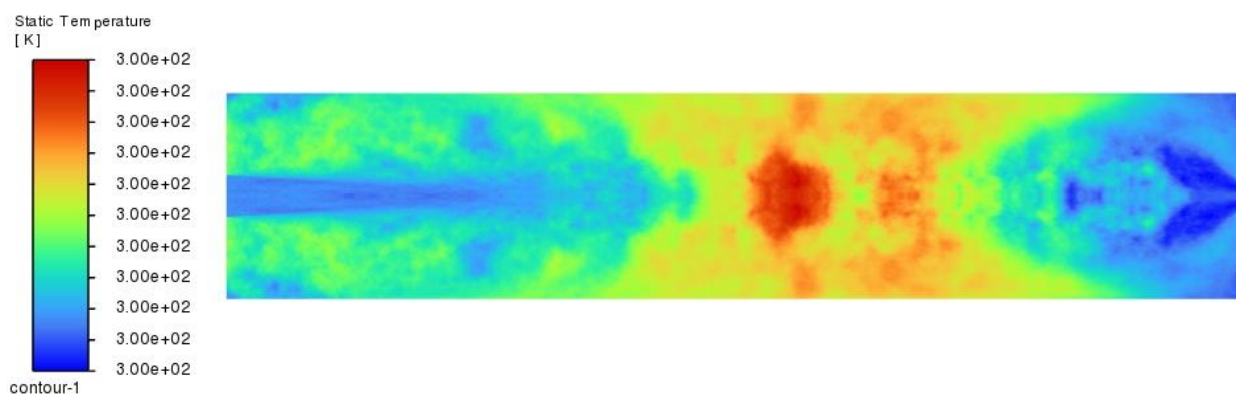


Figure 64 Temperature contour during cold flow